

**UNIVERSITY OF CALIFORNIA
LOS ANGELES**

**Effects of Small Halocarbons on Reverse
Osmosis Membrane Performance**

**A dissertation submitted in partial satisfaction of the
requirements for the degree Doctor of Philosophy
in Civil Engineering**

by

Robert Cheechun Cheng

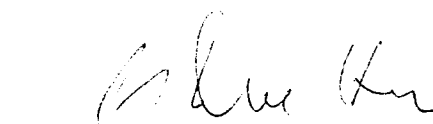
1990


The dissertation of Robert Cheechun Cheng is approved


John A. Dracup


Menacham Elimelech


Vasilios Manousiouthakis


Shane Que Hee


Michael K. Stenstrom, Committee Chair

University of California, Los Angeles

1990

TABLE OF CONTENTS

	Page
List of Symbols	v
List of Tables	vii
List of Figures	viii
Acknowledgements	xi
Vita	xii
Abstract	xiii
1. Introduction	1
2. Membrane Processes.	3
Municipal Wastewater	5
Industrial Water.	6
Agricultural Drainage Water	7
3. Membrane Hardware Configurations	11
Tubular Configuration	11
Spiral-Wound Configuration	11
Hollow Fine Fibers Configuration	14
Flat-Plate Configuration.	16
4. Membrane Types	18
Cellulose Acetate Membranes	18
Aromatic Polyamide Membranes	22
Composite Membranes	24
Summary	27
5. Modelling Membrane Performance.	28
6. Membrane-Chemical Interactions.	36
Membrane Degradation.	36
Membrane Fouling.	37
Inorganic Foulants	37
Particulate Foulants.	38
Dissolved Organic Foulants	39
Biological Foulants	40

Fouling Effects	40
Membrane Permeation	41
Trace Organics in Wastewaters	41
7. Fouling/Degradation Mechanisms	46
Hypothesis	46
Membrane Performance Tests	47
8. Materials and Methods	50
Experimental Apparatus	50
Analytical Methods	50
Experimental Procedure	53
Data Analysis	56
9. Results and Discussion.	59
SDI Tests.	59
Cellulose Acetate Membranes	59
Polyamide Membranes.	66
Advanced Composite Membranes	74
Fouling Reversibility Tests.	83
Membrane/Halocarbon Partition Coefficients	83
Void Fraction Tests.	89
Membrane Performance Summary	91
Organic Rejection vs. Dielectric Constant (ϵ)	97
Comparison of Different Membrane Types	97
Comparison of Experimental and Literature m Values.	100
FTIR Results.	100
NMR Results.	106
SEM Results.	107
10. Conclusions	113
Flux Tests	113
Organic Rejection	114
Halocarbon Partitioning.	114
Membrane Fouling.	115
Fouling Reversibility	116
11. Recommendations for Future Work.	117
References.	118
Appendix: Sample Raw Data and Sample Calculations	122

LIST OF SYMBOLS

A	Water transport coefficient (gal/ft ² -day-psi (GFD/psi))
B	Solute transport coefficient (ft/day)
C _f	Feed concentration (mg/L)
C _p	Product concentration (mg/L)
F	Force of attraction between two charges (N)
F _t	Water flux at time t (gal/ft ² -day (GFD))
J _s	Solute flux (lb/day)
J _s	Water flux (GFD)
K	Membrane constant (GFD)
K _s	Organic distribution coefficient (unitless)
m	Log-log flux decline index (unitless)
MW	Molecular weight (g/mol)
P ₃₀	Plugging at 30 psig feed pressure (unitless)
Q	Amount of permeate per unit area membrane (gal/ft ²)
Q'	Charge on one body (C)
Q''	Charge on one body (C)
Q _f	Feed water flowrate (gal/day)
Q _p	Product water flowrate (gal/day)
r	Distance between two charges (m)
R	Universal gas constant (0.0821 L-atm/mol-K)
SDI	Silt density index (unitless)
t	Time (days)
t _f	Final time, in seconds, required to collect 500 mL sample after test time t _t (usually 15 minutes)

t_i	Initial time, in seconds, required to collect 500 mL sample
t_o	Initial time (days)
t_t	Total test time in minutes (usually 15, but may be less if 75 percent plugging in less than 15 minutes)
T	Temperature (K)
V_f	Feed water volume (gal)
V_p	Product water volume (gal)
w_d	Weight of dry membrane (g)
w_w	Weight of wet membrane (g)
Y	% conversion or recovery (unitless)

Greek Symbols

ΔC	Concentration difference (mg/L)
ΔP	Operating pressure (psi)
$\Delta \pi$	Osmotic pressure difference (psi)
ΔV	Change in volume (cm ³)
ϵ	Dielectric constant of medium (C/V-cm)
ϵ_o	Relative permittivity of vacuum (8.854×10^{-14} C/V-cm)
ϵ_r	Relative permittivity of medium (unitless)
ϵ_v	Membrane void fraction (unitless)
ρ_d	Density of dry membrane (g/cm ³)
ρ_e	Density of wet membrane (g/cm ³)

LIST OF TABLES

No.	Table Title	Page
I	Membrane Separation Processes (<i>from Lonsdale, 1982</i>).	4
II	Comparison of CA, PA, and AC Membrane Properties.	27
III	Selected Properties of Halocarbons Used In This Study (<i>from Weast, 1989</i>)	43
IV	Factors Influencing Rejection by RO Membranes.	44
V	RO Membrane Fixation for SEM Examination (<i>from Weast, 1989</i>).	54
VI	Comparison of m and K values for CA, PA, and AC Membrane	99
VII	Comparison of Experimental and Literature m Values for CA-Type Membranes	101
VIII	Absorption Bands of Characteristic Groups (<i>from Socrates, 1980</i>)	102

LIST OF FIGURES

No.	Figure Title	Page
1	Schematic of Yuma Desalting Plant Facility (<i>from Applegate, 1984</i>)	9
2	Schematic for Tubular RO Configuration (<i>from Eisenberg, 1986</i>)	12
3	Schematic for Spiral-Wound RO Configuration (<i>from Eisenberg, 1986</i>)	13
4	Schematic for Hollow-Fine Fiber RO Configuration (<i>from Eisenberg, 1986</i>)	15
5	Schematic for Flat-Plate RO Configuration (<i>from Eisenberg, 1986</i>)	17
6	Formation of Cellulose Acetate (<i>from Kesting, 1977</i>)	20
7	Formation of Polyamide (<i>from Petersen, 1986</i>)	23
8	Formation of DuPont's ACM (<i>from Pohland, 1988</i>).	25
9	Schematic of One-Pass RO Unit	51
10	Total Product Volume vs. Time for DuPont 7460 CA	60
11	Calculated Flux vs. Time for DuPont 7460 CA	61
12	TDS Rejection vs. Time for DuPont 7460 CA	63
13	Halocarbon Rejection vs. Time for DuPont 7460 CA.	64
14	Water Transport Coefficient (A) vs. Time for DuPont 7460 CA	65
15	Solute Transport Coefficient (B) vs. Time for DuPont 7460 CA	67
16	Total Product Volume vs. Time for DuPont 5930 PA	68
17	Calculated Flux vs. Time for DuPont 5930 PA	69

18	TDS Rejection vs. Time for DuPont 5930 PA	71
19	Halocarbon Rejection vs. Time for DuPont 5930 PA.	72
20	Water Transport Coefficient (A) vs. Time for DuPont 5930 PA	73
21	Solute Transport Coefficient (B) vs. Time for DuPont 5930 PA	75
22	Total Product Volume vs. Time for DuPont 89006 ACM	76
23	Calculated Flux vs. Time for DuPont 89006 ACM.	77
24	TDS Rejection vs. Time for DuPont 89006 ACM	79
25	Halocarbon Rejection vs. Time for DuPont 89006 ACM.	80
26	Water Transport Coefficient (A) vs. Time for DuPont 89006 ACM	81
27	Solute Transport Coefficient (B) vs. Time for DuPont 89006 ACM	82
28	K_s vs. Halocarbon Concentration for DuPont 's CA Membrane . .	84
29	K_s vs. Halocarbon Concentration for DuPont 's PA Membrane . .	86
30	K_s vs. Halocarbon Concentration for DuPont 's AC Membrane . .	87
31	Comparison of K_s for DuPont Membranes.	88
32	Void Fraction vs. Halocarbon Concentration for DuPont Membranes	90
33	Total Product Volumes at 125 Hours for CA, PA, and AC Membranes.	92
34	% Change from Baseline Volumes for CA, PA, and AC Membranes.	93
35	TDS Rejections at 125 Hours for CA, PA, and AC Membranes. .	94
36	% Change from Baseline TDS Rejections for CA, PA, and AC Membranes.	95

37	Average Halocarbon Rejections for CA, PA, and AC Membranes.	96
38	Dielectric Constant ϵ vs. % Organic Rejection	98
39	FTIR Spectrum for CA Membrane (<i>Baseline</i>)	103
40	FTIR Spectrum for CA Membrane (<i>CHCl₃ added</i>).	104
41	FTIR Spectrum for CA Membrane (<i>CHBr₃ added</i>).	105
42	SEM Photograph for CA Membrane, 3670x Magnification.	108
43	SEM Photograph for PA Membrane, 3670x Magnification.	110
44	SEM Photograph for AC Membrane, 3670x Magnification.	111

ACKNOWLEDGEMENTS

The author would like to thank Professor Michael Stenstrom for his valuable advice and support during this research work. Other thanks go out to the other members of this committee, Professors John Dracup, Menachem Elimelech, Vasilios Manousiouthakis, and Shane Que Hee for their comments.

Special thanks go to Professor Julius "Bud" Glater and Dr. J.B. Neethling for providing hours of stimulating discussion and opening my eyes to the world of reverse osmosis research. Without your encouragement and support the completion of this work would have been difficult.

The money for this research was provided by the California Department of Water Resources (DWR) and E.I. duPont Company (Contract numbers B55037 and D881130, respectively). Thanks go out to Brian Smith of DWR and Dr. Irving Moch of DuPont for the technical assistance.

The students in the Water Quality Lab helped with my research problems as well as providing an entertaining place to work. I would like to acknowledge Roger Babcock, David Ching, Chu-Chin Hsieh, Naci Ozgur, Dr. Kyoung S. Ro, Eddie Tzeng, and Kenneth Wong who made the lab a much more interesting place to conduct research.

Finally, to my family, especially my parents, whom never failed to believe in me when the going got tough.

VITA

July 11, 1962	Born, Taipei, Taiwan, Republic of China
1984	B.E., Chemical Engineering Vanderbilt University, Nashville, TN
1985	M.S., Chemical Engineering Vanderbilt University, Nashville, TN
1984-1985	Research and Teaching Assistant Chemical Engineering Department Vanderbilt University, Nashville, TN
1985-1986	Intern Division of Hazardous Waste Management Tennessee Department of Health and Environment Nashville, TN
1986	Intern U.S. Air Force Logistics Command Wright-Patterson Air Base, OH
1986-1987	Teaching Assistant Chemical Engineering Department University of California, Los Angeles
1987-1990	Research Assistant Civil Engineering Department University of California, Los Angeles

ABSTRACT OF THE DISSERTATION

Effects of Small Halocarbons on Reverse Osmosis Membrane Performance

by

Robert Cheechun Cheng

Doctor of Philosophy in Civil Engineering

University of California, Los Angeles, 1990

Professor Michael K. Stenstrom, Chairperson

The effects of small halocarbons, CHCl_3 , CHBr_3 , and CCl_4 at 50 mg/L on the performance of three typical RO membranes were examined. Cellulose acetate, polyamide, and advanced composite membranes were used. Five parameters were evaluated for each membrane/halocarbon combination. Flux, total dissolved solids rejection, halocarbon rejection, partition coefficient, and void volume tests were conducted in order to evaluate the effects of halocarbon addition. In general, the halocarbons were poorly rejected by all three membranes, increased rate of flux decline, and increased total dissolved solids rejection over controls without halocarbons. Partition tests revealed advanced composite membranes absorb all three halocarbons much more strongly than either cellulose acetate or polyamide membranes. The strong halocarbon adsorption for the composite was proposed as the main mechanism for membrane swelling which caused flux decrease and total dissolved solids rejection increase. The strong affinity for halocarbons suggests that the advanced composite membranes should not be used for treating waters containing halocarbons.

1. Introduction

Reverse osmosis (RO) is an advanced demineralization technique for water purification. RO was initially conceived as a method to compete with distillation to obtain potable waters from seawater; recently, RO applications have expanded to other areas such as reclamation of municipal, agricultural, and industrial wastewaters. Each of these waters exhibits very different characteristics such as turbidity, organic content, and salinity. In order to design an effective RO treatment plant for these waters, the engineer must know how membranes respond to a specific water.

The major obstacle to widespread usage of RO as a treatment scheme is a phenomenon known as fouling. Fouling is a decline in product water throughput or flux, and/or a decline in product water quality measured as total dissolved solids (TDS). Fouling results from various sources, one of which is caused by an interaction with organic materials. This type of fouling results because the organic compounds react with membranes in such a way as to lower product water flux and/or quality.

The organic compounds examined in this study are a series of halogenated methanes: chloroform (CHCl_3), bromoform (CHBr_3), and carbon tetrachloride (CCl_4). These organics are byproducts of chlorination or bromination of surface waters and are normally present in trace concentrations ($> 10 \text{ mg/L}$). Studies at Yuma Desalting Plant Facility (YDPF) in Yuma, AZ detected the presence of these constituents in Yuma's feedwaters and are thought to be partially responsible for rapid membrane performance decline. YDPF, located on the Colorado River, is the world's largest facility for reclaiming irrigation water

utilizing RO.

The key to successful RO operations lies in the pretreatment scheme. The goal of pretreatment is to remove, as economically as possible, components from the water which may cause membrane degradation or fouling. Operational cost is increased when membrane cost increases due to membrane replacement. Operational cost is increased when membrane fouling occurs due to additional pumping and cleaning expenses. In either case, downtime for membrane cleaning or replacement incur additional operational costs.

The goals of this dissertation research are threefold. The first goal is to determine whether halocarbons affect various membranes' abilities to produce potable waters. The three membrane types used in this study were provided by DuPont: cellulose acetate (CA), aromatic polyamide (PA), and advanced composite membrane (ACM). Once the effects were determined, possible hypotheses were proposed as to the causes of the halocarbon fouling/damage. If fouling occurs, the reversibility of this effect has to be determined. Knowledge of the causes and effects of membrane fouling/damage by halocarbons will aid in the successful design of wastewater pretreatment.

This work was inspired by the previous research (*Kaakinen, 1985; Glater, 1989*) performed at YDPF and the Los Banos Desalting Facility in California's San Joaquin Valley, both of which indicated organic matter may cause deleterious effects on membrane performance. The latter facility was operated under the supervision of the California Department of Water Resources (DWR) in order to study the economic feasibility of reclaiming agricultural drainage water. Since DWR is responsible for agricultural water quality management in California, the organic matter interaction with membranes was of sufficient interest to warrant further research.

2. Membrane Processes

Abbé Nollet first cited the osmosis phenomenon in 1748 when he noted that a wineskin made of animal bladder had the ability to separate wine and water. In 1865, Fick proposed his now famous diffusion law for interaction between a solution and a membrane. In 1861, Graham set forth his theory on selective gas diffusion dialysis. Van't Hoff, in 1865, discussed principles of osmosis and proposed the formula for osmotic pressure which bears his name to this day. Traube, in 1864, manufactured the first synthetic membrane from cuprous ferrocyanide ($\text{Cu}_2\text{Fe}(\text{CN})_6$).

Commercial membranes were manufactured as early as 1929 by the Sartorius Werke GmbH in Göttingen, Germany from cellulose nitrate and cellophane for microfiltration and dialysis. Millipore Corporation in the United States started developing bacteriological analysis for membranes in 1945. Besides these two companies, Toagepast Natuurwetenschappelijk Onderzoek in the Netherlands and Ionics Corporation in the United States also developed membranes for electro dialysis (*Belfort, 1987*).

The United States Office of Saline Water Research was the first consolidated effort in the US to provide major funding for synthetic membrane research. Under this organization's guidance, Reid and Breton at the University of Florida manufactured the first RO membrane with good salt rejection and acceptable product water flux in 1959. In the early 1960's, Loeb and Sourirajan perfected the first asymmetric cellulose acetate membrane at the University of California, Los Angeles; this type of membrane is the most common type used for low salinity water desalination in the world today.

Table I (*Lonsdale, 1982*) shows various membrane process characteristics.

Table I: Membrane Separation Processes (from Lonsdale, 1982)

Process	Materials Passed	Driving Force	Materials Retained
Dialysis	Ions and Low Molecular Weight Organics (Urea)	Concentration Difference	Dissolved and Suspended Materials with Molecular Weight >1000 amu
Electrodialysis	Ions	Voltage, Typically 1-2 V/cell Pair	All Non-Ionic and Macromolecular Species
Reverse Osmosis	Water	Pressure Difference, Typically 100-800 psi	Virtually All Suspended and Dissolved Material
Ultrafiltration	Water and Salts	Pressure Difference, Typically 10-100 psi	Biological, Colloids, and Macromolecules, Variable Molecular Weight Cutoffs
Gas Separation	Gas and Vapors	Pressure Difference, Typically 1-100 atm	Membrane-Impermeable Gases and Vapors
Microfiltration	Water and Dissolved Species	Pressure Difference, Typically 10 psi	Suspended Materials (Silica, Bacteria, etc.). Variable Particle Cutoffs

RO (or hyperfiltration as it has been known) is the only membrane process which allows water to pass through without other matter entering the product side. Another difference between RO, ultrafiltration, and microfiltration is that RO operates at a much higher pressure. Therefore energy cost for pumping is a higher consideration for RO systems.

In the 1960's, RO emphasis was primarily on desalination for reclaiming potable water from seawater. More recently, usage for RO has expanded to include such varied applications as reclamation of municipal wastewaters, agricultural drainage, and industrial waters. In all these cases, waters which are reclaimed usually do not meet drinking water standards but meet discharge standards for the environment. RO is also used extensively for high-purity water applications such as producing rinse water for semiconductor chips.

Municipal Wastewater

In recent years, one RO application which has met with a good degree of success is reclamation of wastewater from municipal sources. One example of such an application is the Water Factory 21 Plant located in Orange County, CA. Product water from this plant is injected into the groundwater supply to prevent seawater intrusion into groundwater tables; water from this aquifer serves as a potable water supply for Orange County (*Argo, 1979*).

Feedwater undergoes an elaborate pretreatment scheme before RO treatment. Feed is first coagulated with CaO to produce a lime sludge which is settled out in a clarifier. The water is then fed through a series of ammonia stripping towers followed by recarbonation with CO₂ to lower the pH. Next, mixed media filters remove supracolloidal particles are followed by granular activated carbon adsorbers for organics removal and disinfection using

chlorine. A portion of the water is treated using RO (*Allen, 1979*).

This plant was completed in 1977 at a cost of \$18 million (1977 dollars) and processes a total flow of 15 million gallons per day (MGD). Feedwater for this plant is activated sludge process effluent with a total dissolved solids (TDS) content of 1,100 mg/L. The amount of product from RO process totals 6 MGD with an effluent TDS of 40 mg/L. This effluent is blended with 6 MGD of deep well water and 9 MGD of none-RO treated tertiary water. The blended water has a TDS content of less than 500 mg/L; and conforms to standards set by the state of California (*Potts, 1981*) for drinking water.

Industrial Water

Reverse osmosis membranes have been used for industrial water treatment as well. In 1974, the Toray Company of Japan built a pilot plant to test the feasibility of recovering wastewater from a chemical plant. The plant operated for three years using spiral-wound modules, processing 26,420 gallons per day (gal/d) with a feed water TDS of 700 - 2,000 mg/L and effluent TDS of less than 84 mg/L. RO pretreatment consists of coagulation, sand filtration, precision filtration, chlorination, and addition of scale inhibitors. Feed is passed through a 10 µm filter before entering the RO units. Feedwater quality after pretreatment is 151 mg/L TDS. Flux decreased by 19% in the test period which is within acceptable industry standards (*Kojima, 1977*).

The Swissair Maintenance and Overhaul Base in Zurich, Switzerland uses RO as the final wastewater treatment step. Wastewater is generated from various industrial operations, including plating baths and engine cleaning lines. This plant was started in 1977 and has a capacity of 0.19 MGD. Feed to RO modules has an influent quality of 545 mg/L TDS, and product water quality is

17 mg/L TDS. Product water is reused within the plant (*Potts, 1981*).

Agricultural Drainage Water

The largest example of a RO plant for recovering agricultural drainage water worldwide is at Yuma, AZ. The Yuma Desalting Plant Facility (YDPF) has a design capacity of 72.4 MGD. YDPF services the Wellton-Mohawk irrigation district located at the US-Mexican border. The once pristine Colorado River water at its source has a salinity level of 800 - 1,200 mg/L TDS when it reaches the Mexican border.

Increase in salinity may be attributed to irrigation return flows and numerous reservoirs along the river which increase evaporative surfaces. Excess irrigation water carries minerals such as sodium chloride (NaCl) and calcium sulfate back into the Colorado River. When this water reaches the Mexican farmers, the TDS is of greater than 5,000 mg/L, which prevents its use for agricultural purposes. Under a 1974 agreement with the Mexican government, the US agreed to deliver 1.5 million acre-feet of water with a quality of 115 ± 30 mg/L TDS.

The current anticipated operational date for this facility is in 1991. The plant was originally designed to begin production in 1983, but has been plagued by RO membrane problems. The US government contracted two companies to provide membrane and hardware requirements of this plant. The Fluid Systems Division (FSD) of Universal Oil and Petroleum (UOP) was contracted to provide RO equipment capable of handling 50 MGD; Hydranautics Water Systems (HWS) was contracted to provide for the remaining 22.4 MGD. Initial membrane testing using Wellton-Mohawk drainage water showed much greater than anticipated decrease in membrane performance (*Kaakinen, 1985*).

A schematic for this plant is presented in Figure 1. RO pretreatment at this facility consists of chlorination for disinfection, sedimentation for grit removal, lime and ferric sulfate addition for sludge thickening, dual media filtration for turbidity removal, a clearwell for effluent storage, and finally sulfuric acid and/or sulfur dioxide addition for lowering the pH to meet the membrane manufacturers' requirements (*Applegate, 1984*). Even with the described pretreatment scheme, membrane lifetimes do not meet the manufacturers' guarantees.

RO feedwater analysis revealed trihalomethane (THM's) concentrations to be approximately 120 to 140 $\mu\text{g/L}$. Colloidal matter in the form of various clays, including montmorillonite, kaolinite, and illite was between 0.045 and 0.105 g/m^2 of membrane area, depending on the exposure time. The majority of clays (> 90%) had diameters under 2 μm , which was found to contribute to the majority of membrane colloidal fouling (*Winfield, 1979*). The colloids were estimated to have a high surface area of 250 m^2/g . Calculations performed on the water indicated that clays present are in sufficient quantity to completely cover the membranes between 4.5 to 10.5 times over (*Kaakinen, 1985*).

A possible interaction between the THM's and stable colloids present in the RO feed water was proposed by Kaakinen. He speculated that the presence of THM's may cause colloidal destabilization and therefore membrane performance decline was attributed to some synergistic interaction between the two constituents (*Kaakinen, 1985*). Preliminary tests using the Wellton-Mohawk water indicate the effects of fouling are more severe than if either colloids or THM's alone had been present in the feedwater.

Studies performed at the Los Banos Desalting Facility in Central California's San Joaquin Valley showed evidence that THM's affect membrane

Flow Diagram for Yuma Desalting Plant Facility (from Applegate, 86)

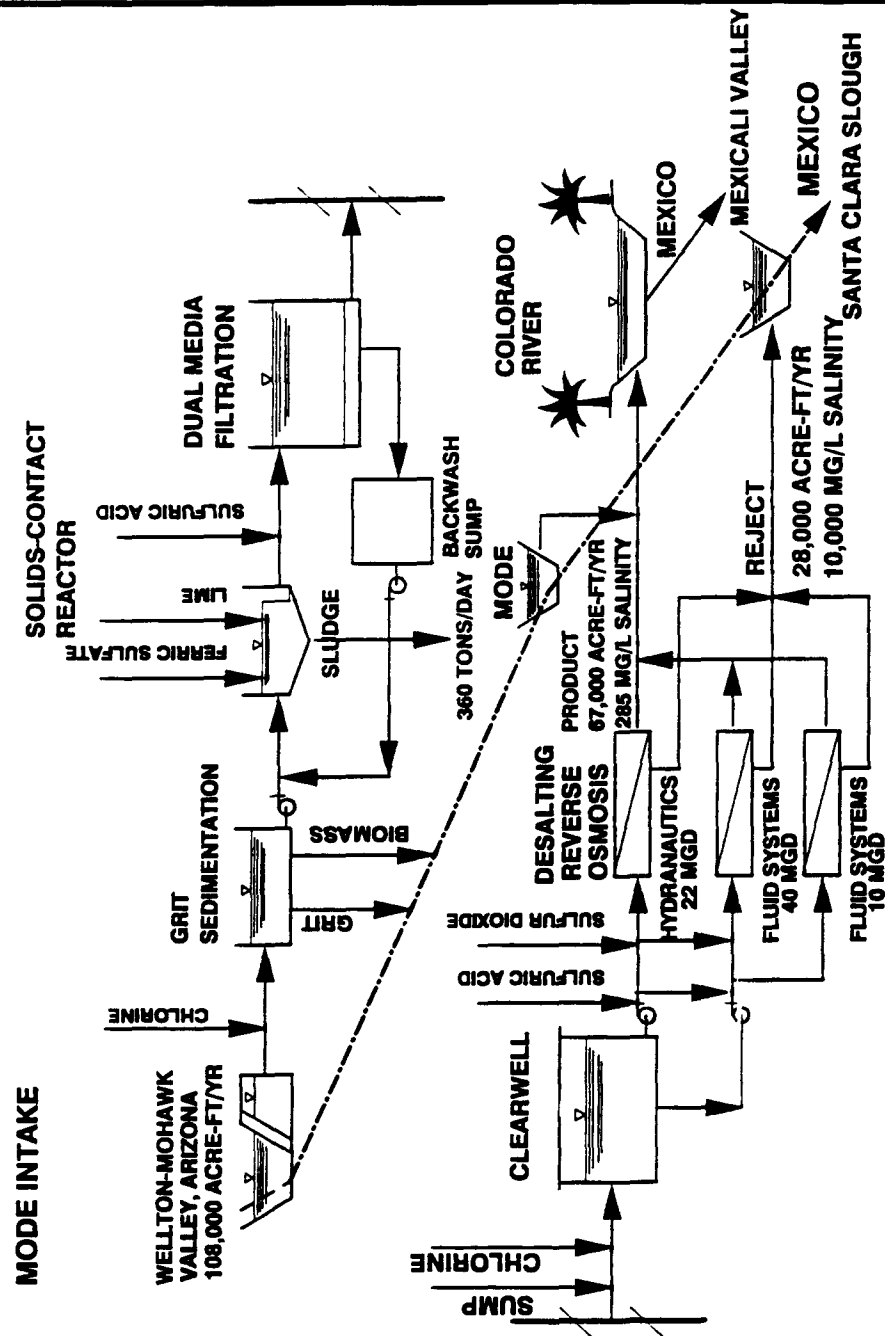


Figure 1: Schematic of Yuma Desalting Plant Facility (from Applegate, 1984)

performance. A demonstration plant was set up at this location to establish the economic feasibility of agricultural water reclamation/reuse. The feed used for this facility comes from tile drainage water produced from overirrigation. The TDS content of this water averaged 9,600 mg/L while the dissolved organic carbon content (DOC) averaged approximately 7.75 mg/L (*Glater, 1989*). These reported values are nearly double the concentration of the Yuma water.

Analysis of the Los Banos tile water reveals a total trihalomethane concentration of 122 µg/L, of which CHBr_3 makes up 44% of the total and CHCl_3 is nonmeasurable (*Wilson, 1988*). Prior to RO treatment, the feed water undergoes pretreatment, including primary chlorination, clarification, dual media filtration, clearwell chlorination, and ion exchange. It was found after the primary chlorination stage THM concentrations increase approximately by 400%.

While the primary focus of Wilson's (1988) study was to analyze the composition of the Los Banos tile water, he also performed a series of preliminary tests on various RO membranes to examine for adverse effects on performance from THM addition. It was found in this testing membrane flux declined faster with the addition of THM's. The THM's were not rejected well by the membranes. Since the initial tests in this area look promising, this study further explores the phenomenon of THM fouling.

3. Membrane Hardware Configurations

Membranes are housed in four different configurations: *tubular*, *spiral-wound*, *hollow fine fiber*, and *flat-plate*. Each of these configurations have inherent advantages and disadvantages and are discussed below.

Tubular Configuration

Figure 2 (*Eisenberg, 1986*) shows the tubular configuration schematic. Material is either coated onto or inserted into the surface of a porous tube. The function of the tube is to provide a support for the delicate membrane. Pressurized feed is introduced from one end of the tube and product water exits through the tube walls. The solute concentrated stream exits through the end of the tube. This configuration was commercially popular during the late 1960's; however, due to the low membrane surface area to membrane volume ratio, and the tendency to foul rapidly, this configuration is not economically feasible.

Spiral-Wound Configuration

Figure 3 (*Eisenberg, 1986*) shows the spiral-wound membrane configuration schematic. Two sheets of membranes with the active layer pointed outwards are glued together with a piece of tricot or nylon membrane spacer separating the two membranes in the center. The space between the membranes is commonly called the tricot product water collection channel. This assembly, "the leaf", has one edge which is not glued together. The membranes at this edge are bent outwards and away from each other. The open edge of the leaf is glued

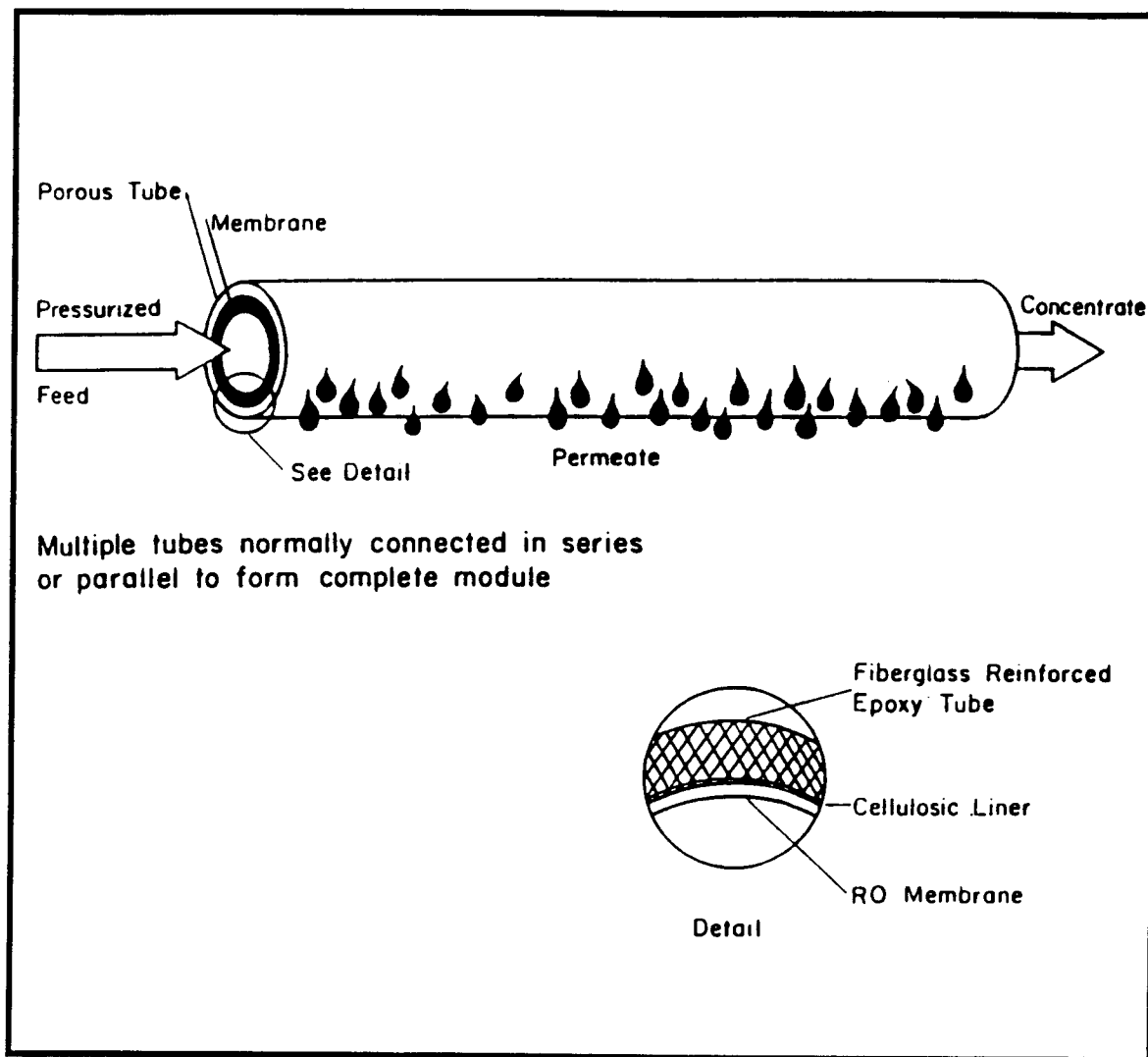


Figure 2: Schematic for Tubular RO Configuration (from Eisenberg, 1986)

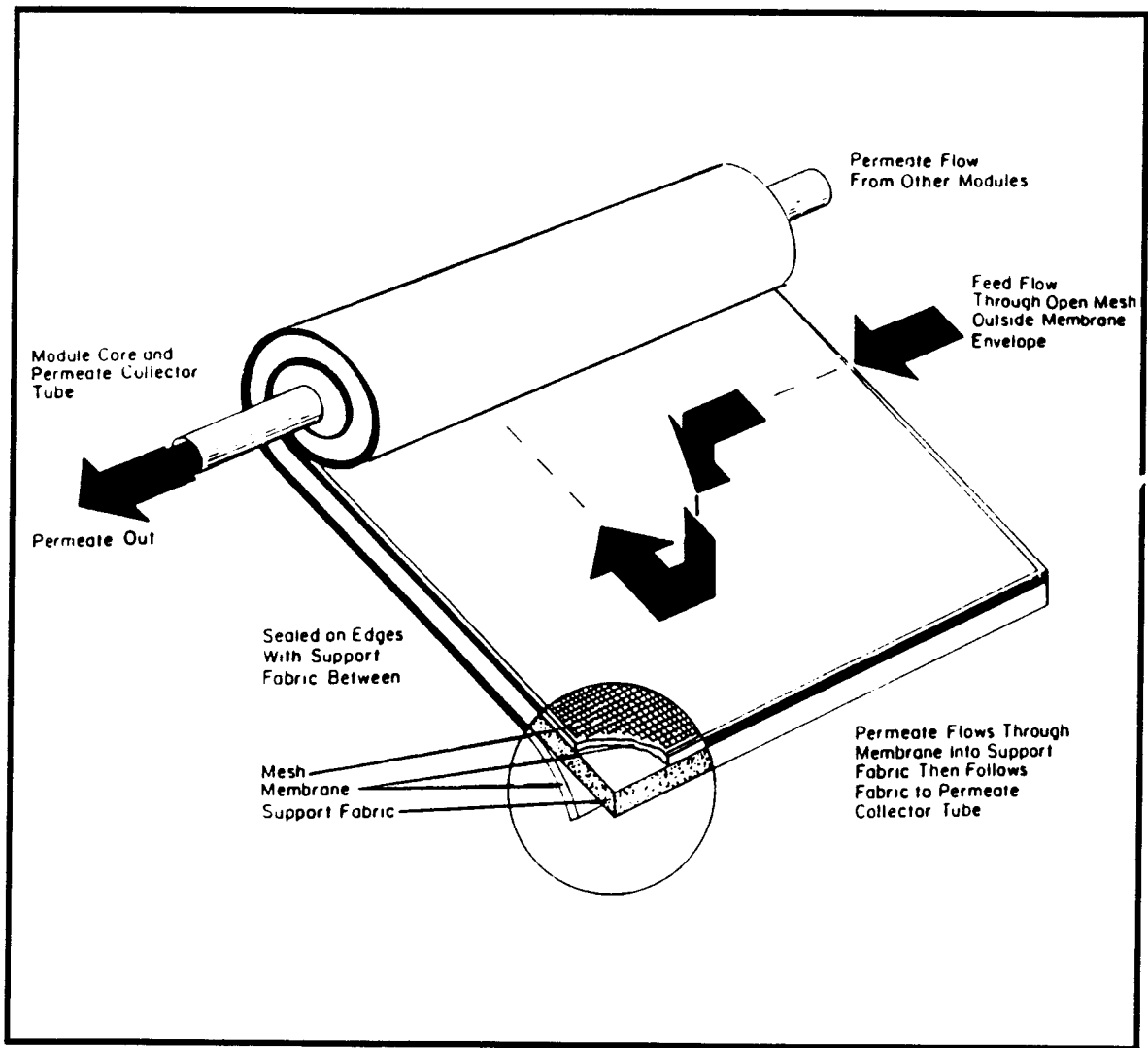


Figure 3: Schematic for Spiral-Wound RO Configuration (from Eisenberg, 1986)

onto a plastic tube with holes predrilled at various locations on the tube. Product water passes through the middle of the leaf via the collection channel into the tube middle. The leaf is wrapped spirally around the tube, hence the name.

In order to allow feed and brine water to pass through this spiral wrap, a plastic netting is placed between each leaf wrap. In this configuration, feed enters one end of the assembly and flows axially with brine exiting the opposite end. A solute concentration gradient is established since brine is more concentrated further down the RO tube. The plastic netting, known as feed-channel spacer, also serves to promote turbulence in the tube and lessens the solute buildup effects on the membrane surface.

A common practice with spiral-wrap membranes is to stagger multiple leaves and glue them onto the product collection tube. In this manner, one may obtain tremendous membrane surface area which is the principal advantage of this configuration. The main disadvantage in this configuration is the difficulty of cleaning. The majority of RO installations in the world presently use this membrane configuration.

Hollow Fine Fibers Configuration

Figure 4 (*Eisenberg, 1986*) shows the hollow fine fiber (HFF) configuration schematic. This design was perfected by DuPont in 1970 with an aromatic polyamide membrane. Asymmetric fibers with an active solute rejecting surface and a hollow core are extruded from a polyamide resin. The fibers have an outer diameter of 85 μm and an inner diameter of 42 μm . As many as 4.5 million of these fibers are bundled together with the product end bonded with an adhesive and the brine end epoxied together into a nub.

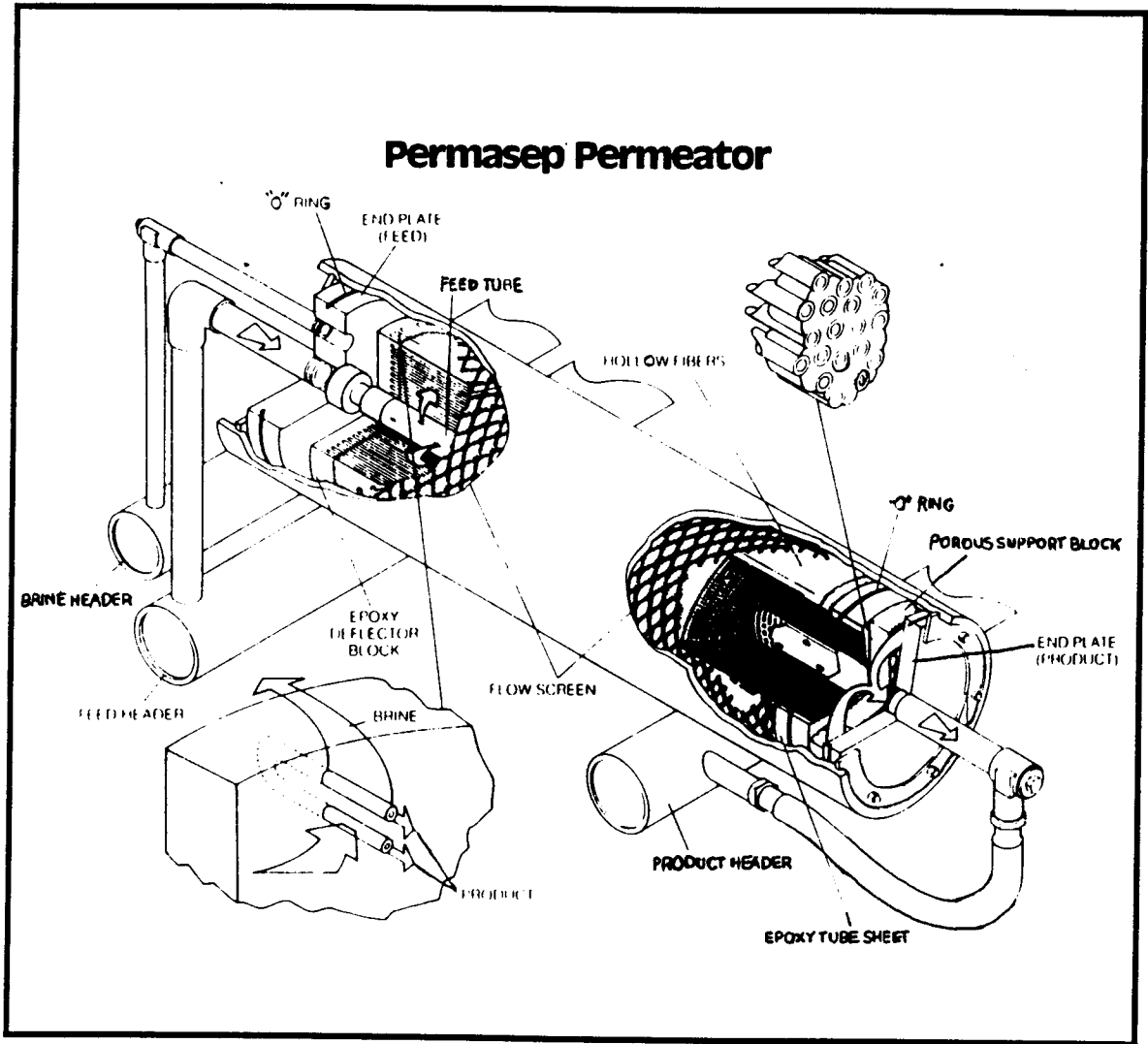


Figure 4: Schematic for Hollow Fine-Fiber RO Configuration (from Eisenberg, 1986)

Feed flows into a plastic center tube to be distributed to the individual fibers. Feed flows radially from the center of the fibers. Product water travels outwards from the fiber and is collected on the outer spaces between individual fibers; brine travels through the center of the fibers and passes out from the assembly (*Applegate, 1984*).

The primary advantage of this membrane assembly configuration is the tremendous surface area. Another advantage of the HFF assembly is the low feed flow rate which is required; this minimizes energy requirements. The disadvantage of this assembly is the difficulty of membrane cleaning. Since individual fibers are so fine, the feedwater pretreatment must be extensive in order to achieve a reasonable membrane life.

Flat-Plate Configuration

Figure 5 (*Eisenberg, 1986*) shows the flat-plate membrane configuration schematic; this is the oldest RO configuration. Two velocities exist in this system, an axial velocity which carries feed and brine across the membrane face and a transmembrane velocity which carries feed through the membrane. Product water flows out the top of the assembly and brine flows out the side opposite from the feed entrance.

The primary advantage to the flat-plate assembly is ease of membrane replacement or cleaning. The primary disadvantage of this configuration is the low membrane surface area. This configuration is not widely used for commercial applications due to its low surface area. The primary use of the flat-plate assembly is for membrane testing and was used in this study.

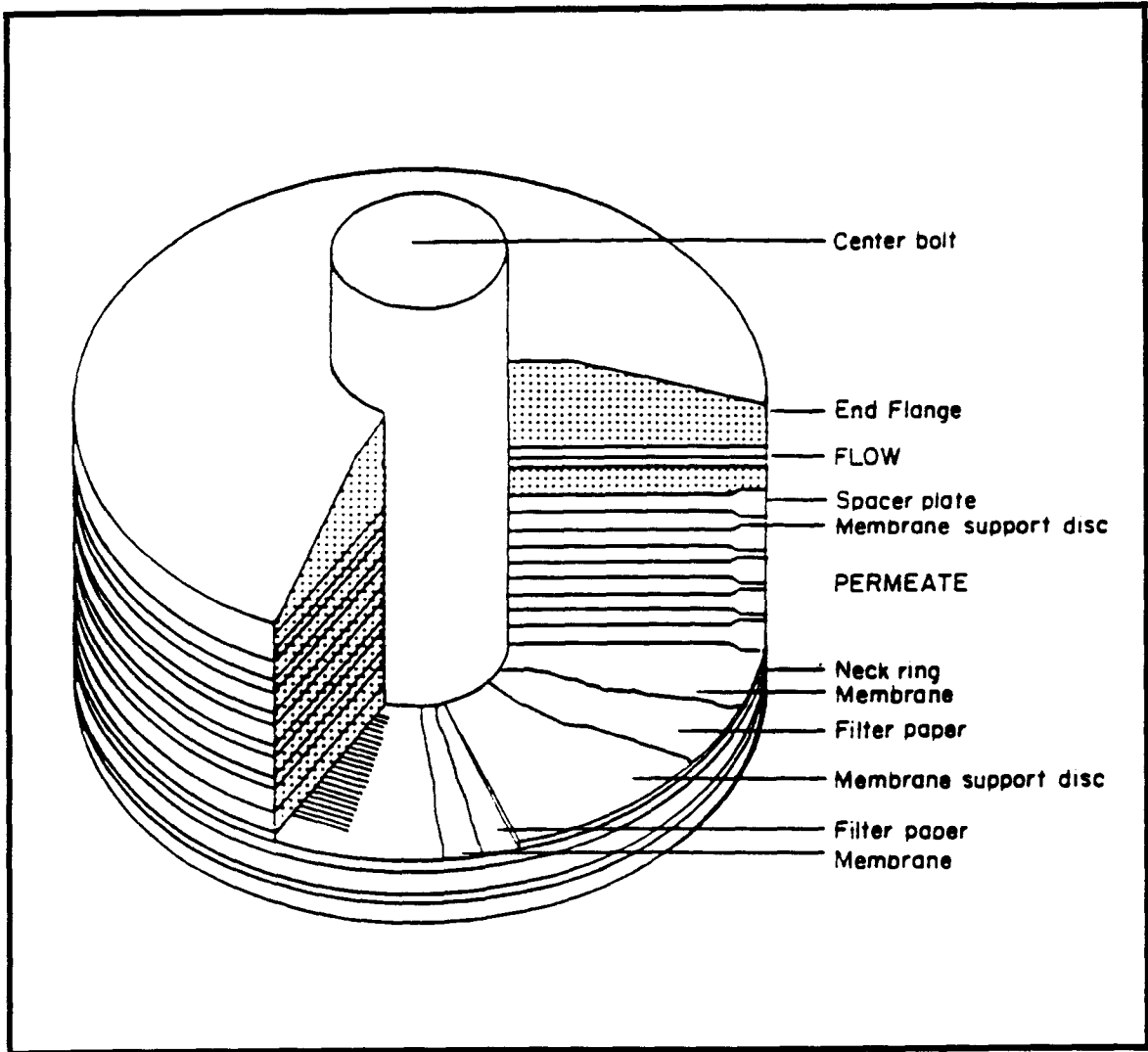


Figure 5: Schematic for Flat-Plate RO Configuration (from Eisenberg, 1986)

4. Membrane Types

Three membrane types are presently in commercial use: *cellulose acetate*, *aromatic polyamide*, and *advanced composite*. Each of these membrane compositions have inherent advantages and disadvantages and not every type of membrane is suitable for every application. Typically, molecular size removal for RO membranes is between 1 to 10 Å which makes its application for demineralization ideal (*Selleck, 1984*). One rule common for product flow is the thinner the membrane, the higher the volume of product output.

In examining material feasibility for RO membranes, two prerequisites appear to be necessary. The materials must contain bonds which bear O and N functional groups, since these groups have been found ideal for hydrogen bonding. Secondly, the materials usually contain five- or six- member rings. These characteristics appear in all of the currently available commercial membranes.

Cellulose Acetate Membranes

Cellulose acetate (CA) is the oldest and most widely used synthetic membrane material available for RO applications. Reid and Breton at the University of Florida synthesized the first cellulose membrane which possessed desalination capabilities in 1959 (*Reid, 1959*). However, product water flux from this membrane was too small to be of any commercial importance. Loeb and Sourirajan at UCLA devised the first functional asymmetric cellulose acetate membrane in 1960 (*Loeb, 1980*). The membrane's asymmetric structure raised solute rejection and product water flux to a level which allowed commercial utilization to be feasible.

A CA membrane is comprised of three layers; a thin, dense *active layer*, a thicker layer known as the *porous substrate*, and a *fabric support*. The purpose of the active layer is to block out dissolved solids, such as salts, in the feed while allowing water to pass through. Typical thickness for this layer is approximately 1 μm . Porous substrate, formed from the same cellulose acetate as the active layer, provides support for the delicate active layer and is typically 5 to 10 μm thick. The fabric support sits on the bottom of this sandwich and is approximately 89 to 96 μm thick. This support may be composed of either fabric or paper.

Formulation for CA membranes is depicted in Figure 6 (*Kesting, 1977*). Many attempts were carried out before a membrane with high rejection and flux was found. CA membrane performance depends on three factors: *nature of casting solution, evaporation time, and curing temperature*. The casting solution is dependent on type of CA used, acetone percentage, and type and percentage of swelling agent used.

CA is made from a solution of cellulose, acetic anhydride, acetic acid, and sulfuric acid. Cellulose is acetylated by the addition of acetic anhydride under these conditions (*Malm, 1971*). The completely acetylated product is known as cellulose triacetate (CTA) and has three acetate groups substituted for the hydroxyl groups on the cellulose unit. CTA is a sparingly soluble polymer and is deacetylated by water to form cellulose diacetate (CDA). The CA that is used in membrane casting solutions is a blend of CTA and CDA.

The degree of substitution on cellulose may range from zero to three, depending on the number of hydroxyl groups which are replaced by acetate subunits. Varying this parameter yields very different membrane performance. One trend which has been noted in cellulose processing is the higher the

Formation of Cellulose Acetate

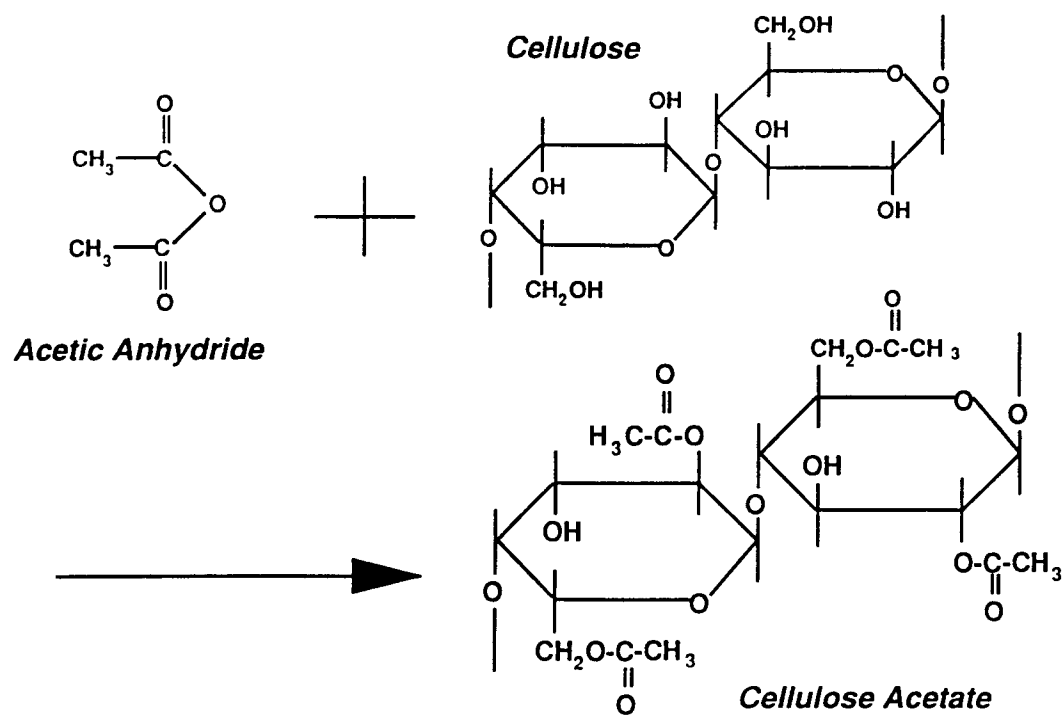


Figure 6: Formation of Cellulose Acetate (from Kesting, 1977)

degree of substitution, the more ordered or crystalline the polymer structure becomes. A degree of substitution of three (CTA) causes an increase in rejection of sodium chloride (NaCl) salts and a decrease in product flux. The lack of hydroxy groups on cellulose is one possible reason for causing poor product water flux in CTA. Hydroxy groups enable hydrogen bonding to occur which facilitates transport of water molecules through the membrane. Zero substitution (pure cellulose) yields a high product flux but poor NaCl rejection. Most of the CA's used in casting solutions for membranes have a degree of substitution of 2.4 to 2.5. This enables the membrane to have good rejection characteristics of CTA and good product flow characteristics of CDA (*Kesting, 1977*).

Acetone in the casting solution allows evaporation of excess water from deacetylation and hydrolysis of CTA and controls the degree of swelling achieved from addition of swelling agents. The swelling agent used in CA processing is usually magnesium perchlorate or formamide. The function of these agents is to increase membrane water content which correlates positively with product permeability as well as to produce proper pore sizes for product water transport through the membrane (*Kesting, 1977*). Too much swelling agent in the casting solution will cause larger membrane voids, which results in a membrane skin too thin to maintain structural integrity. To yield a membrane with good flux and rejection characteristics, a careful balance must be maintained among CA, acetone, and swelling agent used in casting.

Evaporation time and curing temperature are also important factors for establishing proper flow and rejection characteristics. Increasing both time and temperature result in "tighter" membranes, that is, membranes which have good rejection but poor flux characteristics. Water is driven out of the membrane

structure by both these methods, and in doing so, decreases membrane permeability.

CA membranes are currently the most popular membrane types, and may be formed into flat-plate, tubular, HFF, or most commonly, spiral wound configurations. They have favorable rejection and flux performance characteristics for lower salinity waters but are unsuitable for seawater applications. CA may be used under pH conditions from 3 to 8, operating pressures from 400 to 600 psi, and operating temperatures from 32 to 104 °F. CA withstands exposure to free chlorine resulting from disinfection much better than other membrane types. However, CA is subjected to hydrolysis at high pH (basic conditions) or when it is exposed to ozone. CA is also susceptible to bacteriological attacks.

Aromatic Polyamide Membranes

DuPont introduced their version of the aromatic polyamide (PA) membrane in 1975. The structure is presented in Figure 7 (*Petersen, 1986*). This membrane has the ability to form crosslinked hydrogen bonds between different chains. This crosslinking yields a more rigid membrane than CA, and for this reason less pressure compaction is likely to occur. Also, this crosslinking leads to higher product flow and enhances the membrane's ability to withstand biological and chemical attacks.

PA membranes are made from reacting diacid chloride with *m*-phenylenediamine. Products formed from this reaction are polyamides and hydrochloric acid. This polymer is formed in the same manner as CA membranes. Fifteen parts of polyamide are added to 85 parts of *N,N*-dimethyl formamide with slats to create pores in the membrane (*Sundet, 1983*). The

Formation of Polyamide

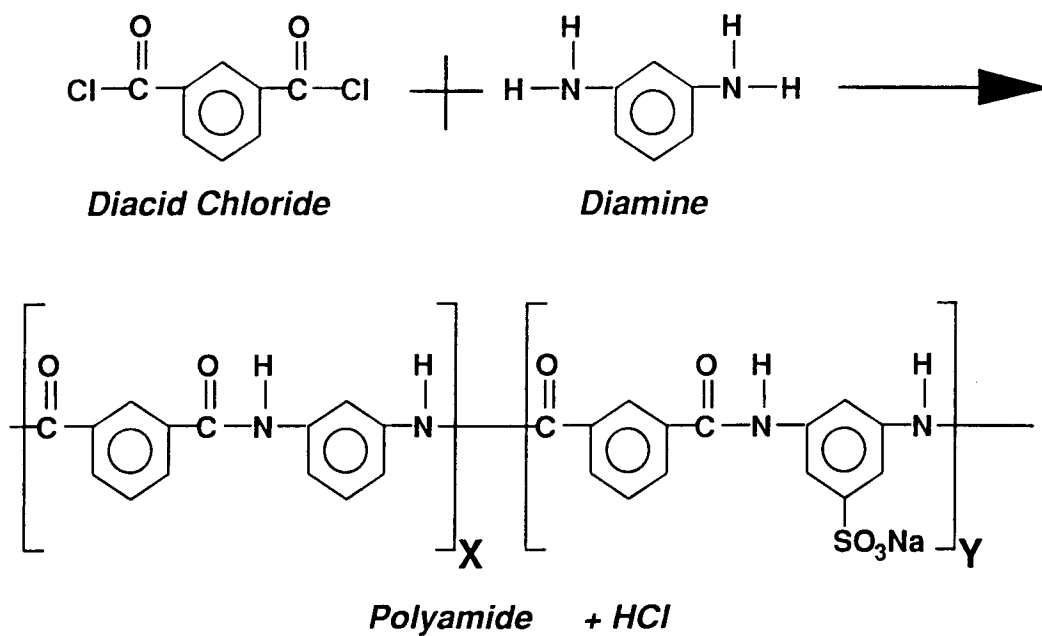


Figure 7: Formation of Polyamide (from Petersen, 1986)

solution is filtered through a 5 μm filter and the filtrate is cast onto clean glass at 100 $^{\circ}\text{C}$. The membrane is dried and extracted in quench water for one hour. Afterwards, the membrane is annealed in 55 $^{\circ}\text{C}$ water for 30 minutes.

PA membranes may be found in flat-plate, spiral wound, or HFF configurations. Its active layer may be as thin as 0.1 μm which makes PA ten times thinner than cellulose acetate and allows more water to be passed through with the same pressure. PA membranes may be used at pressures varying from 350 to 400 psi and at temperatures from 32 to 104 $^{\circ}\text{F}$. The HFF configuration is widely used for demineralizing seawater. PA membranes are also used for other applications such as municipal and industrial water treatment since they are resistant to changes in feedwater conditions.

Composite Membranes

Fluid Systems Division of Universal Oil and Petroleum is the first company credited with the manufacture of a thin film composite membrane which was not formed out of cellulose (*Petersen, 1986*). Since their development, various polymer membranes have been formed and installed for demineralization purposes. DuPont manufactures a composite membrane dubbed the advanced composite (AC) membrane to improve upon cellulose acetate properties.

The formation of AC membrane is depicted in Figure 8 (*Pohland, 1989; Sundet, 1987*) This membrane is formed from aliphatic 1,3,5-cyclohexane tricarbonyl chloride (HT) and aromatic m-phenylene diamine (MPD) via interfacial polycondensation. In interfacial polycondensation, reactants are contacted at an interface; the active layer for the membrane forms here. Another membrane is formed from reacting aromatic 1,3,5-benzyltricarbonyl chloride with MPD to yield a fully aromatic membrane. The aliphatic/aromatic

Formation of DuPont ACM

(from Pohland, 1988)

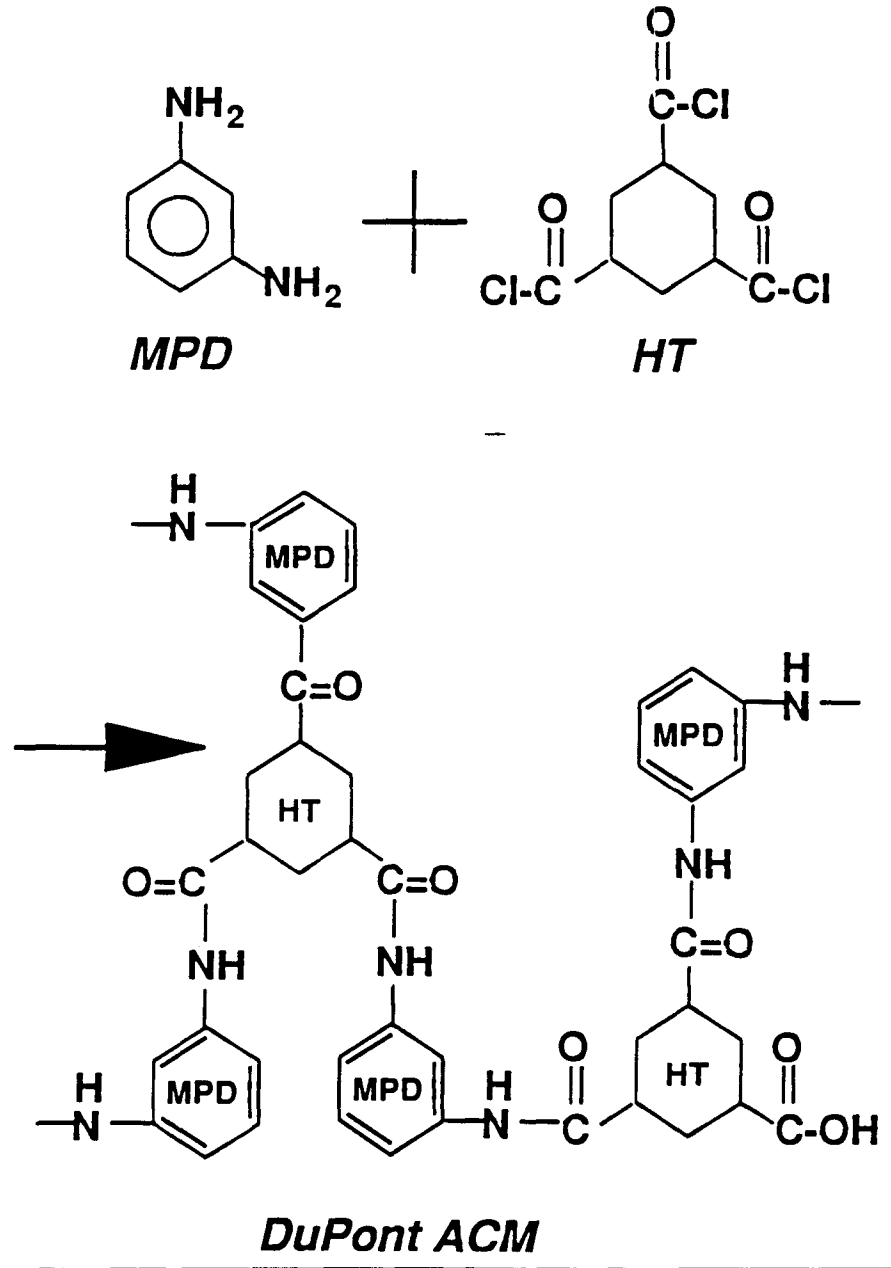


Figure 8: Formation of DuPont's ACM (from Pohland, 1988)

configuration yields a membrane which has better flow and rejection characteristics as well as higher durability than the fully aromatic version. This membrane is structurally stronger than aromatic membranes since it contains more hydrogen bonds (*Pohland, 1989*).

Composite membranes are composed of four layers. The active layer, composed of HT/MPD, is between 250 to 500 Å thick or nearly 20 to 40 times thinner than the average CA active layer. The thinness of this layer offers much less resistance to water transport than CA membranes, therefore, higher product fluxes are attainable with ACM than CA. The second layer in this membrane is known as the intermediate transport layer. This colloidal gel-like layer is composed of polyether/polyamide blend and offers a support for the active layer. The next layer in this sandwich is the porous support layer which may be formed of polysulfone. On the bottom of the membrane is fabric which provides further support for the sandwich.

ACM has distinct advantages over cellulose acetate membranes in almost every area. ACM may tolerate a wider range of operating conditions than CA membranes. Whereas CA membranes are used in the pH region between 3 to 8, ACM may tolerate pH levels ranging from 1 to 11. ACM may be used at pressures between 150 to 600 psi and temperatures between 32 to 115 °F. Unlike CA, ACM is not subject to hydrolytic attacks which may severely reduce membrane life. ACM also has a thinner active layer than CA which translates to higher product fluxes at the same operating pressure. ACM is also resistant to biological attacks which presents a problem for CA. Since ACM has a higher degree of cross-linking than CA, this membrane is also more resistant to pressure compaction effects.

Summary

Table II summarizes the important characteristics of the three membrane types discussed in this chapter. The main advantage of AC membrane is its operational range which is wider than CA and PA. AC membrane has fully cross-linked bonds, extending into three dimensions, which allows it to retain its structure better under pressure than other membranes. The main advantage of CA over ACM is in its ability to withstand the effects from free chlorine. Another advantage of CA over ACM is cost; CA is less expensive than AC membrane. PA's physical and operational characteristics are between CA's and ACM's; its cost is also between CA and ACM.

Table II: Comparison of CA, PA, and AC Membrane Properties

Membrane Type	Active Layer (μm)	Active Layer Material	Cross-Linking	pH Range	Temp Range ($^{\circ}\text{F}$)	Pressure Range (psi)
CA	1.0	Cellulose Acetate	None	3 - 8	32 - 104	400 - 600
PA	0.1 - 1.0	Aromatic Polyamide	Partial (2D)	4 - 10	32 - 104	350 - 400
ACM	0.05 - 0.2	HT/MPD	Full (3D)	1 - 11	32 - 115	150 - 600

5. Modeling Membrane Performance

Since the discovery of cellulose acetate membranes, scientists and engineers have attempted to characterize membrane performance to predict the useful life based on flux and rejection. Two sets of equations seem to work best for quantifying membrane performance. The first set, containing Equations 1 and 2, known as Merten's equations, applies only to steady state conditions. Merten's (1967) equations are useful for comparing different membranes' performances at steady state. High water transport coefficients (A) and low solute transport coefficients (B) are desirable since high A's are associated with high water fluxes and low B's are associated with high percent TDS rejections. Equation 3 is a modified form of Van't Hoff's equation used to predict osmotic pressure.

$$J_w = A(\Delta P - \Delta\pi) \quad (1)$$

$$J_s = B(\Delta C) \quad (2)$$

$$\Delta\pi = \frac{(\Delta C)RT}{MW} \quad (3)$$

$$\Delta C = C_f - C_p \quad (4)$$

where

A	=	water transport coefficient (gal/ft ² -day-psi)
B	=	solute transport coefficient (ft/day)
C _f	=	feed concentration (mg/L)
C _p	=	product concentration (mg/L)
J _s	=	solute flux (lb/day)
J _w	=	water flux (gal/ft ² -day (GFD))
MW	=	molecular weight of solute (g/mol)
R	=	universal gas constant (0.0821 L-atm/mol-K)
T	=	temperature (K)
ΔC	=	concentration difference (mg/L)
ΔP	=	operating pressure (psi)
Δπ	=	osmotic pressure difference (psi)

The second set of equations was also coined by Merten, modified by Wechsler (1977) and applied to unsteady state conditions.

$$F_t = Kt^m \quad (5)$$

Upon integration, this equation is transformed from,

$$\int_0^Q F_t = \int_0^t Kt^m$$

to the following form,

$$Q = \frac{K}{m + 1} (t^{m+1} - t_o^{m+1}) \quad (6)$$

where

- F_t = water flux at any time t (gal/ft²-day)
- K = membrane constant (gal/ft²-day)
- m = log-log flux decline index (unitless)
- Q = amount of permeate per unit area membrane (gal/ft²)
- t = time (days)
- t_0 = initial time (days)

Assuming t_0 be 0 and taking logs of both sides of the equation, the following expression is obtained.

$$\log Q = \log\left(\frac{K}{m+1}\right) + (m+1) \log(t) \quad (7)$$

If $\log Q$ vs. $\log t$ is plotted, the slope is $m+1$ and the intercept is $\log\left(\frac{K}{m+1}\right)$. From these, m and K are estimated easily. Wechsler (*Wechsler, 1977*) states this equation is only valid in periods between membrane cleanings; however, some authors have overlooked this limitation. Since the log-log flux decline index m is negative, it is desirable for this parameter to be as small as possible in order to extend the useful membrane life. It is also desirable for the membrane constant K to be as high as possible for high permeate fluxes.

Another useful parameter for membrane performance characterization is percent rejection. Percent rejection is defined as follows.

$$\% R = \left(\frac{C_f - C_p}{C_f}\right) \times 100 \% = \left(1 - \frac{C_p}{C_f}\right) \times 100 \% \quad (8)$$

where

$$\begin{aligned} C_f &= \text{feed concentration (mg/L)} \\ C_p &= \text{product concentration (mg/L)} \end{aligned}$$

It is desirable for a membrane to have a high percent rejection since this determines permeate quality. In this study, Equation 8 is used to calculate TDS and halocarbon percent rejections.

A parameter which gives an indication of RO efficiency is known as percent recovery or conversion.

$$Y = \frac{Q_p}{Q_f} \times 100\% = \frac{V_p}{V_f} \times 100\% \quad (9)$$

where

$$\begin{aligned} Q_f &= \text{feed water flowrate (gal/day)} \\ Q_p &= \text{product water flowrate (gal/day)} \\ V_f &= \text{feed water volume (gal)} \\ V_p &= \text{product water volume (gal)} \\ Y &= \text{\% conversion or recovery} \end{aligned}$$

High Y values reflect higher efficiency and more water is recovered than at lower Y values. One common problem when operating at high Y values is concentration polarization. Concentration polarization is a buildup of solutes on the membrane surface. Solutes at the membrane surface are usually swept away by the reject or brine water. In a case of high Y's, there is very little reject water to sweep solutes from the membrane surface. This deposition presents a hindrance to product water flow.

An important factor in determining membrane life is the degree of feedwater

pretreatment. Although there is no total agreement within the industry, the most widely accepted empirical test performed on waters presently is the silt index test (SDI) described in a DuPont bulletin (*DuPont, 1982*). In this test, one runs a stream of water at a pressure of greater than 40 psig through a pressure regulator set precisely at 30 psig. This water is passed through a 0.45 μm Millipore[®] filter. One measures the time required to collect a 500 mL sample initially and another 500 mL sample at 15 minutes after test startup. In operations involving RO, feed SDI is usually taken after water has been subjected to clarification. The SDI is defined as:

$$SDI = \frac{\% P_{30}}{t_f} = 100 \times \frac{\left(1 - \frac{t_i}{t_f}\right)}{t_t} \quad (10)$$

where

- P_{30} = percent plugging at 30 psig feed pressure
- t_f = final time, in seconds, required to collect 500 mL sample after test time t_t (usually 15 minutes)
- t_i = initial time, in seconds, required to collect 500 mL sample
- t_t = total time in minutes (usually 15, but may be less if 75 percent plugging in less in 15 minutes)

Equation 10 is used to determine adequacy of water pretreatment. An SDI reading of 1 indicates a very high purity water which needs no pretreatment. Surface waters have SDI values of 10 to 175 which may be attributed to colloidal suspensions. A positive correlation exists between SDI values and a water's fouling tendencies; the higher the SDI of a water, the shorter lifespan one may expect for a membrane. Most manufacturers guarantee their

membranes' lifetimes at prescribed SDI levels for the feedwater.

Although SDI is a widely used parameter in the membrane and its associated industries as the indicator of a feed water's quality, there are still some problems with this test. Since the pore size of the filter used in SDI testing is 0.45 μm , any fouling attributable to particles less than this size is not detected. The problems at Yuma stress this point since colloidal particles, which are suspected to be a major source of fouling, are between 10 Å and 1 μm in size and may easily pass through this filter. Another potential foulant which the SDI test does not detect is the presence of organic matter which may foul the membrane.

A parameter which may be helpful in determining the attraction of organic compounds to a membrane is known as the *partition coefficient* described by Equation 11 (Pusch, 1976).

$$K_s = \left(\frac{\text{mol organic}}{\text{kg wet membrane}} \right) / \left(\frac{\text{mol organic}}{\text{kg solution}} \right) \quad (11)$$

where

K_s = organic distribution coefficient (unitless)

K_s is very similar to K_{ow} , the octanol-water coefficient with one difference. Whereas K_{ow} measures the ratio of the affinity of an organic matter for octanol and for water at equilibrium, K_s quantifies the distribution of organics between the membrane phase and the solution phase at steady state. K_s values less than 1 indicate the organic compound prefers the solution phase while K_s values greater than 1 indicate the organic prefers the membrane phase. K_s values of 1 indicate equimolar distribution of the organic between solution and

membrane phases.

Pusch found phenol prefers the membrane phase to the solution phase with K_s values ranging from 10 to 40 for different types of CA membranes at 25 °C and pH of approximately 7. The large amounts of phenol sorbed by the membranes displaced the water in their structure and thus altered the membrane's performance characteristics. Pusch also discovered the phenol-membrane interactions were irreversible. K_s indicates the degree of interaction between organics and a membrane and may provide indications of how membrane performance characteristics are affected by organic addition.

Another parameter of interest in membrane research is a quantity known as *membrane void fraction*, ϵ_v . This quantity relates the volume of voids to the volume of the entire membrane and is described by Equations 12 and 13 (Pintauro, 1980).

$$\epsilon_v = \frac{\Delta V}{1 + \Delta V} \quad (12)$$

and

$$\Delta V = \frac{\rho_d(w_w - w_d)}{\rho_e w_d} \quad (13)$$

where

- w_d = weight of dry membrane (g)
- w_w = weight of wet membrane (g)
- ρ_d = density of dry membrane (g/cm³)
- ρ_e = density of solution (g/cm³)
- ϵ_v = membrane void fraction (unitless)
- ΔV = change in volume (cm³)

This parameter may also be thought of as the ratio of void volume to membrane volume. If total membrane volume remains relatively constant over the course of an experiment, then any changes in ϵ may be attributed to changes in void volume. In this case, ϵ quantifies the changes in the membrane void volume. Decreases in ϵ indicate decrease in the membrane void volume while increases in ϵ indicate increase in the membrane void volume.

6. Membrane-Chemical Interactions

Membranes may experience two classes of interactions with chemicals during time of operation: *degradation*, *fouling*, and *permeation*. Membrane degradation is often a relatively fast, irreversible phenomenon while membrane fouling occurs over longer periods of time and may be reversible or irreversible. Another difference between degradation and fouling is how the product flux and quality are affected. Flux increases and quality decreases over time for membrane degradation; flux decreases and quality may remain the same or increase for membrane fouling. In permeation, the chemicals pass through the membrane without any chemical interactions.

Membrane Degradation

Membrane degradation involves polymer changes and the effect is usually irreversible. Degradation is caused by chemicals which may break membrane structural bonds. For example, strong acids may cause CA membrane hydrolysis and revert it back to the cellulose form. Cellulose allows both water and solutes to pass through indiscriminately.

Bacterial attacks may also degrade CA membranes. Microbes attach to membrane surfaces and metabolize acetyl groups; with this accomplished, microbes attack cellulose chains, thus breaking membrane bonds and allowing excess water and solutes to pass through the membrane (*Lepore, 1988*). Substrates for bacterial growth are often found in RO feedwaters.

Composite membranes are less susceptible to acid or microbial attacks; nevertheless they may be degraded when exposed to halides such as bromide (Br^-) or chloride (Cl^-). In one study (*Glater, 1981*) benzanilide, used as a model

for DuPont's B-9 aromatic polyamide membrane, was placed into a solution of 6,000 mg Br⁻/L and soaked for 260 hours. Infrared analysis revealed halide uptake and halogen substitution into the aromatic ring structure. Halogen substitution disrupts polymeric intermolecular hydrogen bonding and allows more solutes and water to pass through. This process is irreversible and membrane replacement is required to restore efficiency.

Membrane Fouling

Fouling is the most common problem in membrane process operations. Although there are various definitions of fouling, one of the best found in the literature is by Eykamp(1976).

Fouling is a condition in which a membrane undergoes plugging or coating by some element in the stream being treated, in such a way that its output or flux is reduced and in such a way that the foulant is not in dynamic equilibrium with the stream being ultrafiltrated. In another words, something has occurred that makes the microenvironment near the membrane a nonsteady state situation.

Although there are a variety of foulants, Potts(1981) classifies foulants in four broad categories, 1) slightly soluble inorganics such as salts from calcium or sodium, 2) colloidal or particulate matter, 3) dissolved organic compounds, and 4) biological foulants.

Inorganic Foulants

Potts classifies inorganic foulants as commonly including Ca⁺², Mg⁺², CO₃⁻², SO₄⁻², silica, and iron. The degree of fouling from these inorganics worsens as

percentage recovery increases. Under these circumstances, more water is passed through the membrane which increases inorganic concentration on the feed side. Above a critical concentration, solubility limit for inorganic salts may be exceeded which will result in precipitation, which is commonly known as scaling. Scale formation greatly reduces water transport through the membrane. Besik(1972) and Wechsler(1977) noted these inorganic foulants become a serious problem at recovery levels exceeding 90 - 95%. In a recent study (Allegrezza, 1988) of operating practices at some commercial RO facilities, 10% recovery is a satisfactory guideline used for the prevention of this type of fouling from occurring. In this study, our recovery level is less than 10% so scale formation is not expected to be a problem.

Particulate Foulants

Particulate foulants in water may either be organic or inorganic and vary in size and shape. Cruver (1973) states common inorganic particulates in water are composed of iron, aluminum, and silica with aluminum silicate clays (d_p of 0.3 - 1 μm) being the most ubiquitous. In this case, silica fits into both inorganic and particulate foulant categories.

There is much disagreement among authors on the classification of different sizes of particles which exist in waters. Rudolfs (1952) arrived at the following scheme for classification.

<u>Classification</u>	<u>Size Ranges</u>
Settleable solids	> 100 μm
Supra-colloidal solids	1 μm - 100 μm
Colloidal solids	10 \AA - 1 μm
Dissolved solids	< 10 \AA

Although waters vary from source to source, Rickert and Hunter(1967) found dissolved solids constituted 69% of the total solids in municipal wastewaters. Some researchers have hypothesized colloidal and dissolved solids fractions make the largest contributions to particulate fouling. Winfield(1979) noted removal of particles larger than 5 μm did not decrease membrane fouling and theorized larger particles do not significantly affect fouling since they are carried away by convection. Sugahara(1979) concluded particles less than 45 Å tended to foul membranes more than ones larger than 45 Å.

Dissolved Organic Foulants

In this study dissolved organics are the foulant type which are of the most interest. Organic particulates may be composed of larger constituents such as bacteria or smaller constituents such as humic acids and carbohydrates. Humic acids may further be cleaved or functional groups may break off as a result of exposure to various halogens such as Br^- and Cl^- to form CHBr_3 , CHCl_3 , and various intermediates. These organics are known as trihalomethanes (THM's), and are purgeable and therefore detectable by purge and trap gas chromatography (GC) analysis. Potts(1982) noted dissolved organics together with colloids contribute most to membrane fouling since they are the hardest to remove during pretreatment. Wojcik(1980) noted THM's and phenols present no fouling problems since they permeate easily through the membrane and should not cause any blockage of membrane pores.

Biological Foulants

Biological fouling is caused by viruses or live or dead bacterial cells. This fouling may occur on the membrane surface or in the pores; typical thicknesses for the bacterially-fouled layer is on the order of 10 to 20 μm (Lepore, 1988). Cellulose acetate membranes were found to be the most susceptible to fouling by bacteria and fouling effects increased as the SDI increased (Arora, 1983).

Bacterial growth patterns on CA membranes were established by Ridgway(1985) in tests conducted at the Water Factory 21 Treatment Plant in Orange County, CA. *Mycobacterium* dominated bacterial growth for the initial five week period, followed by a wide variety of bacterial growth including *Acinetobacter*, *Pseudomonas*, and *Flavobacterium*. Longer growth periods revealed presence of *Moraxella*, *Klebsiella*, *Alcaligenes*, and *Shigella*. Optimum pH conditions for growth were observed at between 6 and 6.5. This pH range is also favorable for prevention of CA hydrolysis.

Fouling Effects

In membrane fouling the most recognizable effect is a decline in product flux over time. The reason for this arises from buildup of a foulant layer on the membrane surface or from membrane pore pluggage. Fouling may either be reversible or irreversible. Reversible fouling is characterized by partial or full recovery of product water flux through cleaning. Cleaning procedures include chemical addition, backflushing, or sponge-ball cleaning depending on membrane configuration and its ability to withstand chemical addition. By definition, membrane performance recovery is not possible with irreversible fouling.

Plasticization is another cause for decrease in membrane performance. In plasticization, the addition of certain organics, e.g. phenol, will cause the CA membrane to soften and subsequently harden, reducing product water flux. This effect is reversible at low phenol concentrations; at higher phenol concentrations, asymmetry loss is permanent and the effect is irreversible (Andersen, 1981).

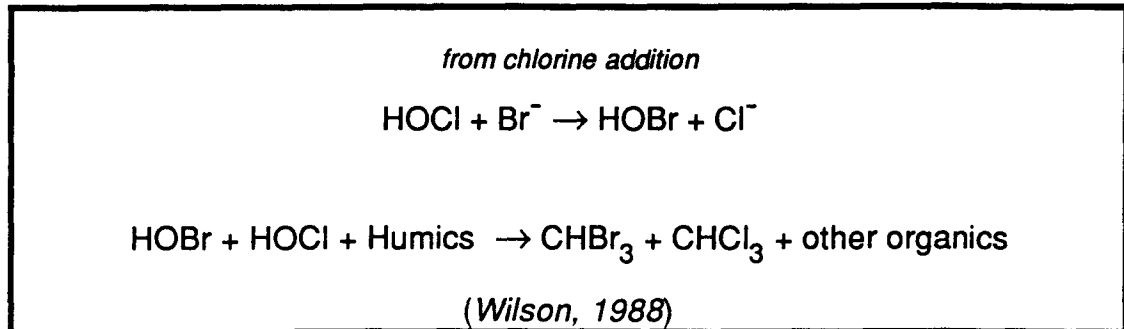
Membrane Permeation

Chemical permeation through membranes is a three step process; *surface adsorption, membrane absorption, and desorption*. In surface adsorption, the chemicals attach themselves to available spaces on the membrane surface. In membrane absorption, the chemicals permeate into the membrane structure but no chemical bonds result. In desorption, the chemicals which were absorbed are transported out of the membrane to the other side. Throughout the permeation process, no chemical bonds are formed.

Trace Organics in Wastewaters

Trihalomethanes (THMs) are one class of organics which have come under close scrutiny by the U.S. Environmental Protection Agency (USEPA). THMs are methanes substituted with three halogens which are formed through reactions with humic acids commonly found in natural bodies of water. Humic acids result from decomposition byproducts of organic matter, such as vegetation. When humics react with bromide, which is also found naturally in water, the result is various methanes substituted with Br. Only tribrominated methane (CHBr_3) is considered a THM. Another source of THMs is the reaction

of chlorine with humic acids during disinfection. Chloroform (CHCl_3) is one byproduct of this reaction and also a THM. Various other brominated and chlorinated methanes, i.e. CHBr_2Cl , CHBrCl_2 , are also THMs.



In 1974, THM's were reported in drinking water and on November 29, 1979, the USEPA passed regulations limiting levels in drinking water to 0.1 mg/L total THM concentration. THMs are the most common organic chemicals found in drinking water and occur at the highest levels. The National Academy of Sciences (NAS) state prolonged exposure to THM's would impose an added health risk to the general population. Although evidence is not conclusive in humans, chloroform is a carcinogen to rats and mice and NAS recommended its regulation in drinking water. During passage of this regulation, a clear and distinct line had not been drawn between effects of chloroform and other THM's on laboratory rats and mice. Hence it was decided to place an overall limit on all THMs. The figure of 0.1 mg/L THM's was decided on not because it was the safe limit for humans but because it achieved a reasonable balance between water treatment economics and health safety (*Cotruvo, 1981*). Some of the halocarbon properties used in this research are listed in Table III (*Weast, 1989*).

Table III: Selected Properties of Halocarbons Used in This Study
(from Weast, 1989)

Type	Solubility (mg/L)	Density (g/mL)	M.W. (amu)	Dipole Moment (debye)	Dielectric Constant ϵ (C/V-m)	Diameter (Å)
CCl ₄	800	1.594	153.84	0	2.228	6.70
CHBr ₃	100	2.890	252.77	0.99	4.390	5.54
CHCl ₃	8200	1.489	119.39	1.02	4.806	5.14

Researchers have examined rejection of various inorganics and organics by RO membranes. Several generalizations are listed in Table IV. Factors 1 and 3 apply mostly to organic rejection while 2 and 4 apply more towards inorganic solute rejections.

Another factor which may be related to percent rejection of organic molecules is the *dielectric constant*. Dielectric constant is defined by the following relationships for two point charges Q and Q' at a distance r apart.

$$F = \frac{Q'Q''}{\epsilon r^2} \quad (14)$$

where

- F = force of attraction between two charges (N)
- Q' = charge of one body (C)
- Q'' = charge of one body (C)
- r = distance between charges (m)
- ϵ = dielectric constant of medium (C/V-cm)

and

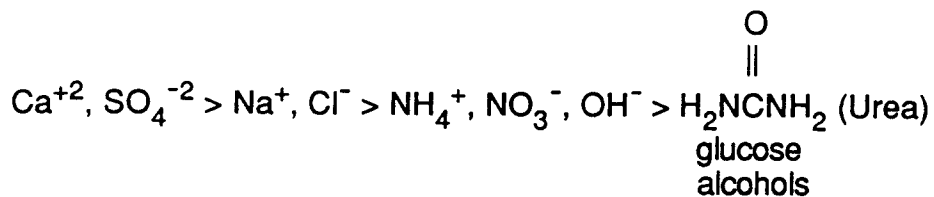
$$\epsilon = \epsilon_f \epsilon_0 \quad (15)$$

Table IV: Factors Influencing Rejection by RO Membranes

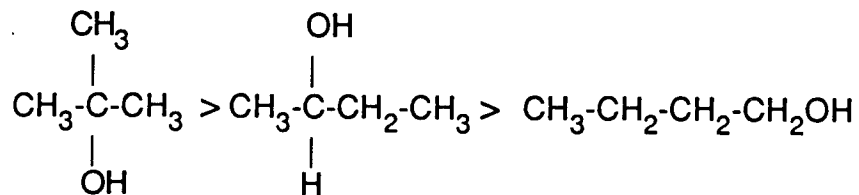
1) In general, larger molecules are rejected more than smaller molecules.

2) Decreasing order of rejection

Divalent ions > Univalent ions > Univalent ions capable of H⁺ bonding > Covalent molecules capable of H⁺ bonding



3) Longer chains and more highly branched molecules are rejected more than shorter chains and less branched molecules.



4) Protonated species are rejected less than nonprotonated species.

where

ϵ_r = relative permittivity of medium(unitless)

ϵ_0 = relative permittivity of vacuum(8.854×10^{-14} C/V-cm)

Dielectric constant is dependent on polarity of solvent molecules. For example, the ϵ_r for water is 78 and is reduced by nearly two orders of magnitude compared with using air as a medium. Higher values of ϵ_r help to reduce attractive forces between two charges. Dielectric constant is directly related to the *dipole moment* of a molecule.

A permanent dipole moment, measured in debyes, is a characteristic which gives molecular structure information (*Atkins, 1982*). More commonly, it is used for testing the suitability between solids and solutes in solvent systems; for example, a polar solvent such as water will dissolve an ionic solute, such as NaCl. The dipole moment is directly related to the polarity of a molecule. Symmetrical molecules, such as CH₄ are nonpolar with a dipole moment of zero, and have low dielectric constants. Water is polar and possesses a large dielectric constant.

The dielectric constant of organic molecules may be correlated with rejection. Molecules which have lower dielectric constants, i.e. non or less polar molecules, are rejected more favorably than molecules with higher dielectric constants. Correlations of organic rejection with dielectric constants are simple since dielectric constant data are readily available.

7. Fouling/Degradation Mechanisms

Hypothesis

In considering halocarbon effects on membrane performance, two questions must be answered. The first question is do halocarbons cause measurable changes in membrane performance? The second question is if observable changes do occur, do the halocarbons cause this by altering membrane structure (i.e. chemical changes) or are the changes physical which involve no chemical bonding between the halocarbons and membrane? Several hypotheses may be proposed for membrane changes and are listed below.

1) *Mechanical swelling* caused by halocarbons penetrating the membrane but not chemically bonding to the membrane. Halocarbon molecules would cause membrane "swelling", thereby decreasing pore space size for water transport. The noted effect would be a decrease in the transport of both solute and product water over time. This phenomena could either be reversible or irreversible.

2) *Weak hydrogen bonding* of halocarbons to O or N atoms in the membrane. This may cause acetate group hydrolysis in CA membranes and intermolecular hydrogen bonding and membrane structure weakening in PA and AC membranes. The result will be solute and product increases over time for all membrane types. This chemical interaction is irreversible.

3) *Physical adsorption* of halocarbons to the membrane. Halocarbons would attach to membrane polymer and cause water channel pluggage; the result is product and solute flux reductions. Physical adsorption is not chemical bonding

and is reversible.

4) *Polymer attachment* by halocarbons to the membrane. These substitutions would occur on the polymer, resulting in formation of new bonds which cause membrane structural changes. The results may be a lower flux and/or lower rejection due to a change in the selective properties of the membrane. This effect is a more pronounced form of hypothesis 2.

A series of experiments may be performed to test whether membrane performance changes are caused by fouling or degradation. Once these effects are determined, instrumental analyses may be used to establish which of the four aforementioned mechanisms occur in the membrane to cause degradation/fouling. The next section details the procedures used in this study.

Membrane Performance Tests

Impact of halocarbons on membrane performance may be determined by measuring product volume, solute (TDS) rejection, and halocarbon rejection over an extended period of time. Flux is determined by measuring product water volume collected as a function of time. A control test is first performed on tap water. Then, individual halocarbons are added to the system and product water volume was monitored over time. A reduction in water volume with halocarbons present indicates membrane fouling or swelling; an increase in product volume with halocarbons present indicates membrane degradation.

TDS rejection also indicates whether membrane fouling or degradation occurs. Measurements of influent and product TDS indicate the membrane's ability to reject solutes. In the case of membrane fouling, solute flow will

decrease with time and TDS rejection will increase. If membrane degradation occurs, solute flow will increase with time and TDS rejection will decrease.

Halocarbon rejection tests are valuable for demonstrating the membrane's ability to separate these organics from water. The possibility of membrane degradation is decreased if a halocarbon permeates through the membrane easily. If the membrane rejects a halocarbon strongly, halocarbon concentration buildup occurs on the membrane surface and the possibility of fouling or degradation is increased. Molecular size, charge, and dielectric constant are all factors influencing halocarbon transport through or rejection by the membrane. Seemingly, larger molecules should be more strongly rejected than smaller molecules. Halocarbons used in this study have molecular diameters of approximately 6 Å and should be rejected well since membrane pores exclude size range from 1 to 10 Å. However, since membranes do not act purely as filters, charge has more influence on molecule and ion rejection. For example, salts such as NaCl may be rejected on the order of 99% + since they are highly ionized and have considerable charge to mass ratio. A combination of charge and molecular diameter determines the behavior of halocarbon transport through membranes.

Another factor which causes the difference in rejections between inorganics and organics is the hydration radius. Inorganic ions such as Na⁺ and Cl⁻ have hydration spheres of approximately 6 to 9 water molecules. The extra waters on the Na⁺ and Cl⁻ ions increase their sizes and increases their rejection (*Luck, 1984*).

Static soak tests were performed on the three membranes to determine the halocarbon uptake. These tests quantify the affinity of the halocarbons to the membranes under nonpressurized situations. Another goal of these soak tests

is to quantify if any changes occur in the void volumes of the membrane. If decreases in the void volume occur with the addition of halocarbons, then this change signifies that halocarbons shrink the water passage channels within the membranes.

Several instrumental techniques, Fourier Transform Infrared (FTIR) spectroscopy, nuclear magnetic resonance (NMR) spectroscopy, and scanning electron microscopy (SEM) may be used to discern membrane surface or structural changes. FTIR is an instrumental technique which measures rotational and vibrational bending and modes of energy adsorption; these data are correlated with functional groups. Since the membrane structures are known, a comparison between membrane spectra before and after exposure to halocarbons will reveal what type of structural changes have taken place.

NMR is another instrumental technique which can provide insight into the presence or absence of functional groups. NMR involves irradiating a material in a magnetic field with constant frequency and varying strength. Since resonance strengths for different compounds and functional groups are known, comparisons of membrane spectra before and after halocarbon exposure will reveal chemical changes.

SEM detects physical changes on membrane surface through enlarging and photographing the surface via electron microscopy. Cross-sectional SEM photomicrographs reveal a membrane's internal physical changes; the difficulty of obtaining a sharp cross-section makes this technique more difficult and the outcome more dubious than for SEM. Comparisons between membrane SEM's before and after halocarbon exposure should reveal a membrane's physical changes, i.e. buildup of foulant layer, pluggage of pores, or structural breakdown.

8. Materials and Methods

Experimental Apparatus

Membrane performance tests are commonly carried out on an apparatus similar to the one shown in Figure 9. Flux decline, TDS rejection, and halocarbon rejection tests were performed on this apparatus. Tapwater held in a 200 L holding tank is fed into a 10 μ m Orlon prefilter before entering the pump. The pump is a Milton-Roy 221A positive displacement pump capable of delivering a maximum of 12.5 gal/min. Halocarbons are fed into a tee junction in the pump suction. Halocarbons in 20 and 40 L feed holding tanks are injected into the pump suction by a Masterflex[®] pump. Feed is split into two parallel membrane holders after exiting the pump. The holders contain membranes with dimensions of 1 inch by 2 inches with a surface area of 2 in² and were custom made. Permeate is forced out into a teflon tube from the top of the membrane holder and brine exits the side. Brine is collected together and fed into a back-pressure regulator set at 400 psi to maintain constant pressure. Brine is drained after passing through the regulator.

Analytical Methods

TDS measurements were conducted with a YSI model 35 conductance meter attached to a YSI probe, model 3403 with cell constant (K) of 1 cm⁻¹. The probe was first calibrated by using a series of NaCl and deionized water solutions between concentrations of 5 to 5,000 mg/L. pH measurements were taken with a Beckman model Φ 21 pH meter with a Beckman model 39836 probe. The pH probe was calibrated using two buffer solutions, one at pH of 4.0

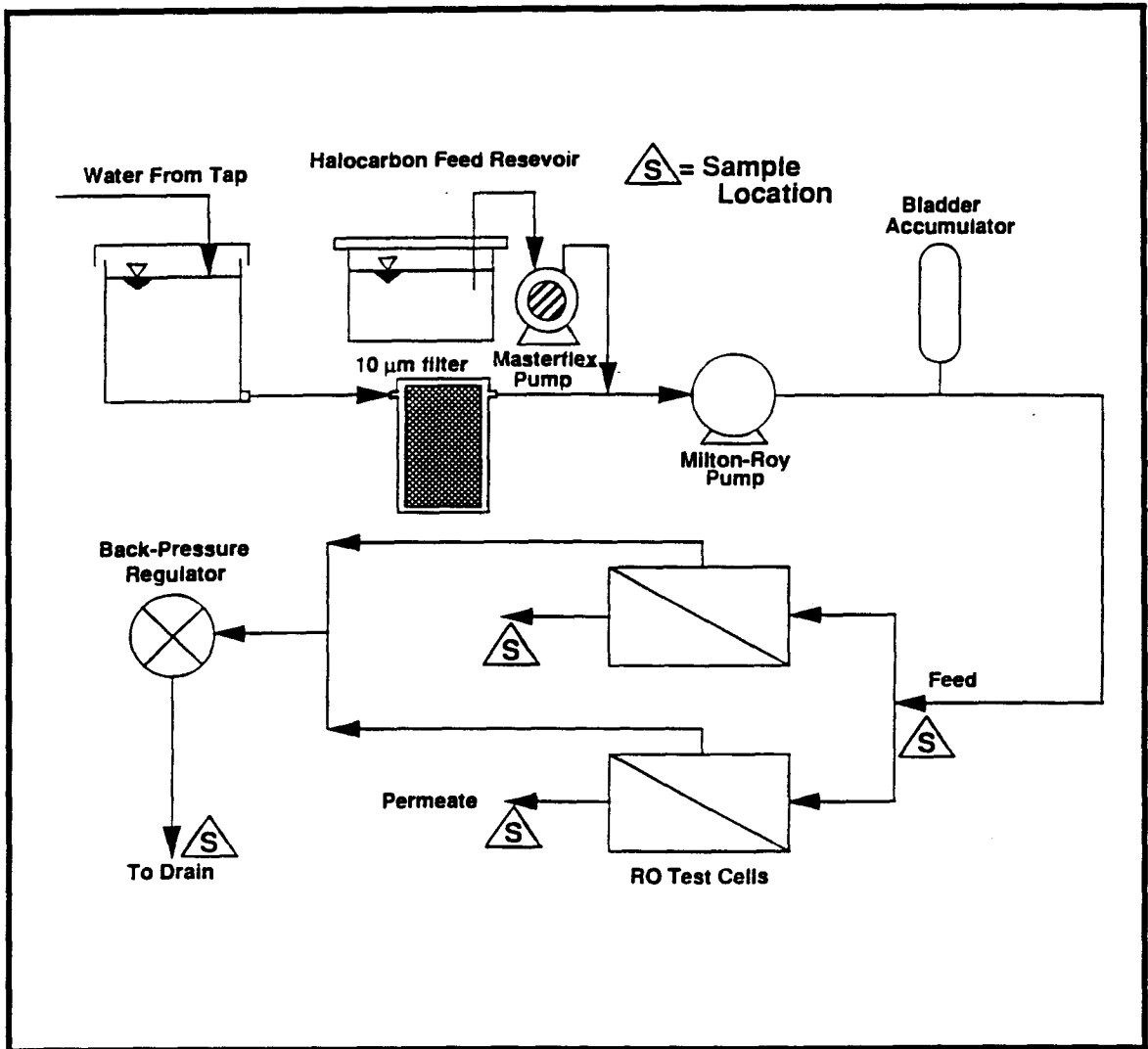


Figure 9: Schematic of One Pass RO Test Unit

and the other at pH 10.

Halocarbon detection was performed using a purge and trap/gas chromatograph (GC). The purge and trap concentrator was a Varian/Tekmar model 00-996367-00 set to the following time and temperature program: 11 minutes purge at 30 °C, 4 minutes desorb at 180 °C, and 8 minutes bake time at 180 °C. The trap was made of Tenax, silica gel, and charcoal and is 12 inches long and 1/8 inch I.D.. The purge and trap concentrator was attached to a Hewlett-Packard model 5890 GC equipped with a flame-ionization detector (FID). FID was chosen over electron capture detector (ECD) since ECD is too sensitive for use with our concentration ranges. The GC capillary column used was a J&W DB-624 silica column, liquid phase, with a 1.8 µm film thickness and dimensions of 30 m by 0.32 mm diameter. GC time and temperature program were: 35 °C initial temperature, 140 °C final temperature, 4 minutes initial hold time, 1 minute final hold time, and a 8 °C/minute temperature program. GC and purge/trap gases flowrates were: helium carrier gas at 5.58 ± 0.07 mL/min, hydrogen combustion gas at 47.2 ± 0.7 mL/min, and dry air purge gas at 315 ± 4 mL/min. The Hewlett-Packard model 3392A integrator used to record GC output had the following settings: attenuation of 2, chart speed of 0.2 cm/sec, peak width of 0.04, and threshold of -1.

Halocarbon concentrations were calibrated by injecting several solutions of concentrations between 1 to 100 mg/L into the purge and trap/GC. The integrated areas were then plotted against halocarbon concentrations to yield a calibration curve. Recovery efficiency of the GC column was also found by injecting a sample to the purge and trap/GC three times. Results of the three runs were totalled and the result from the first run was divided by the total to obtain the recovery efficiency.

FTIR analysis was performed by a FTIR spectrophotometer using a Biorad/Digilab Division model FTS 60 with a scanning resolution of 2 cm^{-1} . The spectrophotometer was a Fourier Transform type using a Michelson infraredometer. A ZnSe disc supported $100\text{ }\mu\text{m}$ thick membrane samples. Scans were performed using a FTIR microscope.

^1H (proton) NMR analysis was performed using a Bruker AF 200 spectrophotometer set at 200.133 MHz frequency. The solvents used to dissolve the membranes' active layer were dimethylsulfoxide (DMSO) and acetone supplied by Cambridge Isotope Laboratories at 99% and 99.5% product purity. The glass tubes used in NMR analysis were supplied by the Wilmad Glass Company with a 5 mm ID.

Membrane samples were prepared and SEM photographs were taken by the Department of Microbiology and Immunology at the University of Arizona in Tucson. The membrane fixation technique (Table V) was described by Kutz(1985) and the instrument used was an International Scientific Instruments model DS-130 scanning electron microscope. Photographs were taken at two magnifications, 367x and 3,670x, at an accelerating voltage of 20 keV. In addition AC membrane samples were also examined under 9,600x magnification.

Experimental Procedure

Twelve sets of measurements were conducted in this project, each with a duration of 125 hours with the exception of the AC membranes which were run for a period of 175 hours. Procedures for sample collection were the same for all tests. Feed SDI was taken via a procedure described in DuPont Bulletin 504 (Dupont, 1982). Total product volume was collected over a known period of

Table V: RO Membrane Fixation for SEM Examination (from Kutz, 1985)

1. Fix membrane samples overnight in 4% glutaraldehyde in 0.1 M Millonig's buffer at pH of 7.2.
2. Rinse the samples three times in Millonig's buffer for 5 minutes each time.
3. Rinse the samples three times in HPLC grade water for 5 minutes each time.
4. Fix the membrane for 30 minutes in 1% ruthenium tetroxide solution.
5. Rinse nine times in HPLC grade water.
6. Incubate membrane for 30 minutes in a saturated thiocarbazide solution. Prior to use, the thiocarbazide should be allowed to stand for one hour at 50 °C in solution. Decant the liquid and add solution until the color has reached a pale straw tint. Allow temperature to cool before using. Use only HPLC grade water.
7. Rinse nine times in HPLC grade water.
8. Incubate in 2% osmium tetroxide solution for 30 minutes.
9. Rinse nine times in HPLC grade water.
10. Repeat steps 4 through 9 once more.
11. Dehydrate through an ethanol series (30% to 100%).
12. Critical point dry with CO₂.
13. Sputter coat the sample with 30 nm of Au/Pd alloy (60/40).
14. Observe under microscope with voltages of up to 20 keV.

time, i.e. one hour. Feed, permeate, and brine specific conductances were measured at the time of product volume collection. If CHBr_3 , CHCl_3 , or CCl_4 were fed into the system, feed, product, and brine samples were collected for gas chromatograph (GC) analysis once every two hours. Product water was collected in 7 mL capped bottles with a teflon tube inserted through the cap top; this minimized volatile halocarbon loss. Temperatures and pHs of the feed and brine were also measured at time of product volume collection.

Three different membrane types were used: CA, PA, and AC. Four experiments were performed for each membrane type. The initial test established baseline performance by using filtered tapwater as feed. GC analyses showed tapwater halocarbon levels were below detection limits; therefore, no GC analyses were performed in baseline tests. In subsequent tests, CHBr_3 , CHCl_3 , and CCl_4 were added to feedwater to maintain constant halocarbon concentration of 50 mg/L.

Fouling reversibility tests were performed on an AC membrane with a total test time of 175 hours. In these tests, the AC membranes were exposed to 50 mg/L of the respective halocarbons for the initial 125 hours. After 125 hours, halocarbon feed was shut off and the membranes were only exposed to tapwater for an additional 50 hours. The product volumes and TDS data were collected for the entire 175 hours while GC analyses were performed for the first 125 hours.

Static soak tests were also performed on the three membranes using mixtures of CHBr_3 , CHCl_3 , and CCl_4 and DI water in concentrations of 0, 50, 100, 250, 500, 1,000, and 2,000 mg/L. Two pieces of membrane, each with a diameter of 2 inches, were placed in 20 mL vials with aluminum lined caps and the vials were completely filled with the halocarbon mixtures. After 10 days, both

pieces of membrane from each vial were removed and rinsed and blotted dry. One piece was used for weight and thickness measurements. Thicknesses were measured by using a Starret Model Number 1230 Micrometer, accurate to ± 0.0005 in. These membranes were then placed in a oven set at 104 °C for four days. After this drying period, the membranes were removed from the oven and reweighed and the thicknesses remeasured. The data were subsequently used to calculate the membrane void fraction using equations 12 and 13.

The other piece of membrane was placed in a 10 mL aluminum-capped vial and filled with 8 mLs of trimethylphosphate (TMP) for extraction. The membranes were removed from the vials after four days. A 0.5 mL aliquot of the TMP/halocarbon solution was then diluted with 9 mLs of DI water and mixed. A 5 mL sample was then injected into the purge and trap/GC for concentration analysis. The concentration of the adsorbed halocarbons on the membrane was subsequently backcalculated from this data.

FTIR analysis was performed by scanning a membrane sample mounted onto a ZnSe disc. Absorbances were plotted against their respective wavenumbers. The peaks and wavelengths were compared to IR spectra of known functional groups in the literature (*Socrates, 1980*). Since membrane functional groups are known, any changes detected by FTIR may be quickly observed.

^1H NMR analysis was performed by soaking CA membrane in acetone and PA in DMSO. The glass tubes holding the membranes and solvents were passed rapidly over a Bunsen burner for warming; this ensured the dissolution of the membranes' active layer into the solvent. The membranes were then removed and approximately 1 mL of the solvent with extract was poured into the NMR tubes for observation.

Data Analysis

Six graphs were generated to compare baseline, CHBr_3 , CHCl_3 , and CCl_4 effects on each membrane. The first graph compared total product volume vs. time. This was plotted by totaling permeate volume and graphed as a function of time. Weschler's equation (Equation 7) along with linear regression were used to evaluate membrane constants m and K . Equation 5 was used to calculate flux once these values were known; flux data were also plotted against time.

Percent TDS and halocarbon rejections were calculated in similar fashions. Concentrations of TDS and halocarbons of the feed, product, and brine streams were calculated by using prepared calibration plots. Equation 8 was used to calculate percent rejection. These data were also plotted against time.

The water transport coefficient (A) and the solute transport coefficient (B) were calculated and plotted against time. This procedure involved several calculations. Water fluxes were calculated from volume data and osmotic pressures were calculated from Equations 3 and 4. Coefficient A was evaluated by using Equation 1. Coefficient B was evaluated by first calculating solute flux J_s by multiplying water flux with product flux with product TDS. J_s was then divided by osmotic pressure to yield B. These coefficients may be plotted against time.

Statistical analyses (Student t-tests) were performed on the data to make comparisons between baseline runs and runs with halocarbons added to be sure the differences noted were not due to experimental error. Confidence intervals (95%) were calculated based on variances in the data. If overlap existed between two sets of confidence intervals, the comparison was deemed nonsignificant and attributable to experimental error.

Partition coefficients (K_s) were calculated and plotted against concentration. This procedure involves several backcalculations. First, sample concentration was obtained by injecting a 5 mL sample into the purge and trap/GC and divided by the column efficiency. Since the sample injected into the GC was made up by membrane extraction in 8 mL of TMP and 0.5 mL of this was diluted with 9 mL of water, these quantities are taken into account when calculating the halocarbon concentration originally in the membrane. K_s for each membrane was calculated by Equation 11.

The membrane void fraction ϵ was calculated by Equations 12 and 13. The dry and wet membrane densities were calculated by dividing the respective weights by their volumes. Membrane volumes were calculated by multiplying the areas by the measured thicknesses. ϵ was plotted as a function of halocarbon concentration.

9. Results and Discussion

SDI Tests

A total of 12 runs were made for silt density index (SDI) calculations on feedwater, prior to each experiment, yielded an average value of 6.47 ± 0.11 . Initial times needed to collect the 500 mL volume ranged between 30 to 90 seconds while final times for the 500 mL collection ranged between 32 to 40 minutes. Our results indicate the water used in this experiment is of poor quality.

Cellulose Acetate Membranes

Figure 10 shows total product volume vs. time plot for DuPont 7460 CA. The data are present in clusters since no data were collected at night. Normally, each cluster of data points represent one experimental day. The baseline and CHCl_3 lines are parallel, i.e. same flux, while CHBr_3 and CCl_4 lines decline after approximately 40 hours. Addition of CHBr_3 causes a larger flux decline than the addition of CHCl_3 or CCl_4 . The predicted lines in Figure 10 were calculated from Equation 6. Predicted and actual volumes are in good agreement with correlation coefficients of 0.999.

Figure 11 shows calculated flux vs. time plot for DuPont's CA. The lines for this graph were generated by Equation 5. This plot further illustrates the impact of adding CHBr_3 to the system. While baseline flux decreases from 24.5 GFD to 22.5 GFD over the experiment, CHBr_3 flux drops from 24 GFD to 17 GFD. This is a 8% decrease as opposed to a 29% decrease in flux, a statistically significant change after their respective 95% confidence intervals were calculated. Both CHCl_3 and CCl_4 experiments indicate flux increases over time.

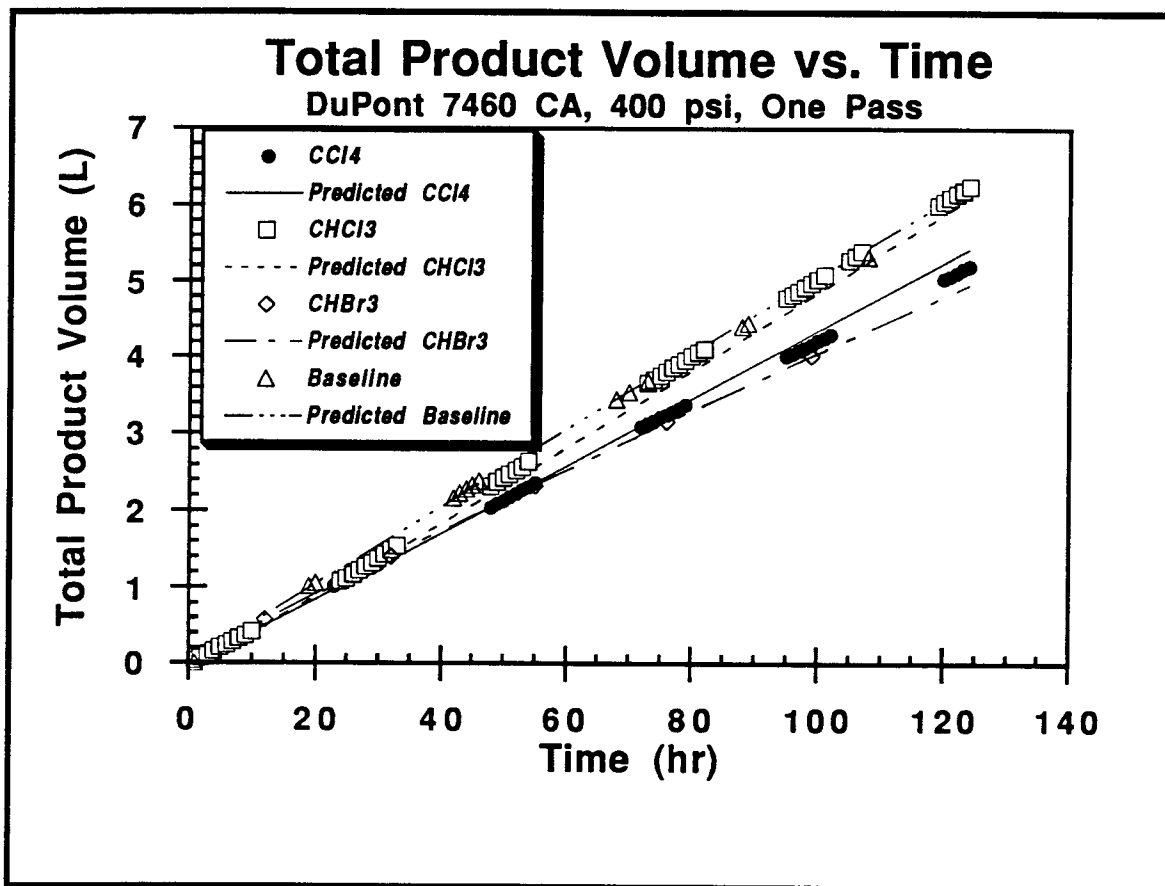


Figure 10: Total Product Volume vs. Time for DuPont 7460 CA

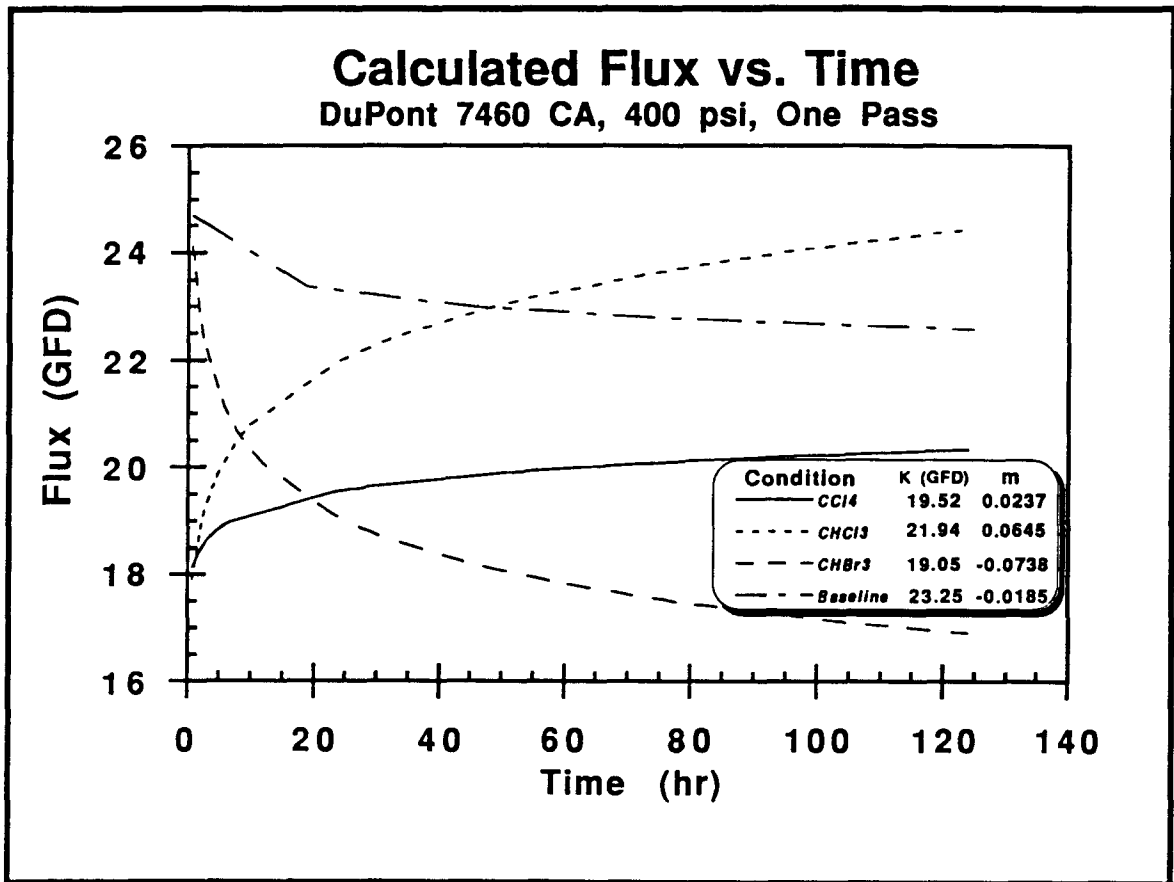


Figure 11: Calculated Flux vs. Time for DuPont 7460 CA

CHCl_3 flux shows a 37% increase over initial flux and CCl_4 flux shows a 12% increase over course of the experiment. Increase in flux indicate membrane degradation may be present.

Figure 12 shows TDS rejection over time for DuPont's CA. Baseline data show an initial rejection of 87% and quickly reaching equilibrium between 97% and 98%. TDS rejection for CHCl_3 also shows rapid equilibration from 84.5% to 99.5% within 16 hours. CHBr_3 and CCl_4 both reach equilibrium rejection between 98% and 99%. While the halocarbons decrease total product volume from baseline, they actually increased percent TDS rejection. This may be accounted for by membrane swelling which results in flux declines and TDS rejection increases.

Figure 13 shows halocarbon rejection vs. time for DuPont's CA. Although some data scatter exists, average percent halocarbon rejections for CHCl_3 , CHBr_3 , and CCl_4 are $4.6 \pm 0.4\%$, $13.2 \pm 1.3\%$, and $31.9 \pm 1.7\%$, respectively. (Note: the number before the \pm sign represents the average data value and the the number after \pm represents the 95% confidence interval range for the data.) Even though CCl_4 is rejected more strongly than CHCl_3 or CHBr_3 , the halocarbons all passed easily through the CA membrane. The results of soak tests, shown later in this chapter, confirms that the halocarbons do permeate through the membranes readily.

Figure 14 shows calculated water transport coefficient A vs. time for the CA membrane. CHCl_3 and CCl_4 lines actually increase over time, indicating the membrane allows more water to pass through over the experimental time period. This observation supports the flux increases presented in Figure 11. The final values for coefficient A for CHCl_3 , CCl_4 , CHBr_3 , and baseline are 0.058 ± 0.001 , 0.048 ± 0.001 , 0.041 ± 0.001 , and 0.041 ± 0.001 GFD/psi, respectively.

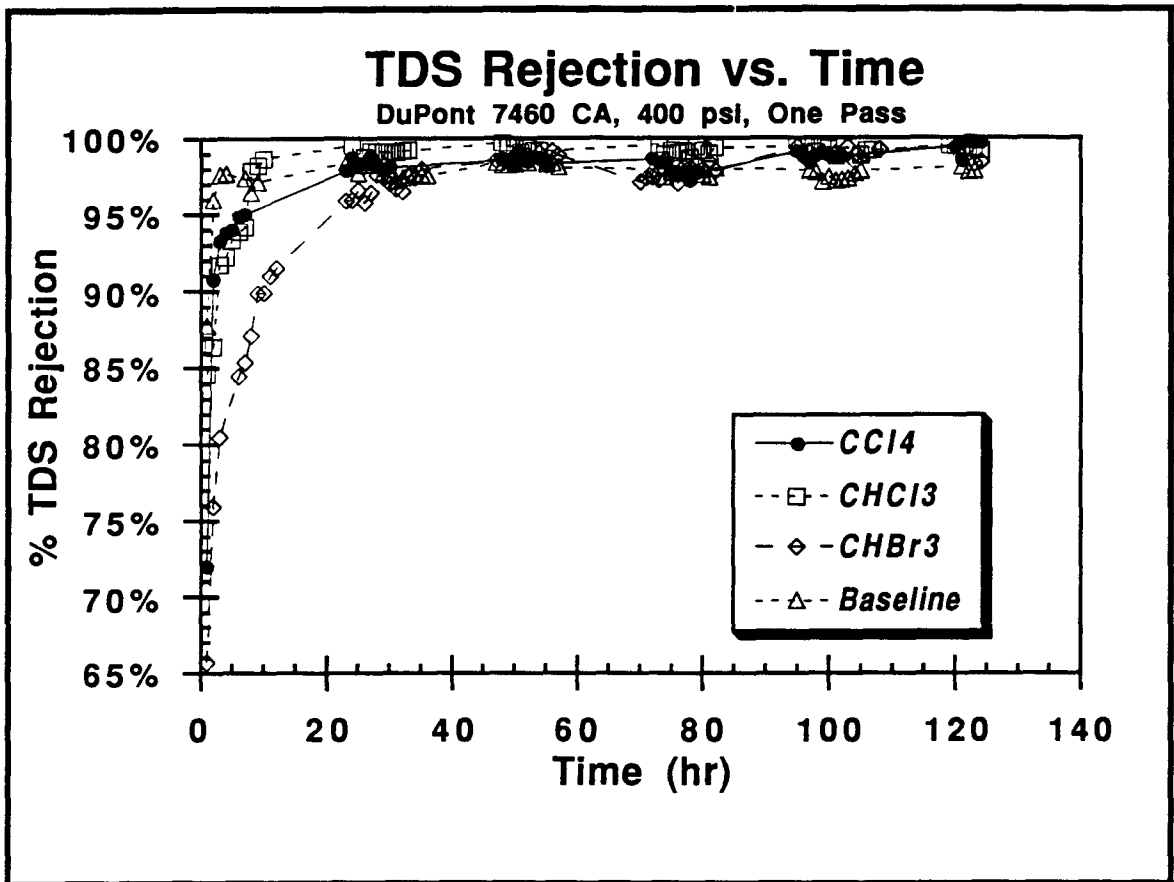


Figure 12: TDS Rejection vs. Time for DuPont 7460 CA

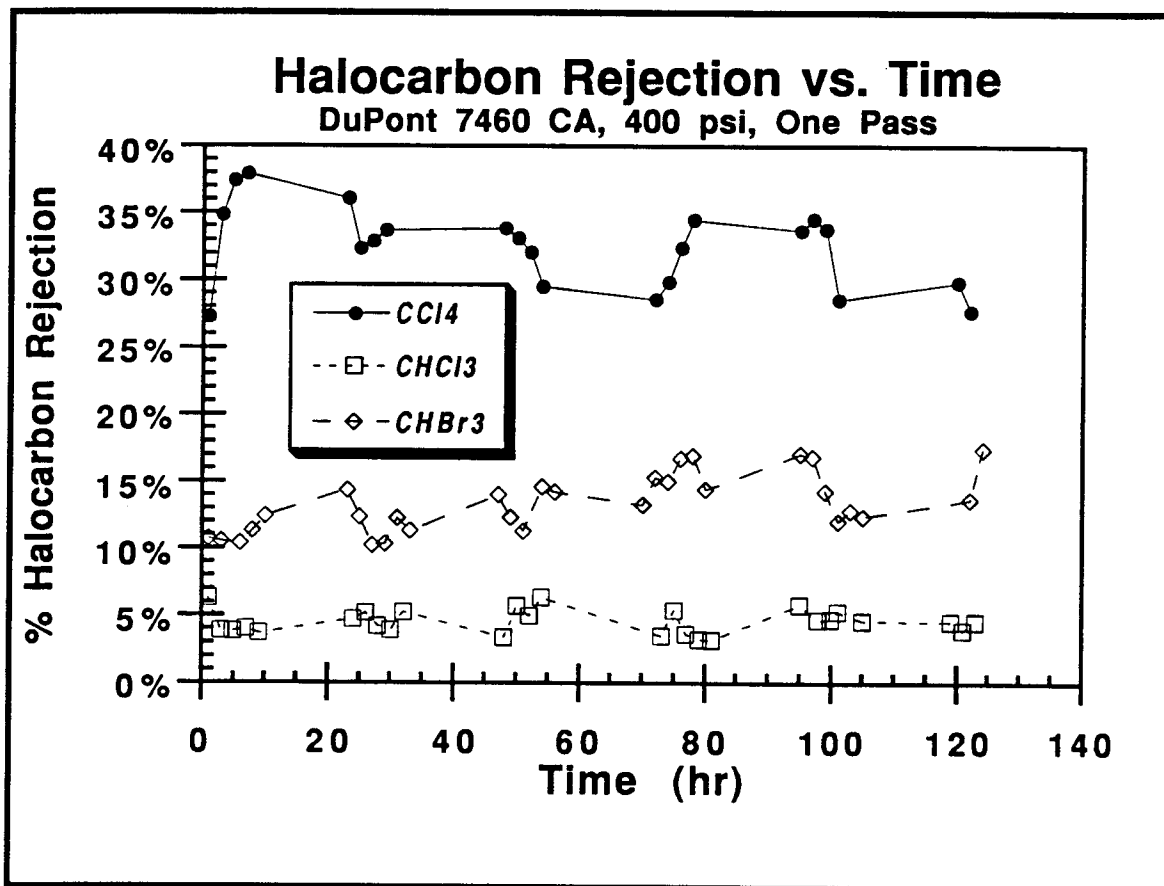


Figure 13: Halocarbon Rejection vs. Time for DuPont 7460 CA

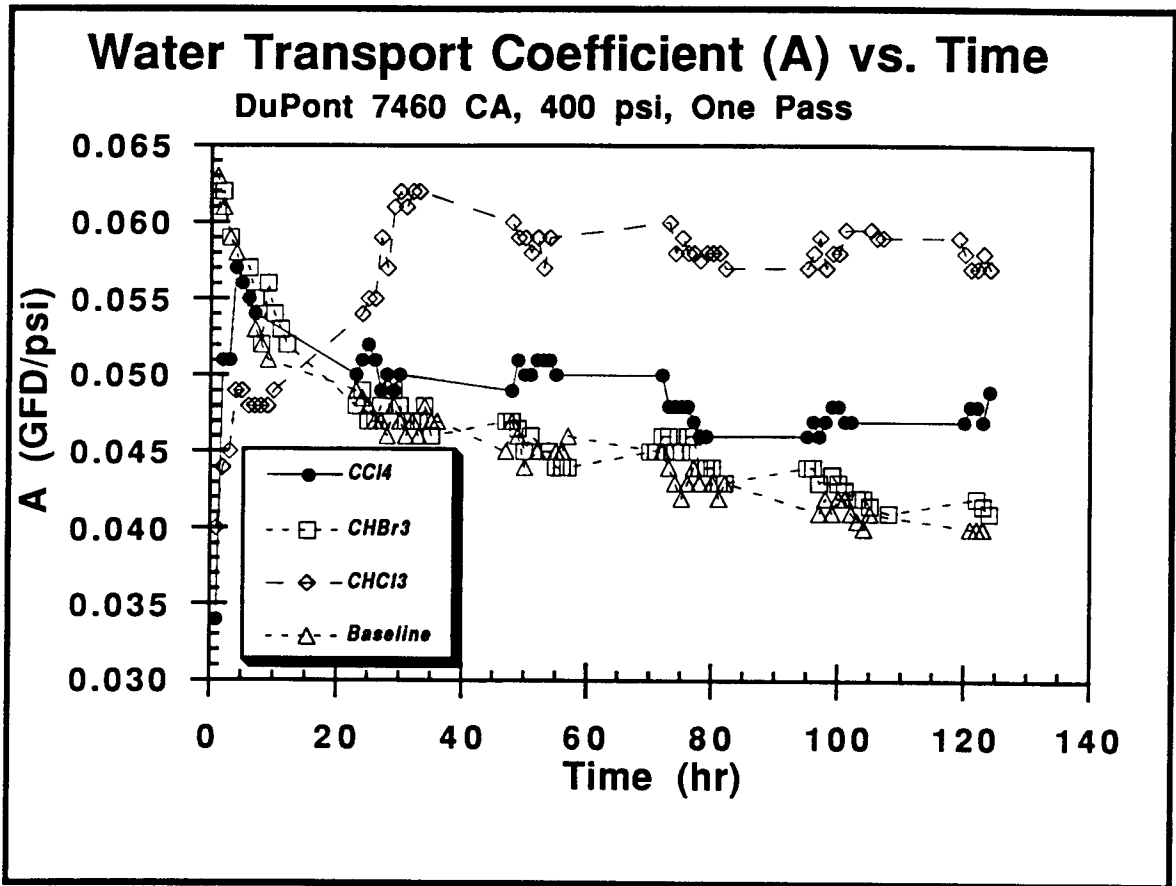


Figure 14: Water Transport Coefficient (A) vs. Time for DuPont 7460 CA

The same values obtained for both baseline and CHBr_3 addition indicates CHBr_3 does not hinder the CA membrane's ability to transport water.

Figure 15 shows calculated solute transport coefficient B for the CA membrane as a function of time. Baseline, CHCl_3 , CHBr_3 , and CCl_4 B coefficients at the end of the test period are 0.045 ± 0.002 , 0.027 ± 0.001 , $0.016 \pm .001$, and 0.011 ± 0.004 ft/day, respectively. Since a lower B coefficient corresponds to less solutes being transported across the membrane, this in turn indicates a higher percent TDS rejection. The data from this graph reinforce the results in Figure 12 that the addition of either CHBr_3 or CCl_4 results in the highest TDS rejection by the CA membrane, followed by CHCl_3 addition, and finally the baseline run.

Polyamide Membrane

Figure 16 shows total product volume vs. time for DuPont's 5930 PA membrane. In the presence of CHCl_3 and CHBr_3 , product flux is greatly reduced. Without halocarbons present, 6.85 ± 0.13 L of product are collected over the 125 hour period and with the two THM's present, the total product volume collected is only 5.15 ± 0.08 L; this represents a 24.8% decrease. With CCl_4 present, only 5.52 ± 0.08 L of product are collected, representing a 19.4% decrease compared to baseline performance. The lines in this figure represent predictions based on Equation 6 and show good agreement with the actual volume data. Linear regression of the data shows correlation coefficients in excess of 0.999.

Figure 17 shows calculated flux vs. time for PA membrane. CHCl_3 and CHBr_3 fluxes are very similar while CCl_4 flux is nearly constant in the experiment. Comparing fluxes at the end of the experiments, baseline, CHBr_3 ,

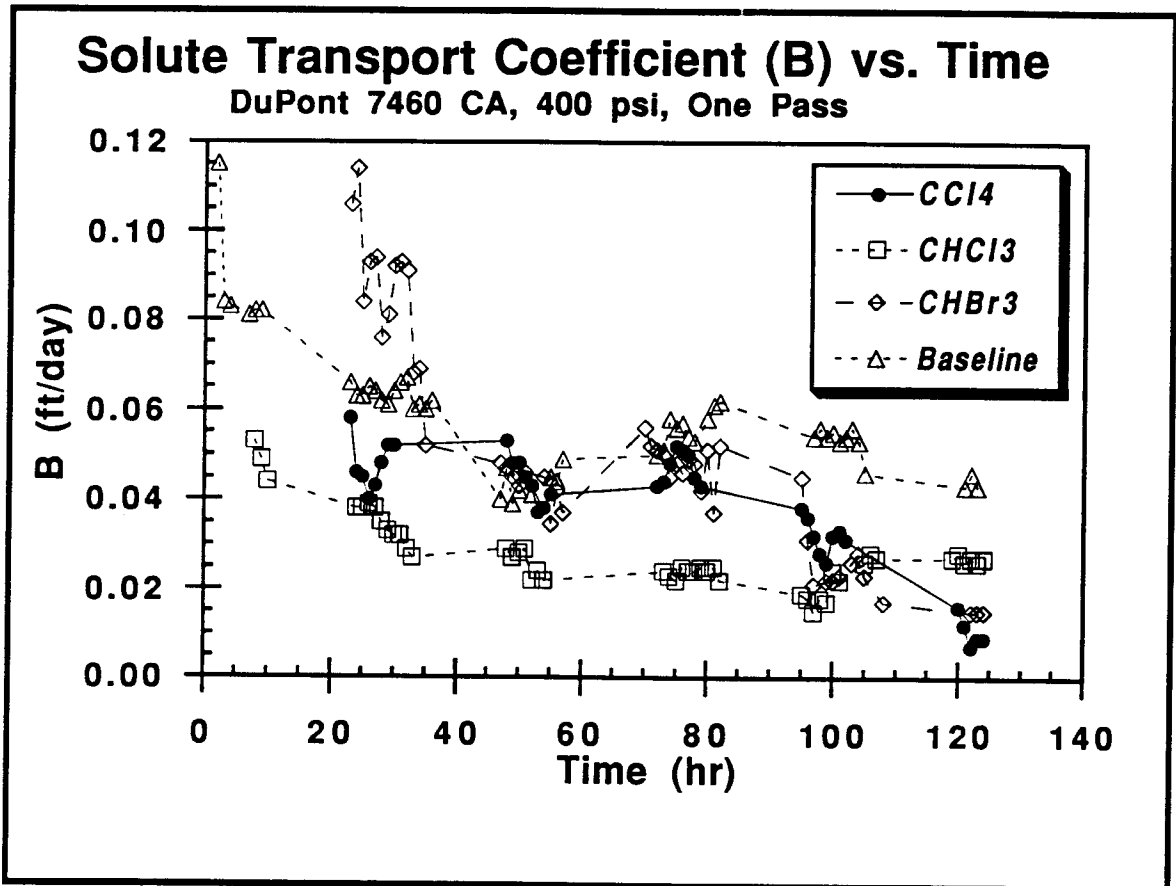


Figure 15: Solute Transport Coefficient (B) vs. Time for DuPont 7460 CA

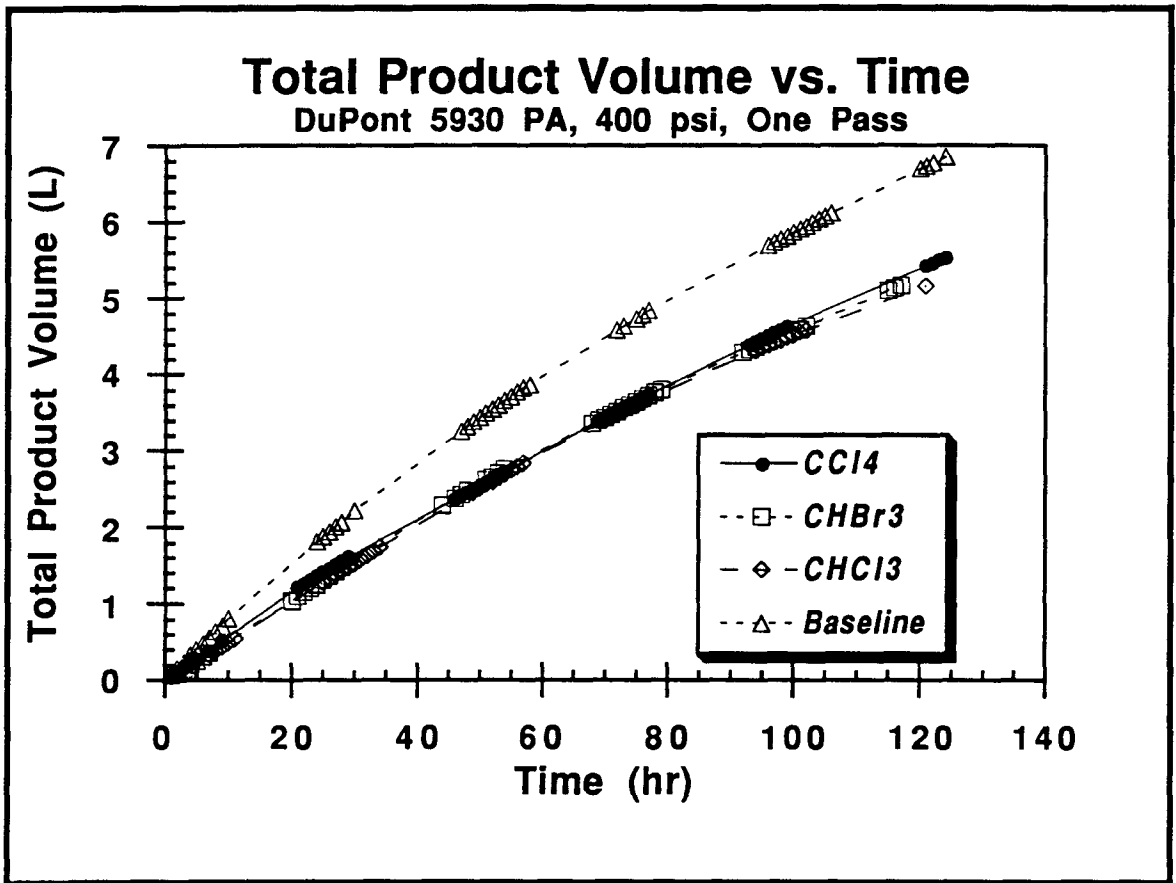


Figure 16: Total Product Volume vs. Time for DuPont 5930 PA

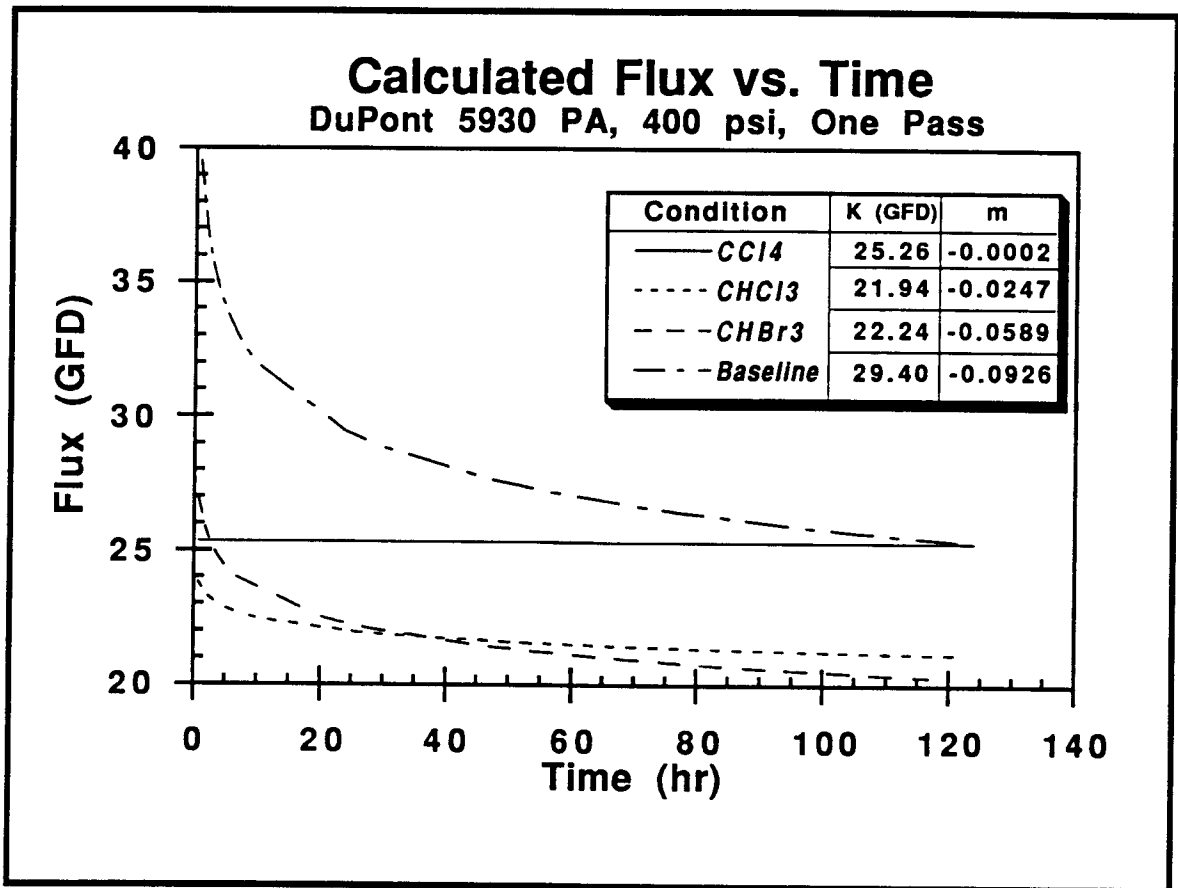


Figure 17: Calculated Flux vs. Time for DuPont 5930 PA

CHCl_3 , and CCl_4 yield fluxes of 25, 20.5, 21.5, and 24.5 GFD respectively. Additions of CHBr_3 , CHCl_3 , and CCl_4 decrease fluxes by 18%, 14%, and 2% respectively, from baseline. Addition of CHBr_3 and CHCl_3 cause nearly the same effects in flux decline while CCl_4 showed no appreciable decline.

Figure 18 shows TDS rejection vs. time for DuPont's PA membrane. Baseline TDS rejection stabilized between 96% and 97%. CHCl_3 did not affect TDS rejection since equilibrium value stayed around 97.7 ± 0.2 %. Additions of CHBr_3 and CCl_4 actually decreased TDS rejection from baseline, showing identical equilibrium rejection values of 91.5 ± 0.5 %. This observation indicates an inconsistency with total product volume and flux data since both graphs indicate decreases from baseline. In the presence of fouling, flux usually decreases but TDS rejection increases.

Figure 19 shows halocarbon rejection as a function of time for DuPont's PA membrane. Although some data scatter occurs, average CHCl_3 , CHBr_3 , and CCl_4 rejections are $10.1 \pm 1.4\%$, 11.5 ± 2.0 %, and $59.3 \pm 2\%$, respectively. These data show the PA membranes reject the two THM's to the same extent, while CCl_4 is rejected more strongly. The same order of halocarbon rejection occurs with PA as with the CA membrane with CCl_4 being rejected more strongly than CHBr_3 which in turn is rejected more strongly than CHCl_3 .

Figure 20 shows calculated water transport coefficient A plotted against time for the PA membrane. No steady-state values were reached in the experimental time. CHCl_3 , CHBr_3 , and CCl_4 values at the end of the experimental period are nearly identical, indicating similar halocarbon influences on PA's water flux. The coefficients for baseline, CCl_4 , CHBr_3 , and CHCl_3 are 0.049 ± 0.001 , 0.045 ± 0.001 , 0.041 ± 0.001 , and 0.039 ± 0.001 GFD/psi, respectively, at the end of the experiment. These data indicate halocarbons reduce the flux of PA membranes.

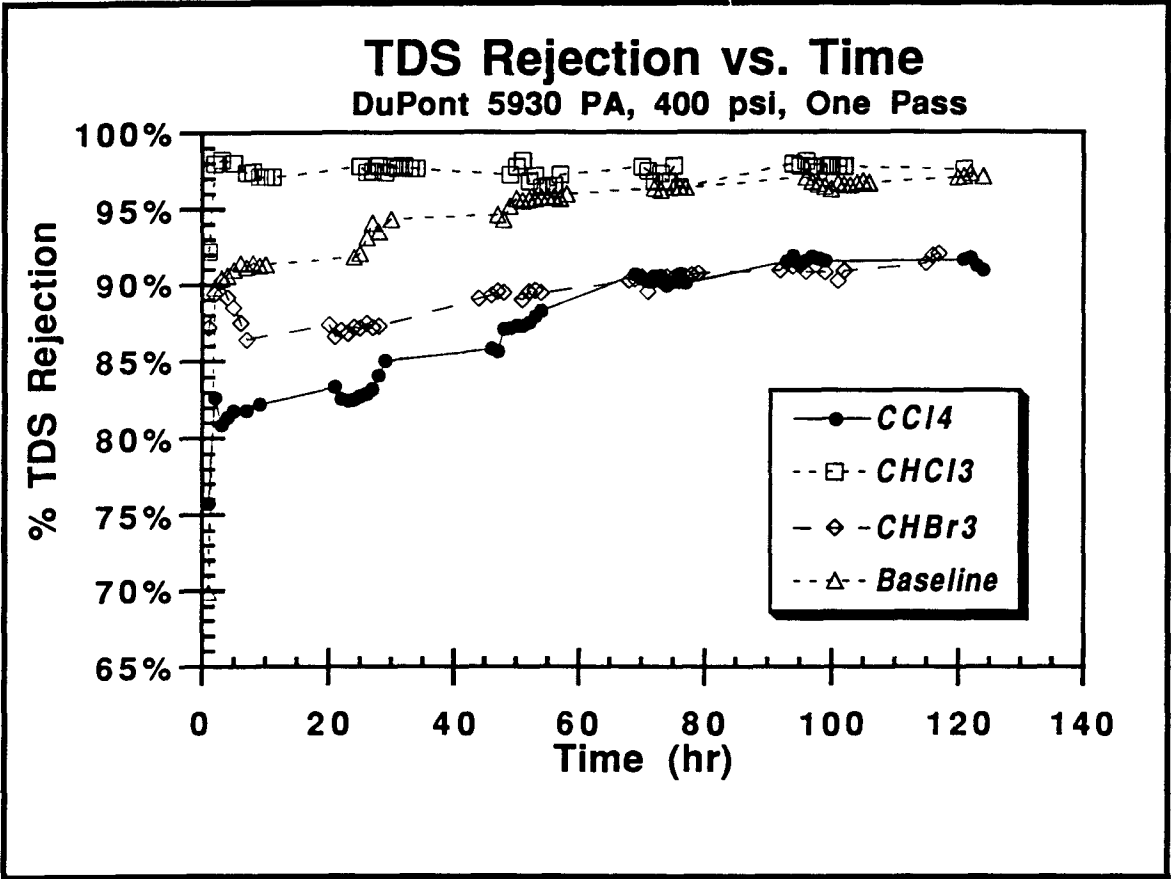


Figure 18: TDS Rejection vs. Time for DuPont 5930 PA

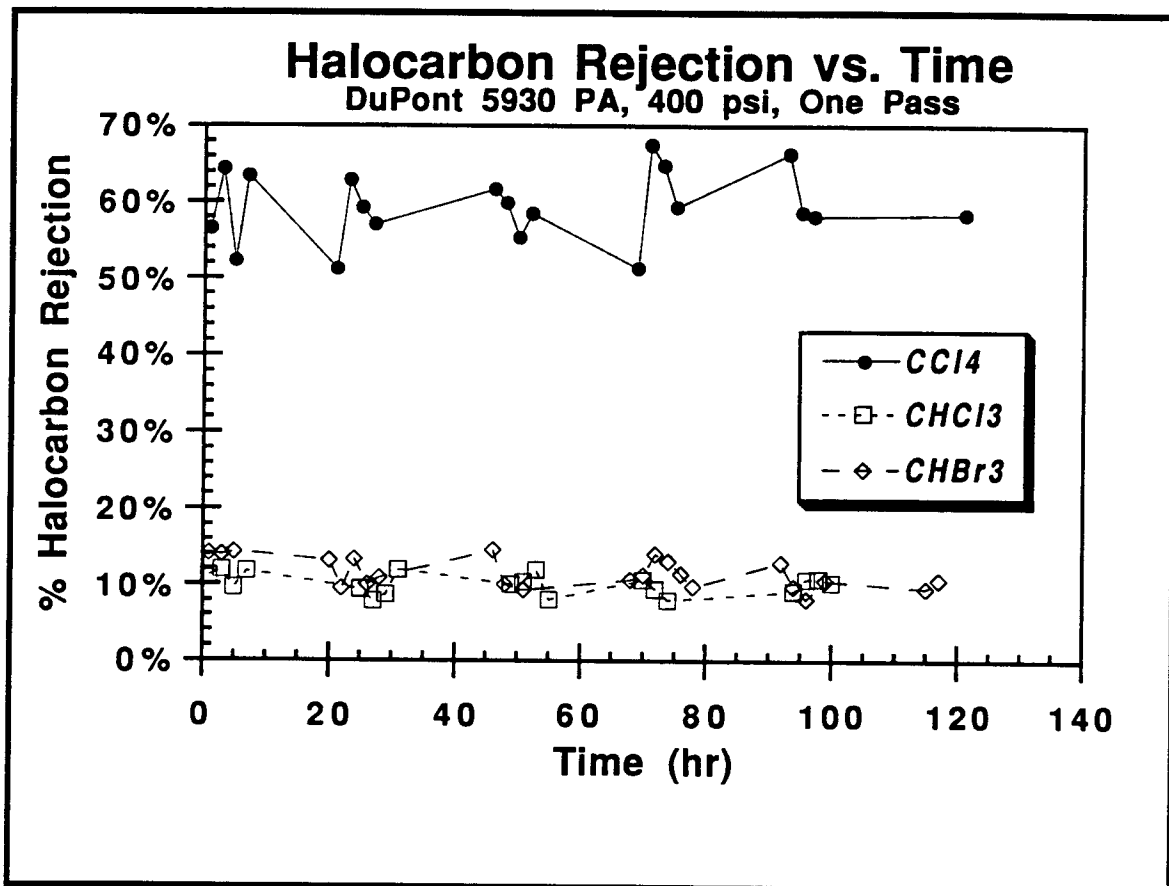


Figure 19: Halocarbon Rejection vs. Time for DuPont 5930 PA

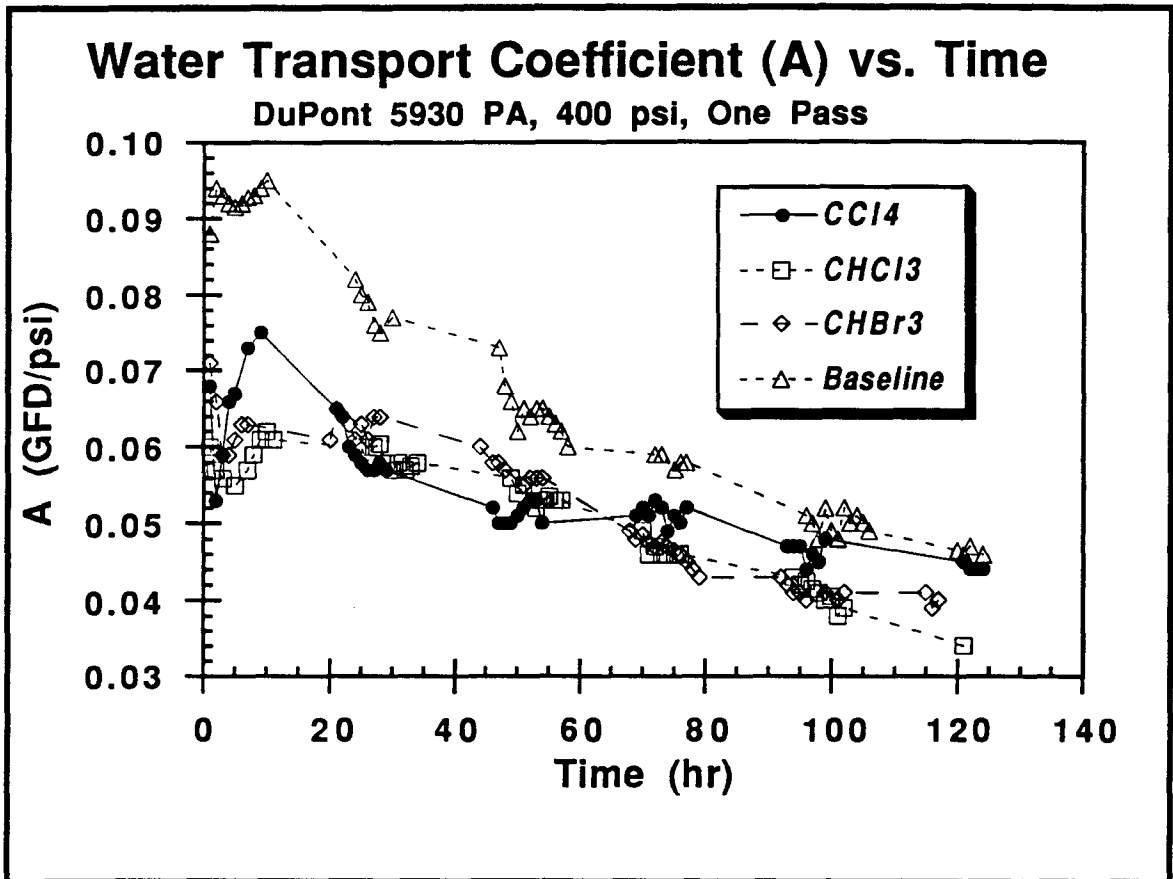


Figure 20: Water Transport Coefficient (A) vs. Time for DuPont 5930 PA

Figure 21 shows the calculated solute transport coefficient B vs. time for DuPont's PA membrane. This coefficient does not reach equilibrium within the experimental time span which is similar to coefficient A. These results support Figure 18 results. At the end of 125 hours, the solute transport coefficient for CHCl_3 , baseline, CCl_4 , and CHBr_3 are 0.047 ± 0.002 , 0.088 ± 0.005 , 0.22 ± 0.01 , and 0.21 ± 0.01 ft/day, respectively. As may be seen, data for CCl_4 and CHBr_3 are nearly identical. Since a lower B value indicates better solute rejection abilities, adding CHCl_3 to the feed improves this membrane's solute rejection capability while additions of CCl_4 and CHBr_3 hinder the PA's solute rejection ability.

Advanced Composite Membrane

Figure 22 presents the results from the product volume experiment for DuPont's 89006 AC membrane. Merten's unsteady-state equation overpredicts the baseline membrane performance while the calculated lines and experimental data are in good agreement for halocarbon additions with correlation coefficients of 0.999. Halocarbon addition decreases the membrane's flux since all product volume lines are below the baseline value. The CCl_4 and CHCl_3 tests were conducted for 170 hours since we were also testing for fouling reversibility. At 125 hours, total product volume collected for baseline, CHCl_3 , CHBr_3 , and CCl_4 are 7.81 ± 0.08 , 5.91 ± 0.08 , 5.88 ± 0.09 , and 5.43 ± 0.08 L, respectively. CHCl_3 and CHBr_3 caused approximately 25% decrease in the ACM membrane's flux while CCl_4 caused a 30.5% decrease.

Figure 23 shows calculated flux vs. time curve for DuPont's AC membrane. The shapes of curves for baseline, CHCl_3 , and CCl_4 are nearly identical while CHBr_3 's shape is nearly flat. Based on predictions from Equation 5, final

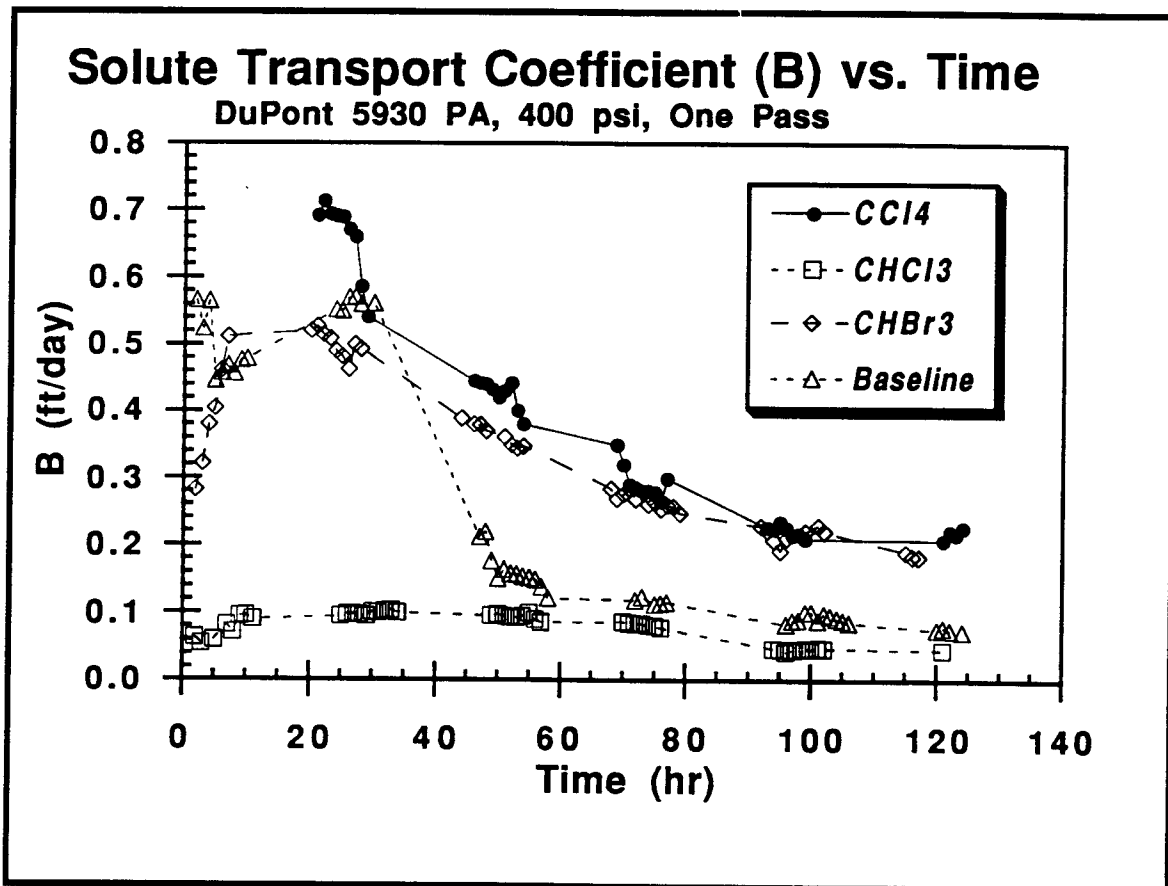


Figure 21: Solute Transport Coefficient (B) vs. Time for DuPont 5930 PA

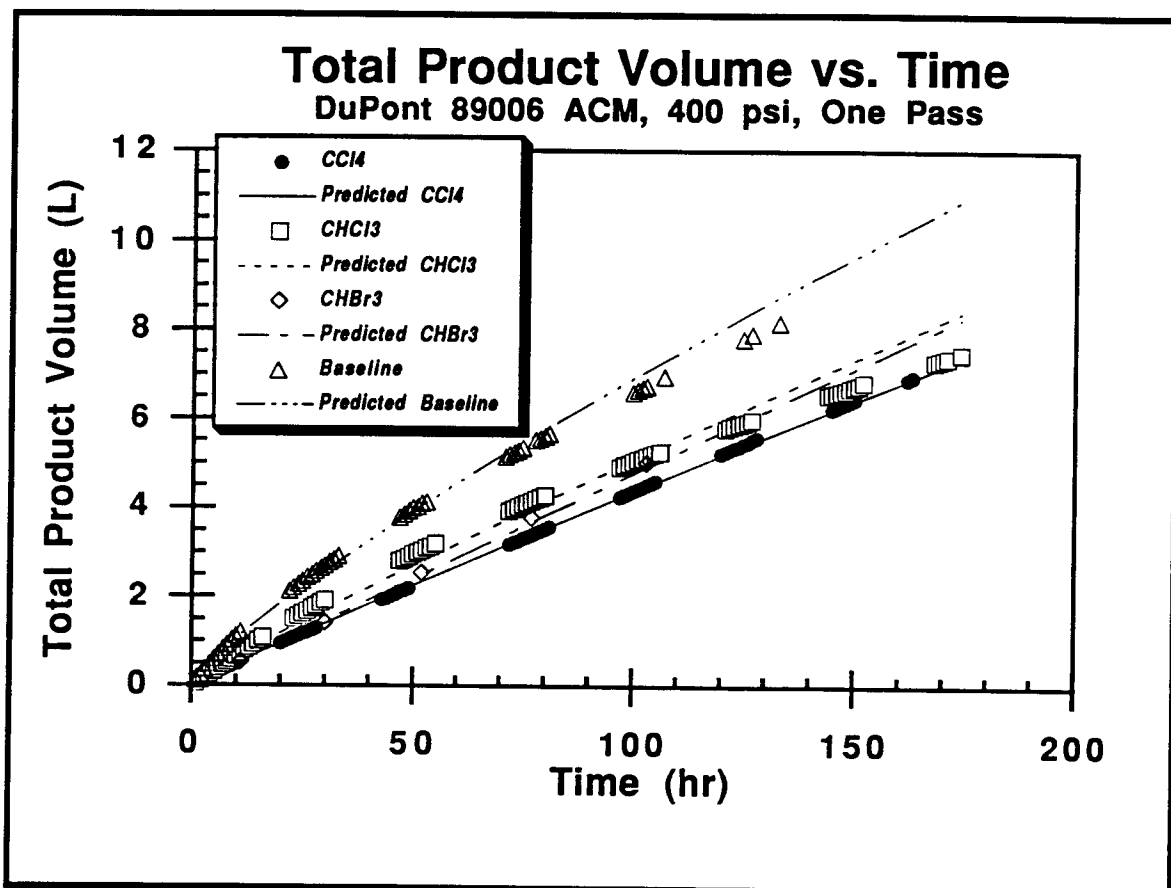


Figure 22: Total Product Volume vs. Time for DuPont 89006 ACM

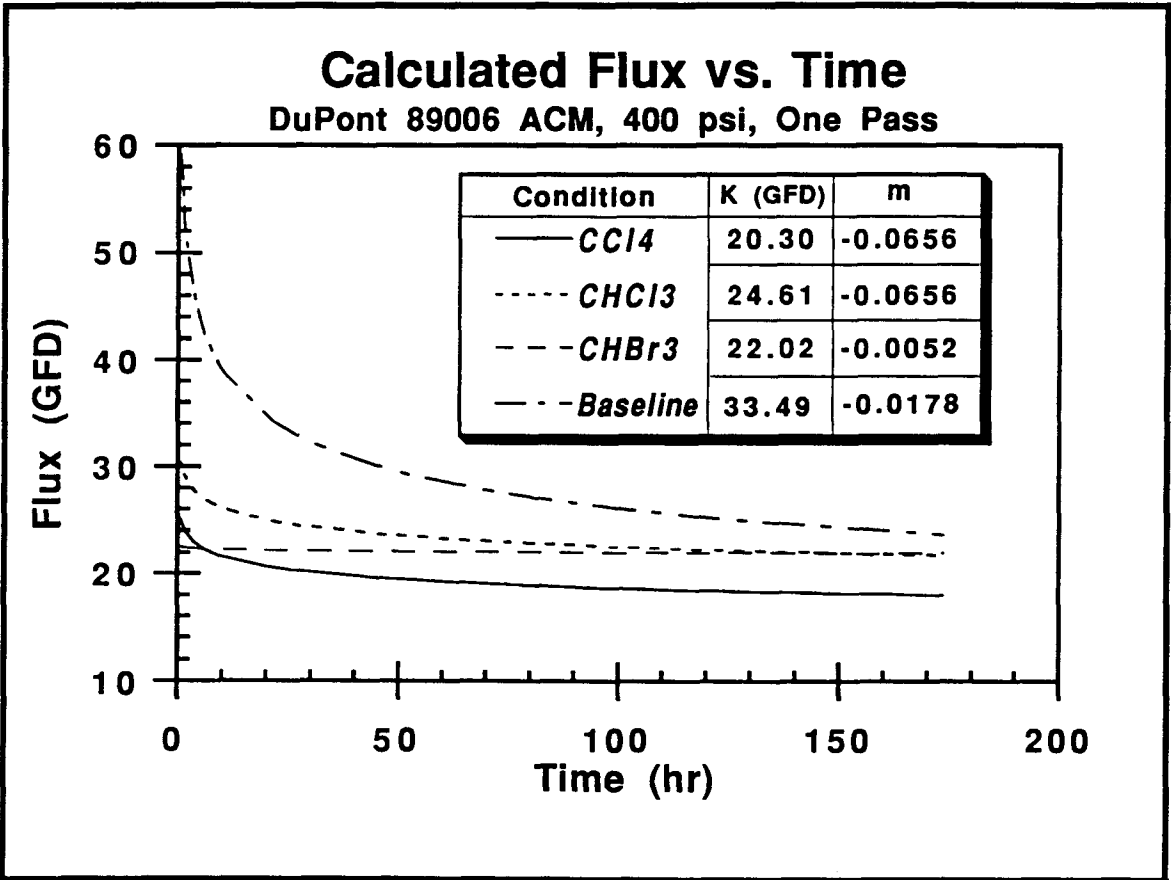


Figure 23: Calculated Flux vs. Time for DuPont 89006 ACM

calculated fluxes for baseline, CHBr_3 , CHCl_3 , and CCl_4 are 23.54, 21.79, 21.61, and 17.83 GFD. CHBr_3 and CHCl_3 cause approximately 8% decrease in flux while CCl_4 causes 24.3% decrease from baseline flux. This reflects the same general trend as depicted in Figure 22.

Figure 24 shows TDS rejection vs. time data for DuPont's AC membrane. While no equilibrium is achieved in these experiments, the general trend is all halocarbons improve the membrane's rejection capability. At the end of 125 hours, TDS rejection for CHBr_3 , CCl_4 , CHCl_3 , and baseline cases are $97.5 \pm 0.2\%$, $96.6 \pm 0.2\%$, $94.3 \pm 0.2\%$ and $90.3 \pm 0.3\%$. This data, combined with the volume data presented in Figure 22, indicate membrane swelling is occurring.

Figure 25 presents data obtained for halocarbon rejection vs. time experiments for the AC membrane. Although data scatter is present, average values obtained for CCl_4 , CHBr_3 , and CHCl_3 are $80.3 \pm 2.5\%$, $48.9 \pm 1.7\%$, and $36.4 \pm 1.3\%$, respectively. Although the AC membrane rejects halocarbons better than both CA and PA membranes, the order of halocarbon rejection is the same for all three: $\text{CCl}_4 > \text{CHBr}_3 > \text{CHCl}_3$.

Figure 26 shows the calculated water transport coefficient A as a function of time for the AC membrane. Equilibrium is established after approximately 50 hours and it is evident halocarbons cause decreases in A from baseline. The values for baseline, CCl_4 , CHBr_3 , and CHCl_3 cases are 0.059, 0.050, 0.050, and 0.043 GFD/psi, respectively. CCl_4 and CHBr_3 cause a 15.4% decrease from baseline value and CHCl_3 causes a 27.1% decrease. These decreases are consistent with the trends observed in the volume data.

Figure 27 shows the calculated solute transport coefficient B vs. time for the AC membrane. These data show halocarbon additions decrease B values from baseline which translate to a higher TDS rejection. Solute transport coefficients

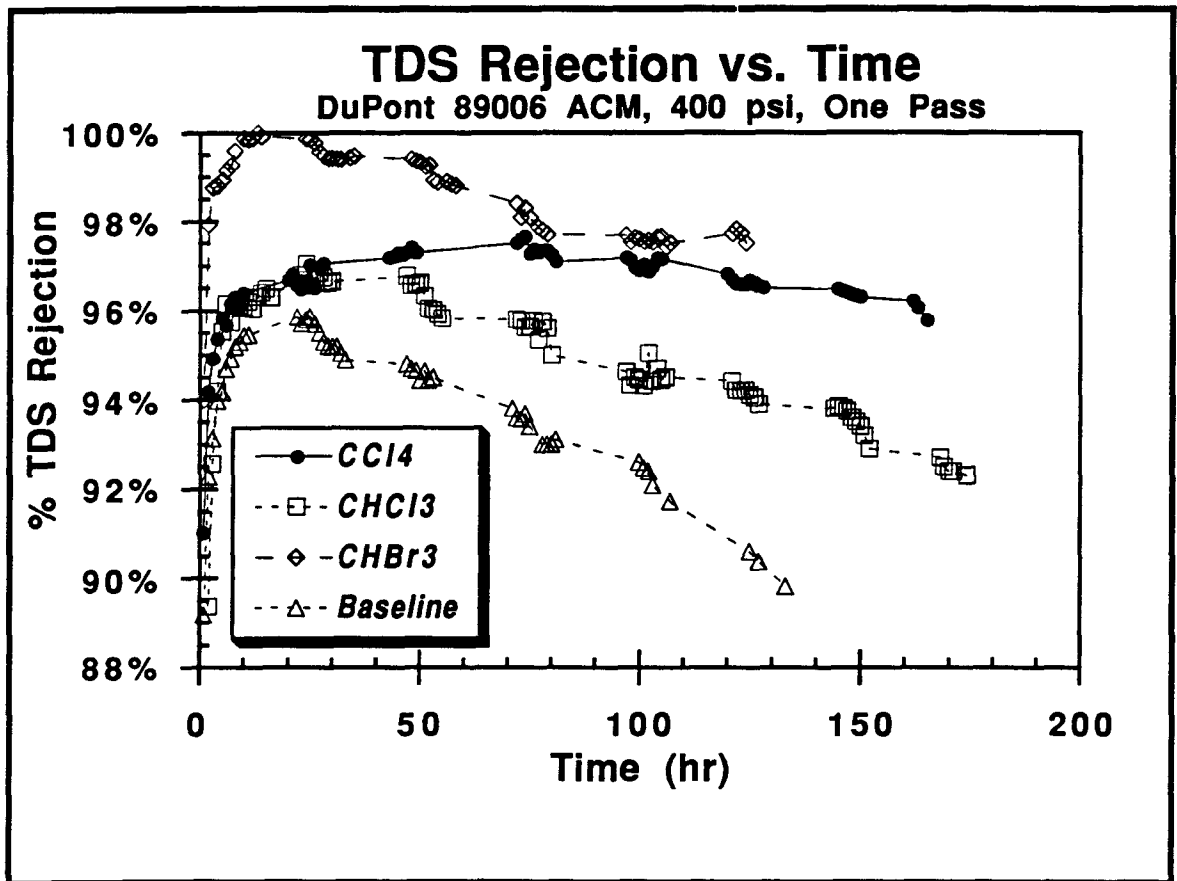


Figure 24: TDS Rejection vs. Time for DuPont 89006 ACM

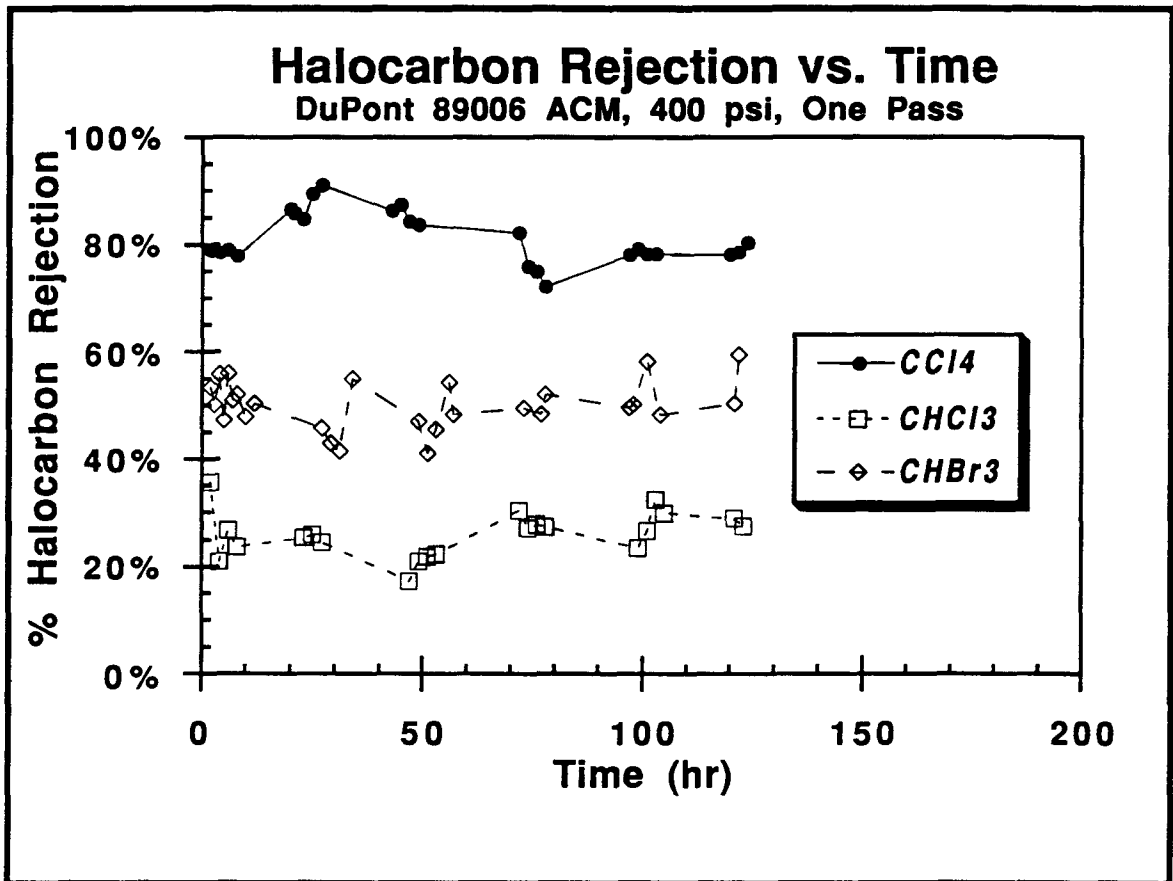


Figure 25: Halocarbon Rejection vs. Time for DuPont 89006 ACM

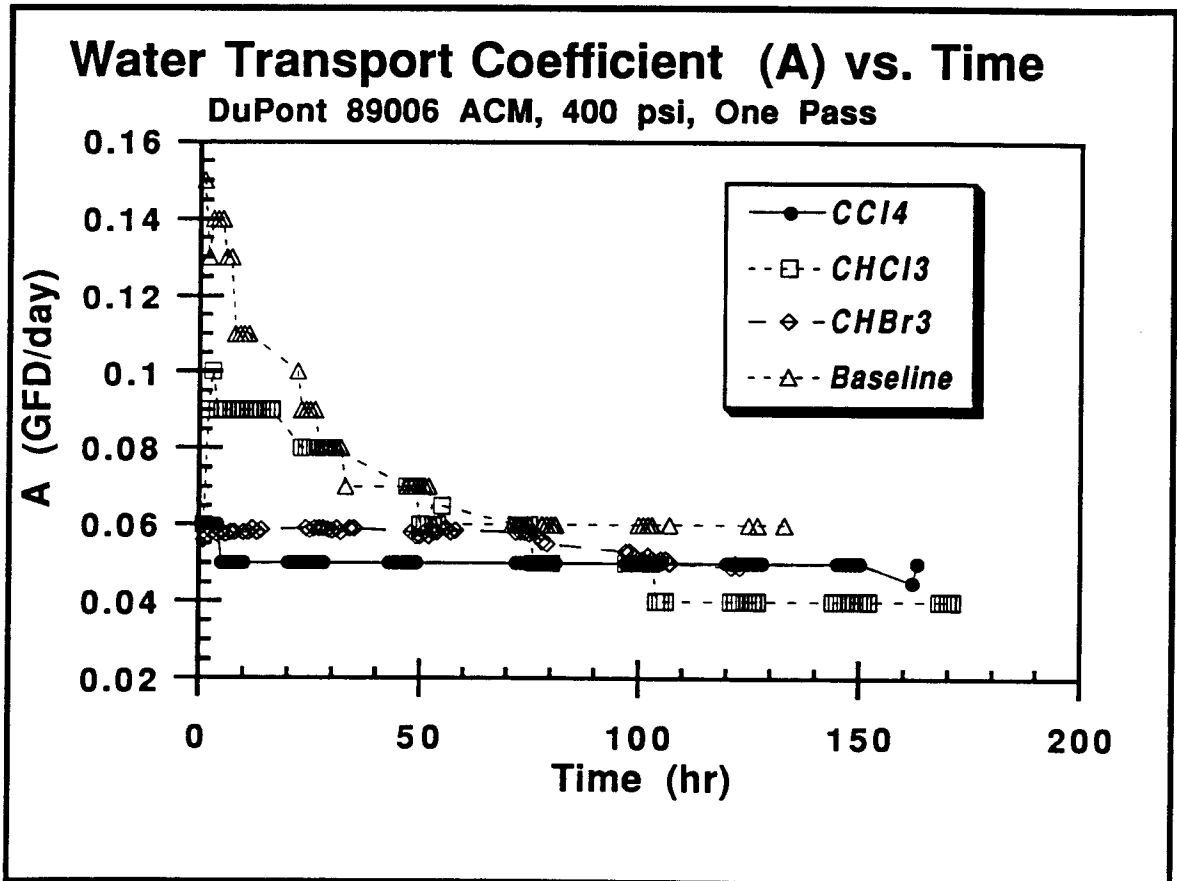


Figure 26: Water Transport Coefficient (A) vs. Time for DuPont 89006 ACM

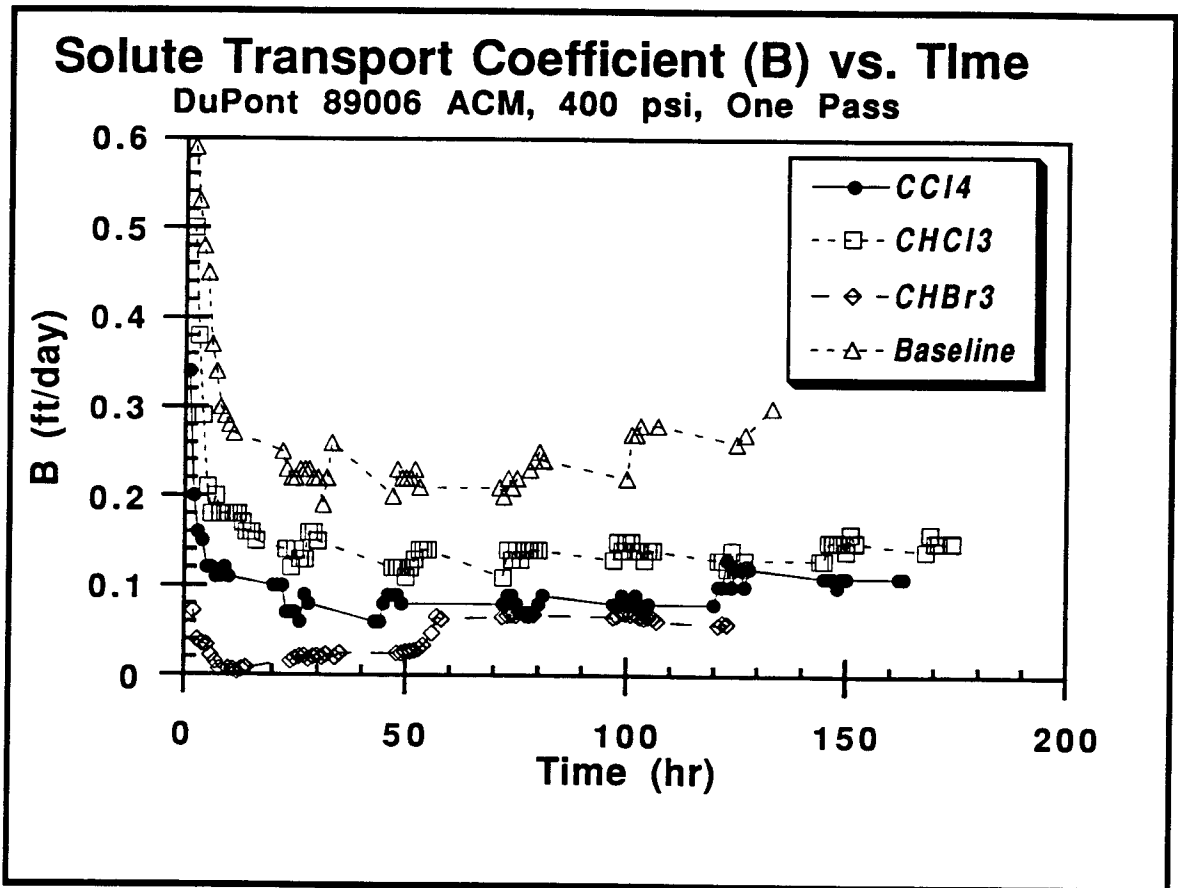


Figure 27: Solute Transport Coefficient (B) vs. Time for DuPont 89006 ACM

for CHBr_3 , CCl_4 , CHCl_3 , and baseline are 0.064 ± 0.003 , $0.085 \pm .005$, 0.139 ± 0.015 , and $0.28 \pm .01$ ft/day, respectively. This data reinforces the TDS rejection trends presented in Figure 24.

Fouling Reversibility Tests

Fouling reversibility test data performed on AC membranes are presented in Figures 22 to 27. The membranes were subjected to 50 mg/L of halocarbon during the first 125 hours, after which the halocarbon feed pump was shut off. Between 125 and 175 hours, the final shutdown, the membranes were exposed to only tapwater. If fouling was reversible, increases in flux and rejection would have occurred. In these figures, no visible increase in volume and TDS rejection data could be detected from the previous 125 hours. The conclusion is halocarbon fouling is irreversible with AC membranes under these conditions. One possible method to recover performance is to flush the membrane with a polar solvent such as an alcohol; this was not tried in our experiments.

Membrane/Halocarbon Partition Coefficients

Figure 28 presents data for the dependence of the partition coefficient K_s on halocarbon concentration with DuPont's CA membrane. The membranes were soaked for 10 days before extraction and K_s values were calculated according to Equation 11. These data show the partition coefficient is nearly constant above halocarbon concentrations of 250 mg/L. In the region where K_s is not concentration dependent, the partition coefficients for CHBr_3 , CHCl_3 and CCl_4 are 0.46 ± 0.02 , 0.32 ± 0.02 , and 0.09 ± 0.01 . This shows CHBr_3 partitions 30% greater than CHCl_3 and 80% greater than CCl_4 into the CA membrane. These

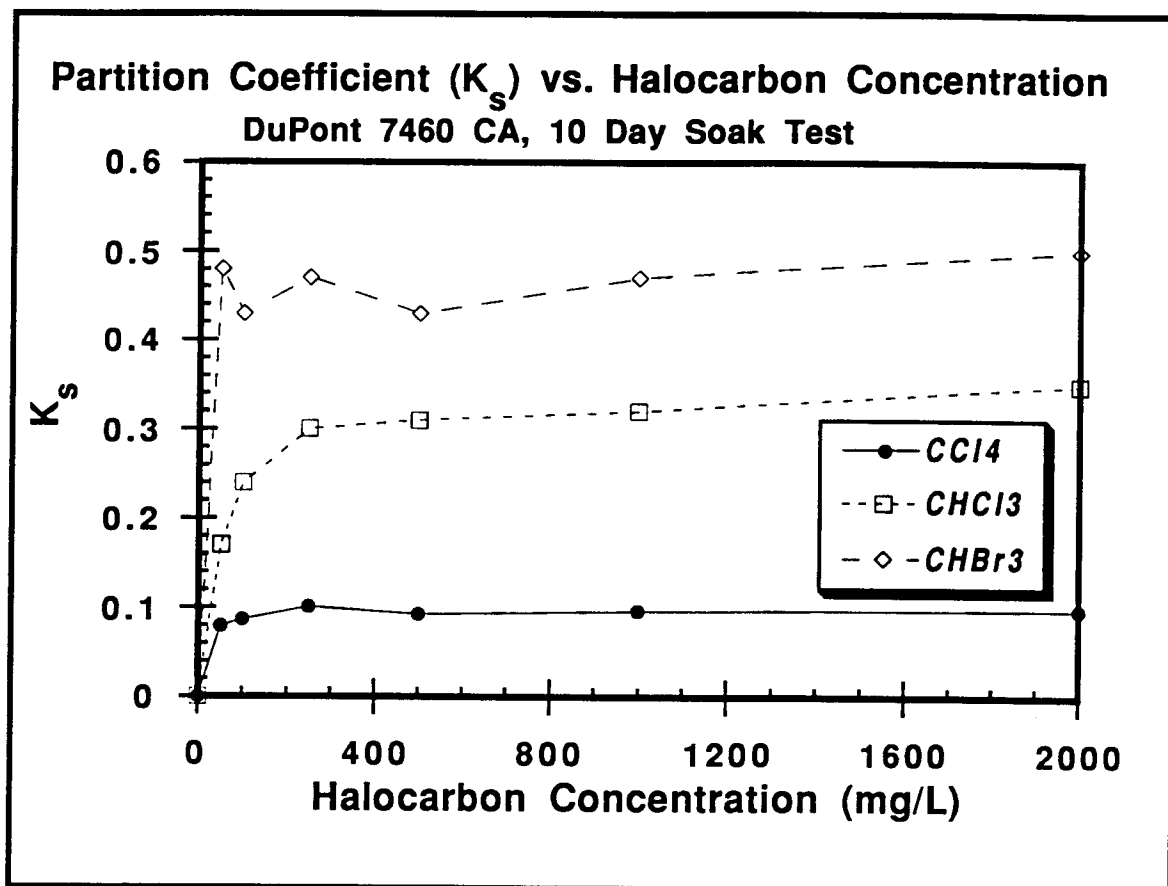


Figure 28: K_s vs. Halocarbon Concentration for DuPont's CA Membrane

data also show haloforms prefer the solution phase to the membrane phase since all the K_s values are significantly less than 1.

Figure 29 shows partition coefficient K_s vs. halocarbon concentration using DuPont's PA membrane; this graph and Figure 28 are very similar. None of the halocarbons partition strongly into the PA membrane; the value for CHBr_3 with an external concentration of 2,000 mg/L is 0.36 which indicates these halocarbons partition more into the solution phase than the membrane phase. Again, the halocarbon partitioning order is CHBr_3 partitions greater than CHCl_3 which partitions greater than CCl_4 into the PA membrane. The concentration independent region appears to start above a halocarbon concentration of 500 mg/L; the values for CHBr_3 , CHCl_3 , and CCl_4 in this region are 0.36 ± 0.02 , 0.24 ± 0.02 , and 0.02 ± 0.001 . This indicates CHBr_3 partitions 33% more than CHCl_3 and 94% more than CCl_4 into the PA membrane. Comparisons between CA and PA data show the halocarbons consistently partition greater into the CA membrane.

Figure 30 shows partition coefficient K_s vs. halocarbon concentration using DuPont's AC membrane. Halocarbons partition more strongly into the AC membrane than either CA or PA. The halocarbon partitioning order changes slightly with $\text{CHCl}_3 > \text{CHBr}_3 > \text{CCl}_4$. No concentration independent region exists; for comparison purposes we will use the average values above 500 mg/L halocarbon concentration. The values for CHCl_3 , CHBr_3 and CCl_4 here are 2.49 ± 0.23 , 1.82 ± 0.29 , and 0.72 ± 0.06 . This indicates CHCl_3 partitions 27% greater than CHBr_3 and 71% greater than CCl_4 into the AC membrane.

Figure 31 presents a comparison between the K_s values for the three halocarbons with CA, PA, and AC membrane at halocarbon levels of 2,000 mg/L. This graph shows AC membrane adsorbs halocarbons much more

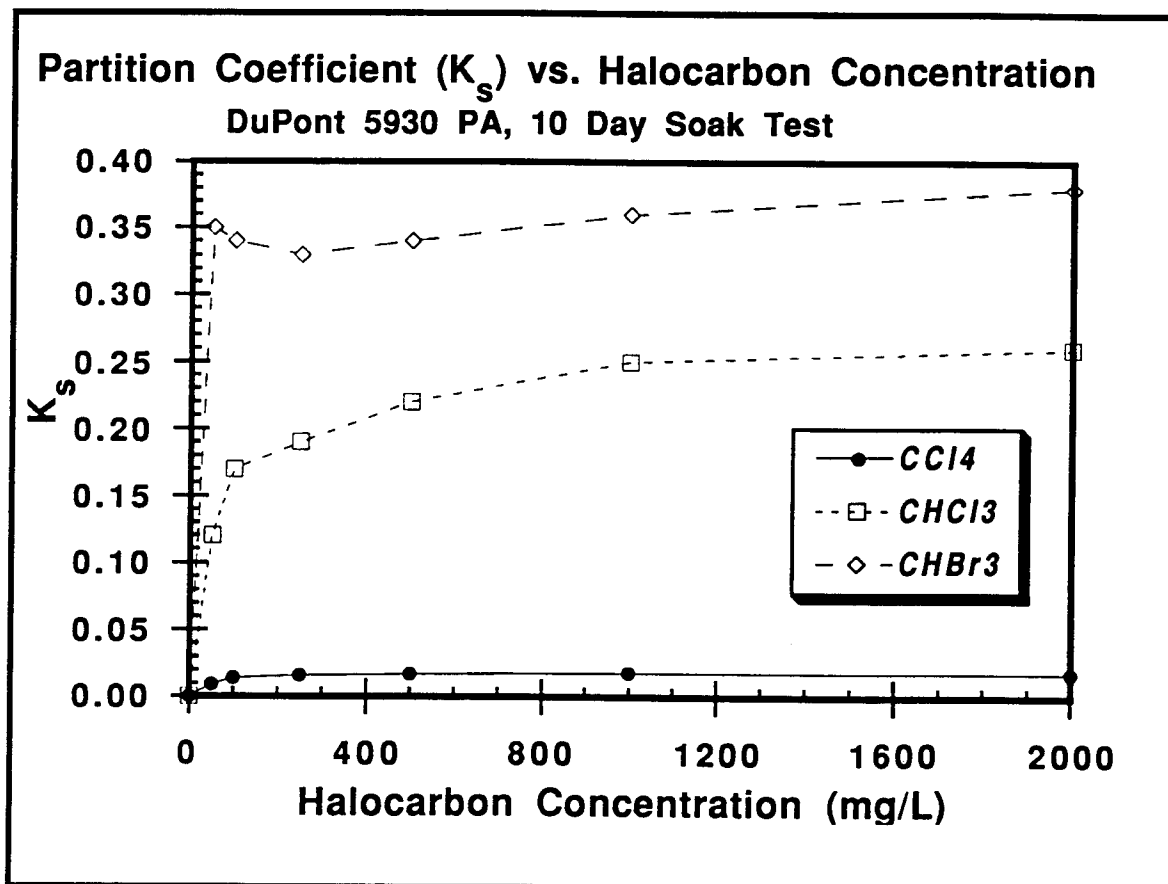


Figure 29: K_s vs. Halocarbon Concentration for DuPont's PA Membrane

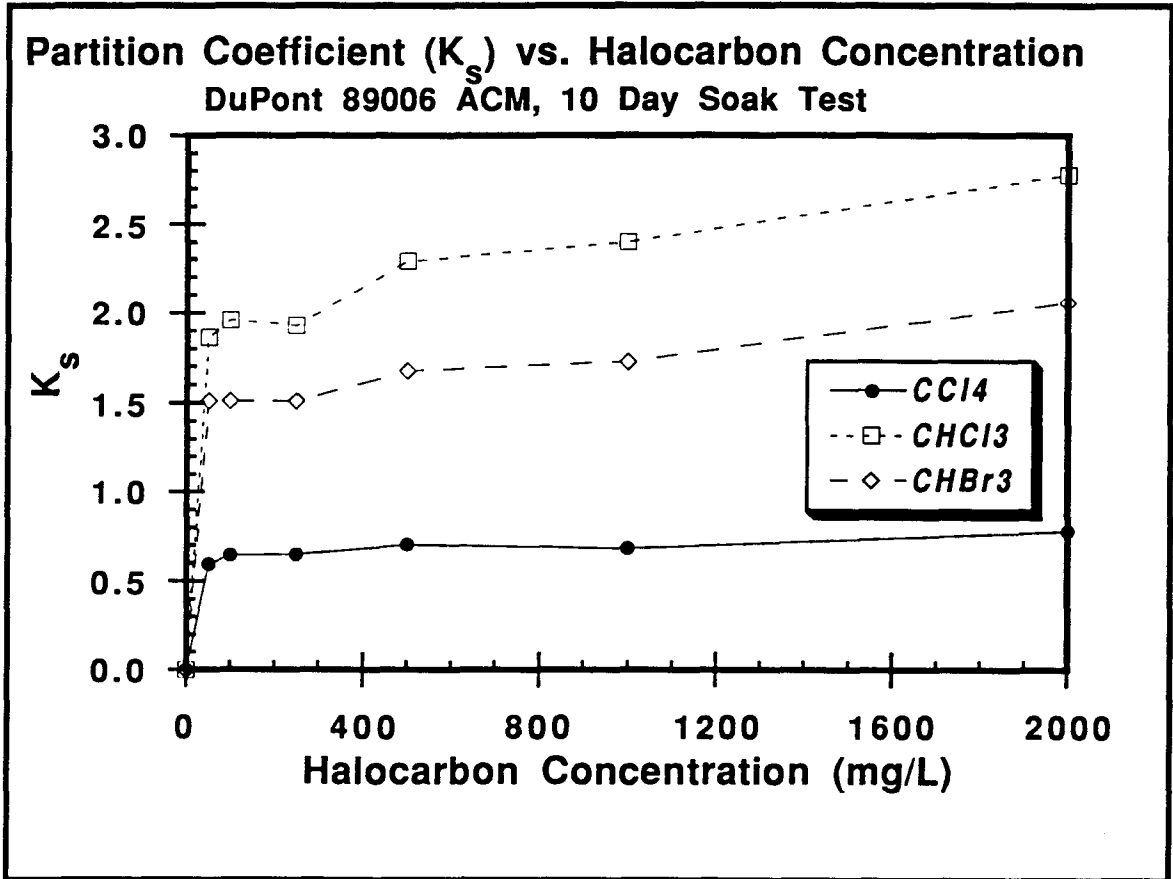


Figure 30: K_s vs. Halocarbon Concentration for DuPont's AC Membrane

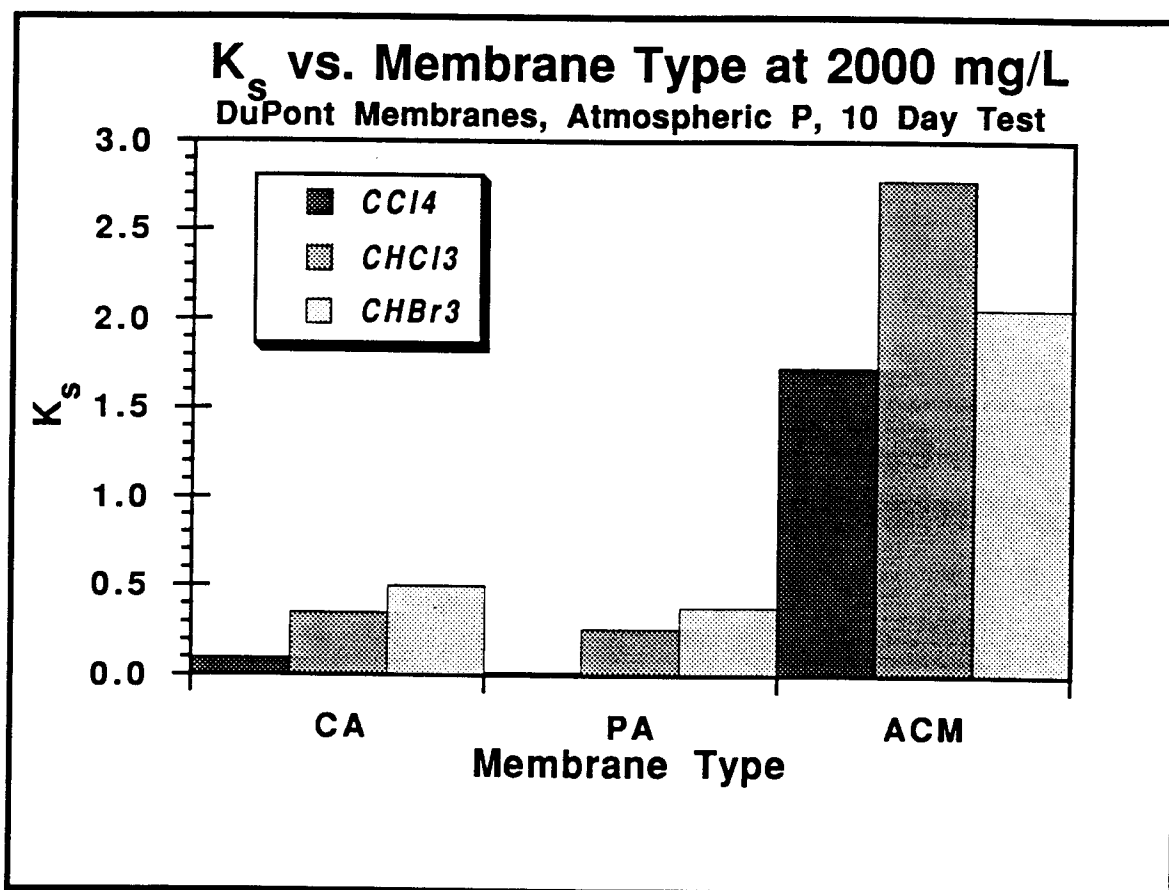


Figure 31: Comparison of K_s for DuPont Membranes

strongly than either CA or PA membranes which adsorb halocarbons almost equally. We noted before that AC membrane rejects halocarbons better than either CA or PA membranes. From this graph, it seems AC membrane is not rejecting the halocarbons; instead ACM adsorbs the halocarbons.

Void Fraction Tests

Figure 32 shows the results obtained from void fraction vs. halocarbon concentration test. The points presented were calculated by using Equations 12 and 13. As may be seen, each membrane's void fraction decreased with increasing halocarbon concentration. If we examine Equation 12, the decrease in ϵ may occur as a result of a decrease in numerator ΔV or an increase in the denominator $1 + \Delta V$. If the numerator represents the membrane void volume and the denominator is the total membrane volume, including the voids, and if we assume total membrane volume remains constant over the course of the experiment, the decrease in ϵ may be attributed solely to the decrease in the void volume. If the previous assumption holds true, then the addition of halocarbons cause the void volume in the membranes to shrink. This observation supports the theory that halocarbon fouling causes membrane swelling which reduces the size of water passage channels in the membrane.

The data show that all three void fractions decreased with halocarbon addition. A comparison between the void fractions at 0 mg/L and 2,000 mg/L halocarbon addition show the percentage decreases for AC, CA, and PA membranes to be 50%, 40%, and 23%, for one sample of each membrane, respectively. This indicates AC membrane's void fraction is reduced the most by halocarbon addition while PA's void fraction is decreased the least. This trend parallels the pattern shown in the halocarbon uptake experiments where ACM

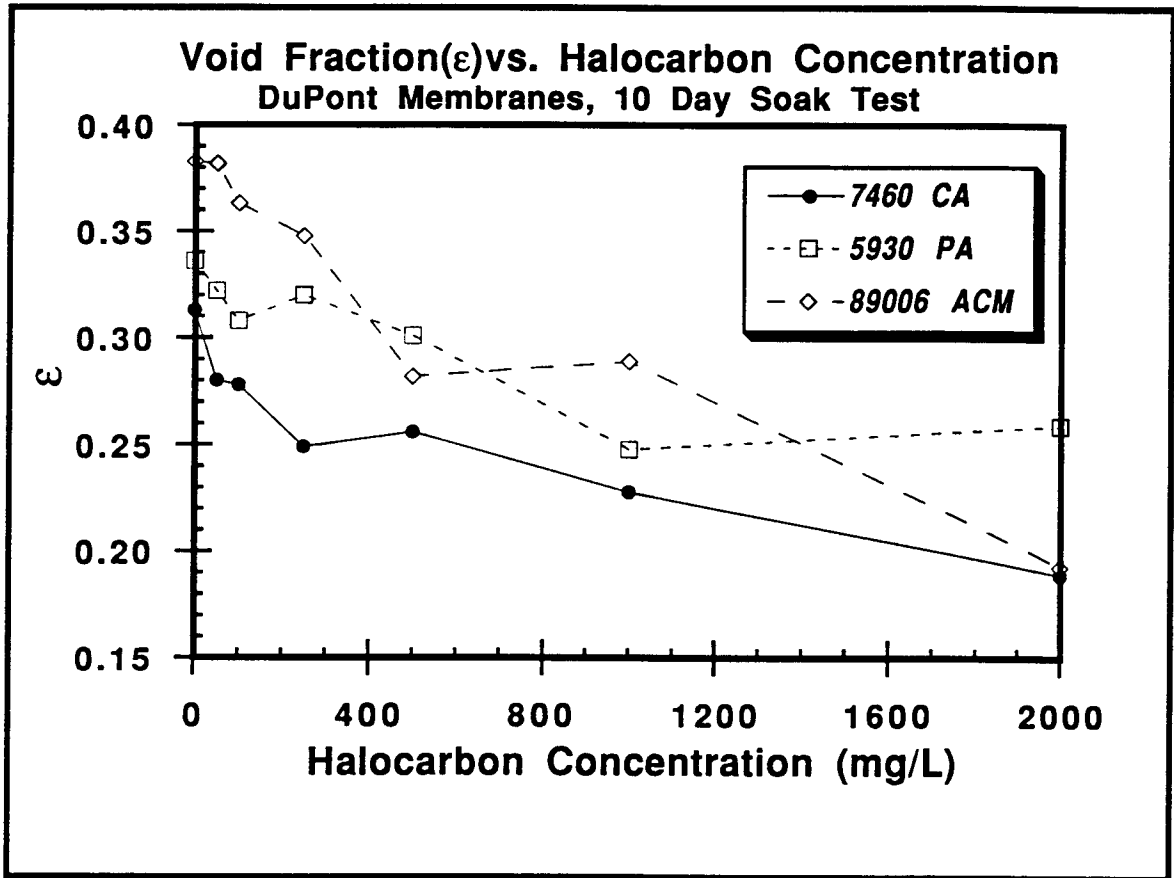


Figure 32: Void Fraction vs. Halocarbon Concentration for DuPont Membranes

adsorbed the greatest amount of halocarbon and PA adsorbed the least. Based on this data, one might conclude the decrease in membrane void fraction is attributable to the membranes' halocarbon uptake capabilities.

Membrane Performance Summary

Figure 33 shows total product volumes collected at 125 hours for all three membranes and Figure 34 shows the percent change from baseline which occur upon halocarbon addition. The AC membrane yields higher fluxes than either CA or PA but is affected more by halocarbon addition. CA has the lowest baseline flux and is affected the least by halocarbon addition. CHBr_3 affects all three membranes equally by decreasing product volume collected by approximately 20%. In addition, both CHBr_3 and CHCl_3 decrease PA and AC membranes' flux by 20%.

Figure 35 shows TDS rejection at the end of the 125 hour test period and Figure 36 shows percent change from baseline TDS rejection caused by halocarbon addition with the membranes. CA shows the best baseline TDS rejection followed by PA and AC membranes. Halocarbon addition improves TDS rejection slightly for CA membrane, ranging from 1 to 1.5% increase, while AC membrane's TDS rejection characteristic improved by 4 to 8%. Additions of both CHBr_3 and CCl_4 decreased PA's TDS rejection capabilities. These two figures show flux decreases are accompanied by TDS rejection increases except for PA membrane; this supports the membrane fouling hypothesis caused by membrane swelling.

Figure 37 shows average halocarbon rejection for the three membranes. CA shows the worst halocarbon rejection of the three membranes with a maximum rejection for CCl_4 of 32%. PA rejects the two THM's poorly at less than 12% but

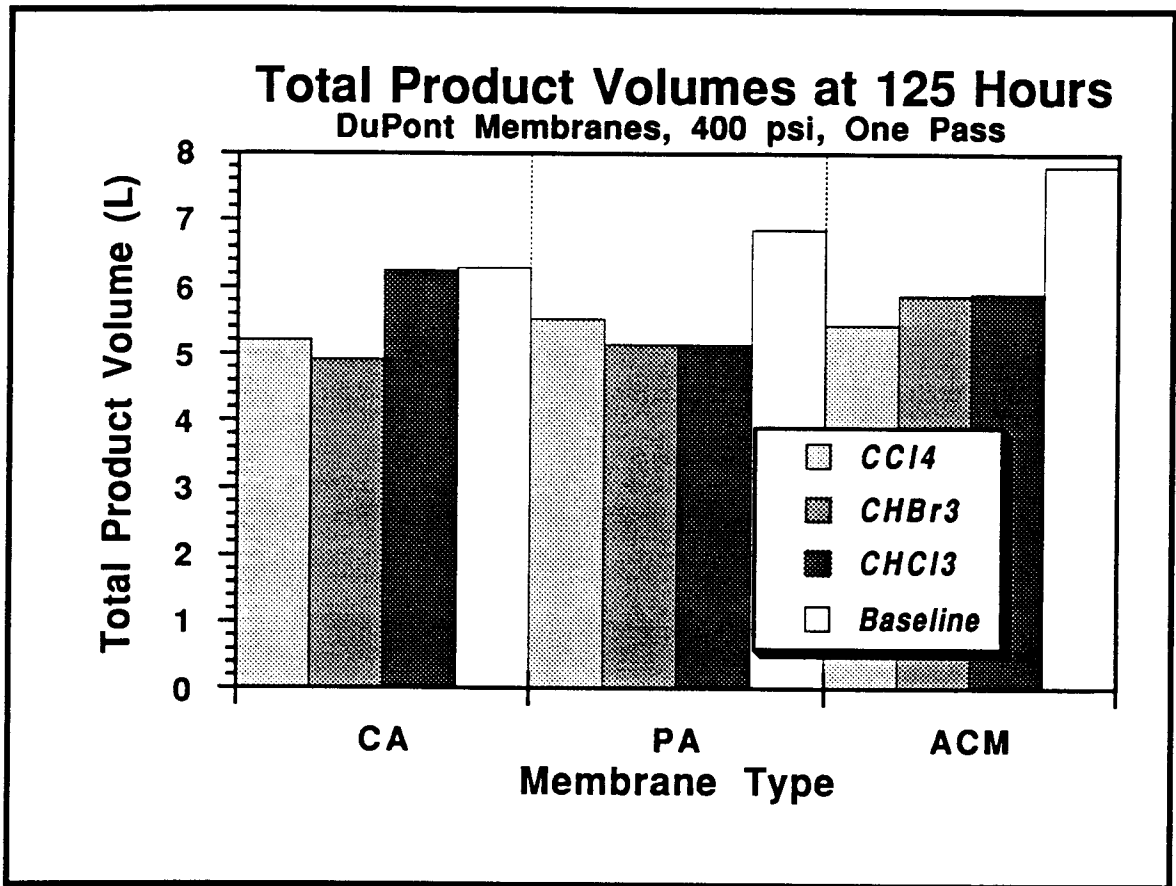


Figure 33: Total Product Volumes at 125 Hours for CA, PA, and AC Membranes

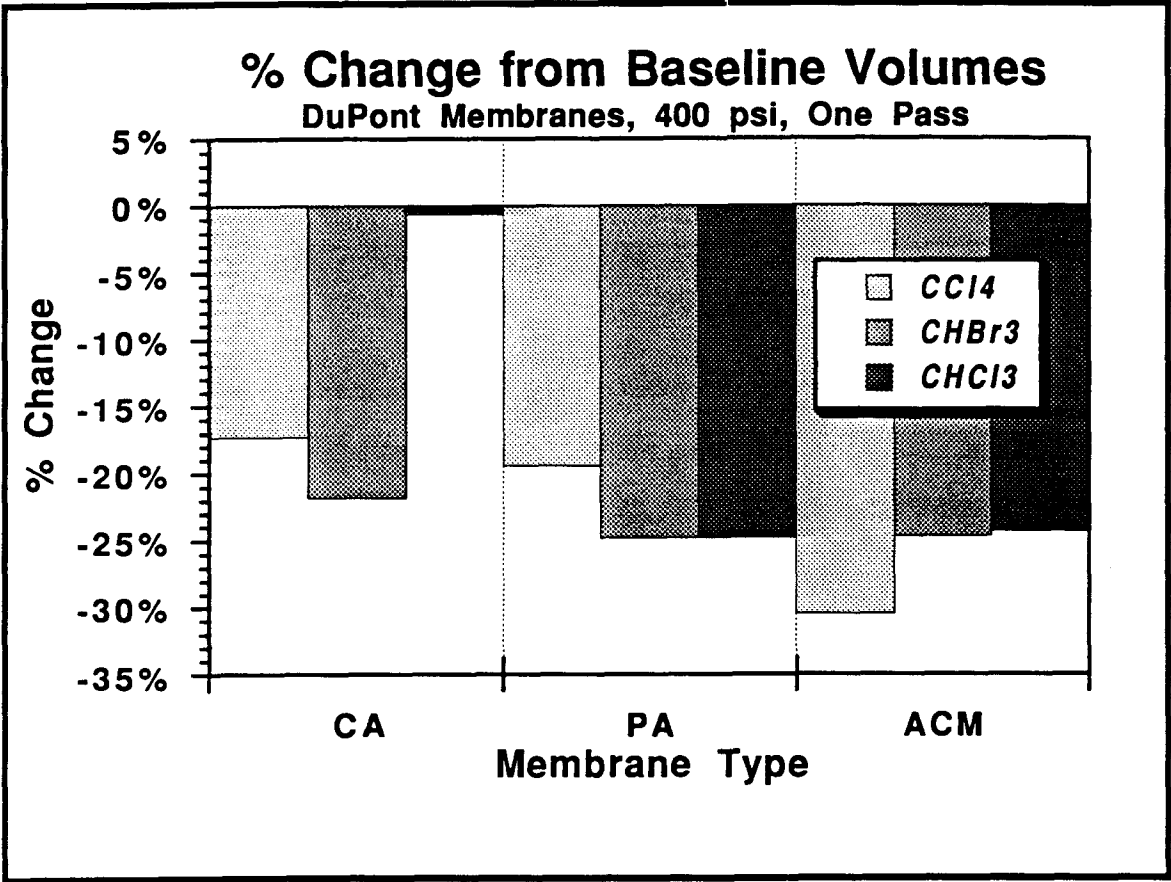


Figure 34: % Change from Baseline Volumes for CA, PA, and AC Membranes

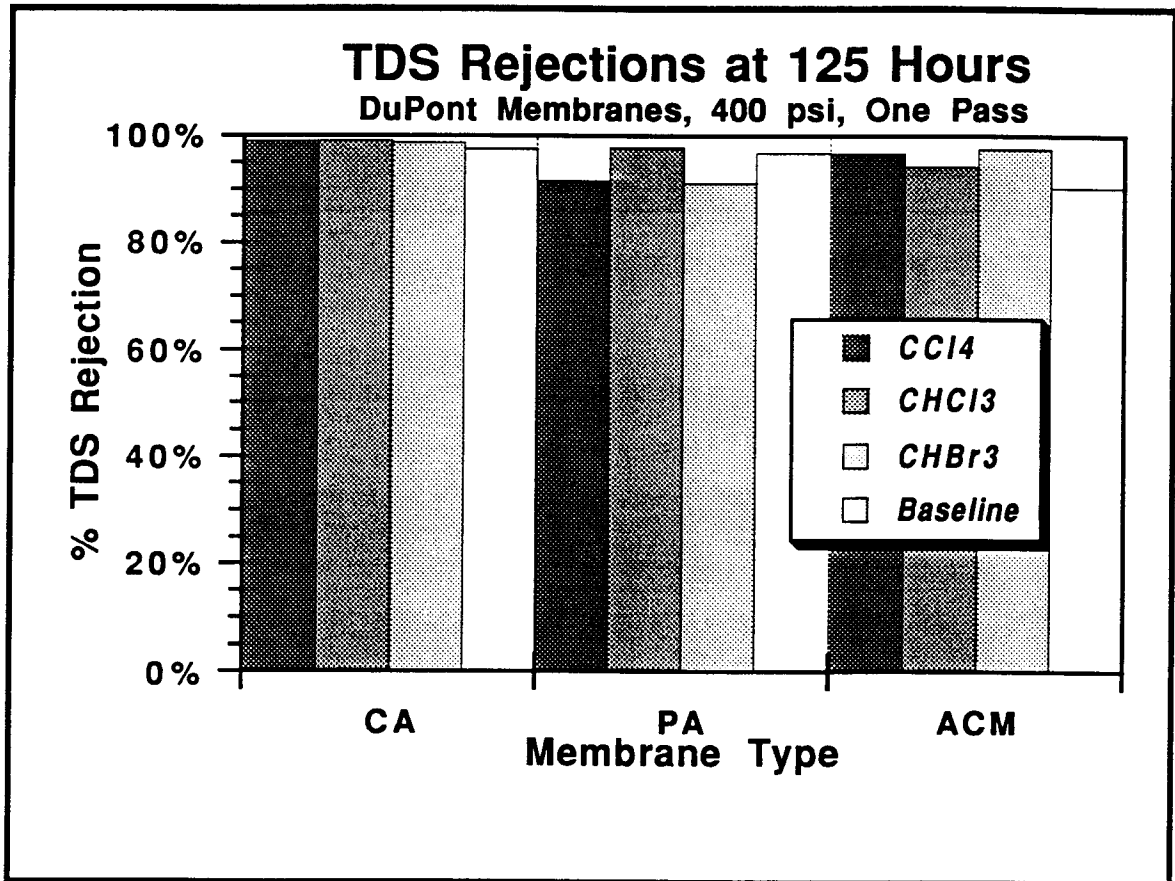


Figure 35: TDS Rejections at 125 Hours for CA, PA, and AC Membranes

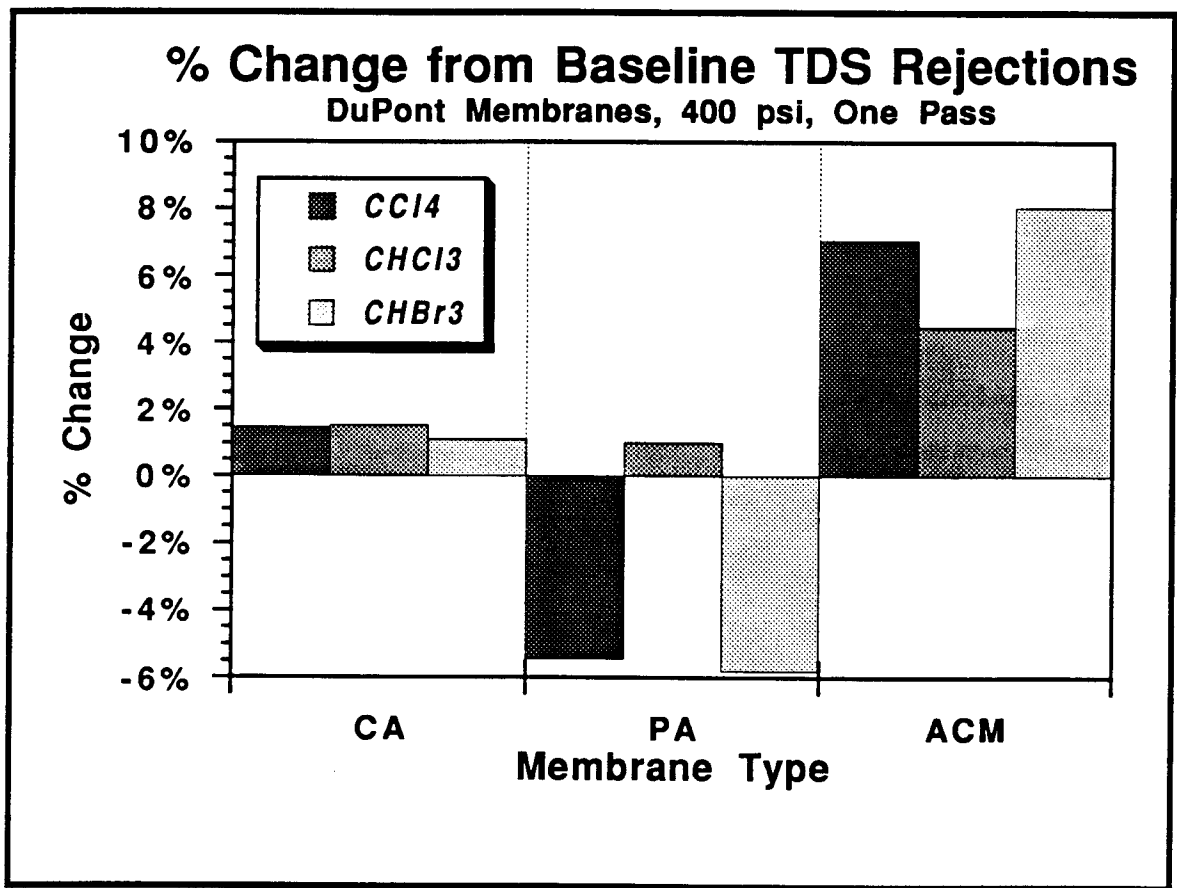


Figure 36: % Change from Baseline TDS Rejections for CA, PA, and AC Membranes

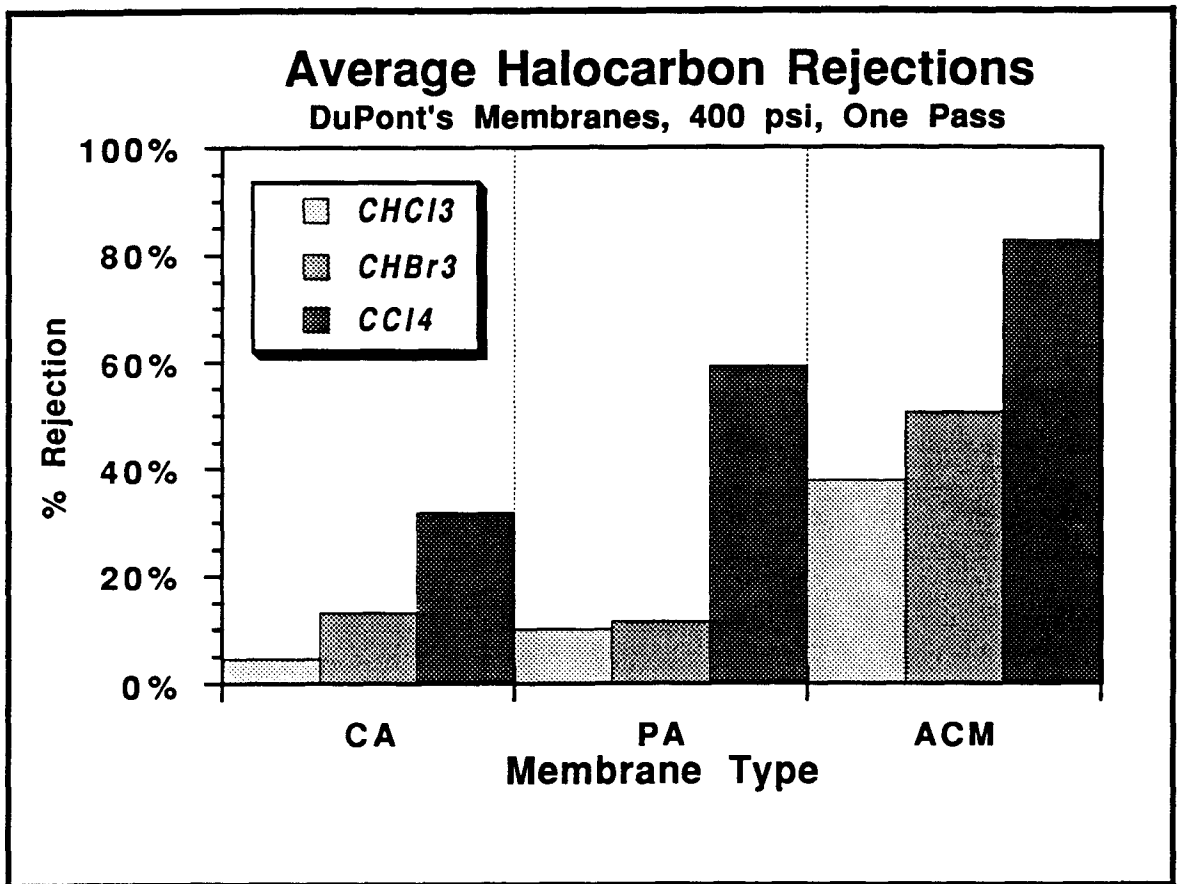


Figure 37: Average Halocarbon Rejections for CA, PA, and AC Membranes

it rejects CCl_4 well at approximately 60%. ACM shows the best halocarbon rejection, ranging from 38% for CHCl_3 to 83% for CCl_4 . In each case, CHCl_3 is rejected the least and CCl_4 is rejected the most by each membrane. This observation supports the theory that larger molecules in this study of test compounds are rejected better than smaller molecules.

Organic Rejection vs. Dielectric Constant (ϵ)

Figure 38 shows the relationship between dielectric constant and percent organic rejection using DuPont's CA membrane. Data points for CHBr_3 and CHCl_3 were obtained from this experiment. The rest of the data were obtained from DuPont's literature (*Pohland, 1989*). This figure shows that as a compound's dielectric constant increases, i.e. worse insulators, its rejection decreases. Also, this figure shows that organic rejection does not just depend on its size.

Comparison of Different Membrane Types

Table VI shows comparisons between different membrane's log-log flux decline indices and K values. Membranes with higher initial flux values (K), such as AC and PA membranes, have higher flux decline coefficients than lower flux membranes such as CA. Flux decline coefficients were in the following order, $\text{ACM} > \text{PA} > \text{CA}$, for all cases. This indicates the addition of halocarbons affected AC membrane more, i.e., faster flux decline than either CA or PA membranes. The phenomena of high flux membranes fouling faster than low flux membranes has been documented previously (*Beckman, 1973*).

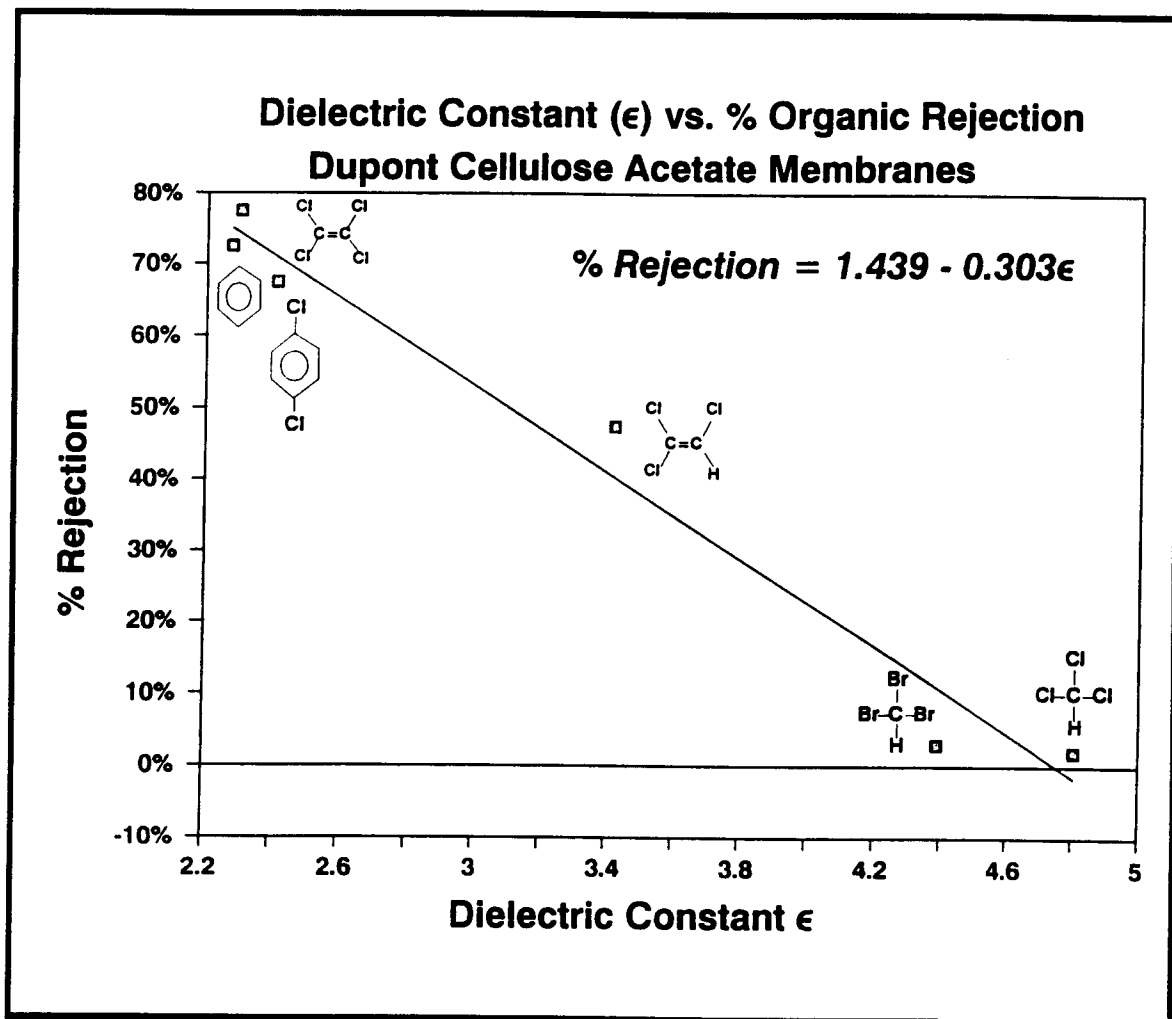


Figure 38: Dielectric Constant ϵ vs. % Organic Rejection

Table VI: Comparison of m and K values for CA, PA, and AC Membranes

Condition	m CA	m PA	m ACM	K (GFD) CA	K (GFD) PA	K (GFD) ACM
Baseline	-0.0185 ± 0.0033	-0.0923 ± 0.0076	-0.178 ± 0.007	23.69 ± 0.34	29.43 ± 2.20	33.91 ± 2.28
CHCl ₃	0.0645 ± 0.0018	-0.0247 ± 0.0053	-0.090 ± 0.001	21.24 ± 0.75	21.94 ± 1.03	23.96 ± 2.73
CHBr ₃	-0.0738 ± 0.0017	-0.0589 ± 0.0059	-0.006 ± 0.003	19.05 ± 0.31	22.40 ± 1.23	22.04 ± 0.05
CCl ₄	0.0237 ± 0.0068	-0.0002 ± 0.0095	-0.052 ± 0.006	19.52 ± 0.92	24.43 ± 2.11	20.30 ± 1.19

Comparison of Experimental and Literature m Values

Table VII presents comparisons of our experimental m values with values obtained from literature for CA-type membrane. As may be seen, the m values obtained in our experiment are much larger than ones obtained from the literature, signifying higher flux declines. The water used as feed for the Kaakinen experiment was actual Colorado River water from Yuma while the water used in the Milstead paper was a synthetic feed mixed up to simulate the conditions for the feedwater at Yuma. The duration of the Milstead test was approximately 530 hours or 22 days (*Milstead, 1982*) and the Kaakinen tests lasted between 484 and 1829 hours, averaging 76 days (*Kaakinen, 1985*). Table VII also shows flux decreases from baseline upon CHBr_3 addition for the three experimental time periods. Although there is a large variation in this comparison due to different feedwater conditions and membranes used, Table VII nevertheless serves to illustrate higher flux declines occur at higher halocarbon concentrations.

FTIR Results

Table VIII shows the absorption bands and characteristic groups which were examined experimentally. From analysis performed on the CA membrane, some changes in FTIR scans are observed with both CHCl_3 and CHBr_3 additions. If structural changes occur either *new* absorbance peaks would show up or the *sizes* of the existing absorbance peaks would change. For CA membranes, one would expect any reactions to occur in either the hydroxyl groups or in the carbonyl groups.

Figures 39 to 41 show typical scans obtained from FTIR analysis. Every

Table VII: Comparison of Experimental and Literature m Values for CA-Type Membranes

	<i>Milstead, 1982</i>	<i>Kaakinen, 1985</i>	<i>This Work, 1990</i>
Baseline m	-0.0012	-0.0284	-0.0185
CHBr ₃ m	-0.0076	-0.0610	-0.0721
CHBr ₃ conc.	10 mg/L	not given	50 mg/L
% change from baseline, 5 days	1.02 %	5.11 %	8.52 %
% change from baseline, 22 days	1.96 %	9.59 %	15.71%
% change from baseline, 76 days	2.73 %	13.17 %	21.30 %

Table VIII: Absorption Bands of Characteristic Groups
(from Socrates, 1980)

Absorption Bands (cm^{-1})	Vibrations Responsible
4500 - 4200	Aliphatic C-H stretch
4200 - 4000	Aromatic C-H stretch
3650 - 3100	O-H stretch
3550 - 3200	C=O stretch
3300 - 2500	O-H stretch on $\begin{array}{c} \text{O} \\ \\ \text{C-OH} \end{array}$ group
2950 - 2800	C-H stretch
1820 - 1630	C=O stretch
1445 - 1330	C-H bend
1320 - 1210	O-H stretch on $\begin{array}{c} \text{O} \\ \\ \text{R-C-OH} \end{array}$ group
1190 - 1070	C-O-C asymmetric stretch, saturated aliphatic ethers
995 - 980	C-H out of plane bending
880 - 785	Benzene ring vibration
750 - 595	C-Cl stretch
690 - 515	C-Br stretch

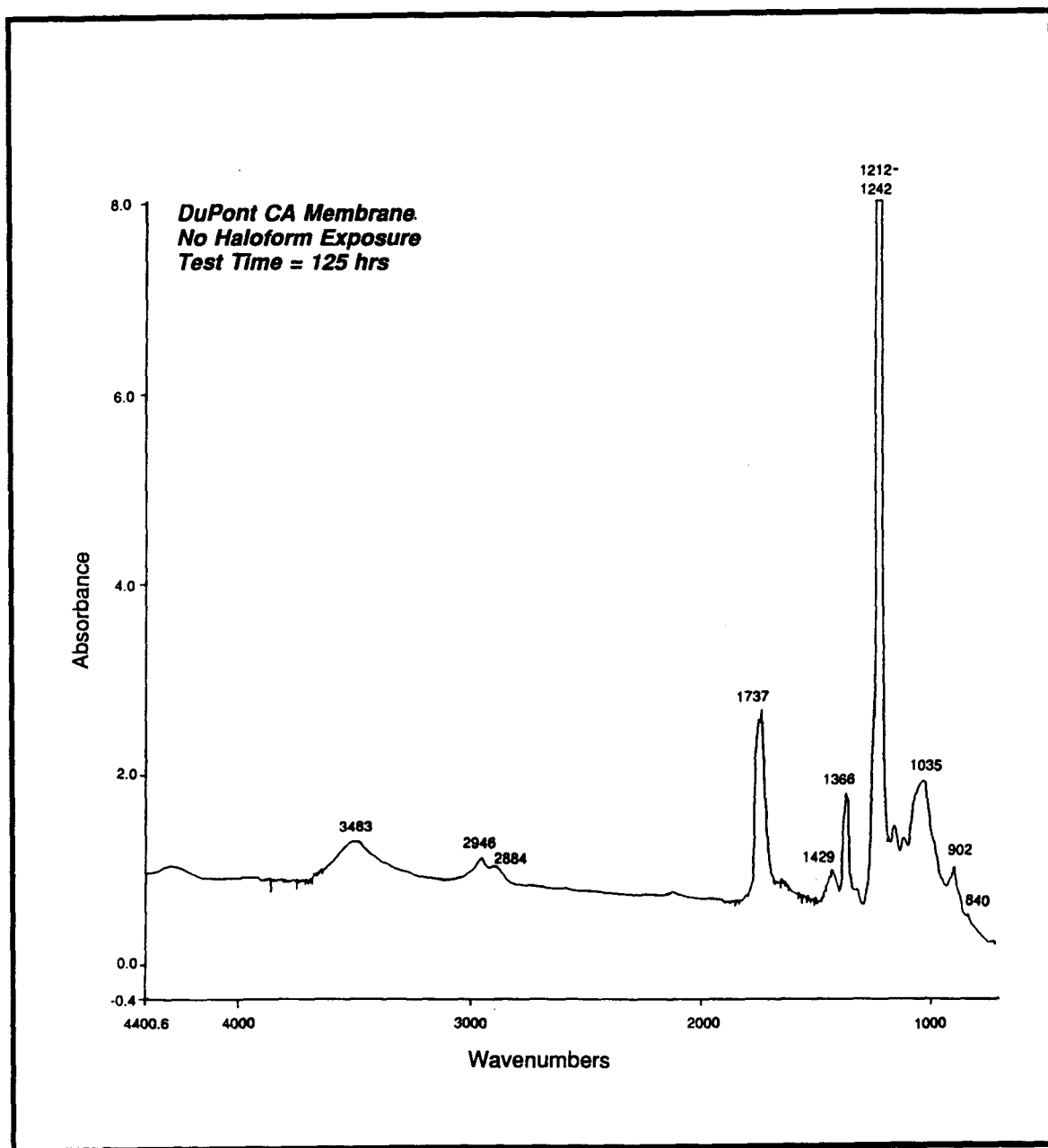


Figure 39: FTIR Spectrum for CA Membrane (Baseline)

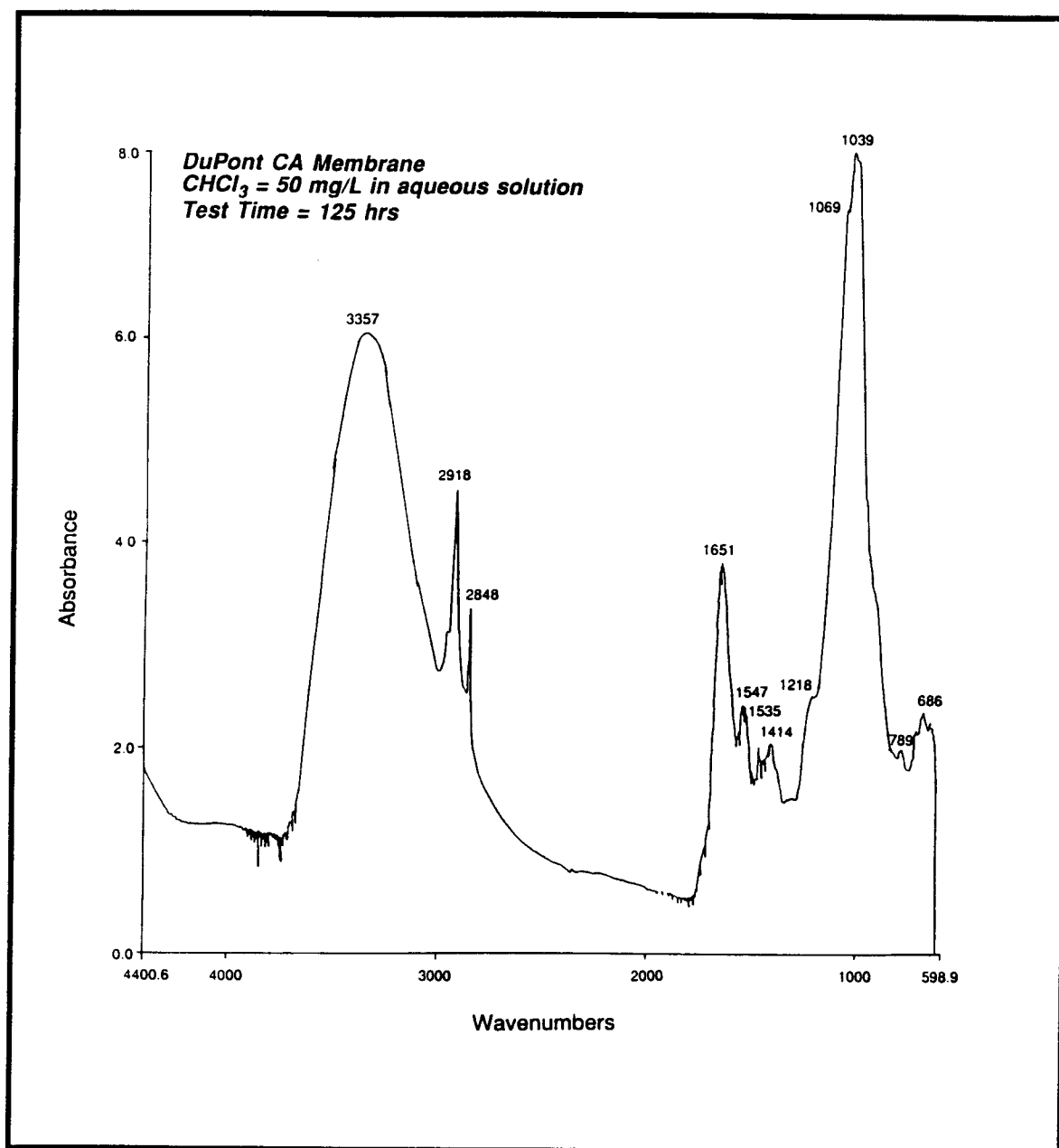


Figure 40: FTIR Spectrum for CA Membrane (CHCl_3 added)

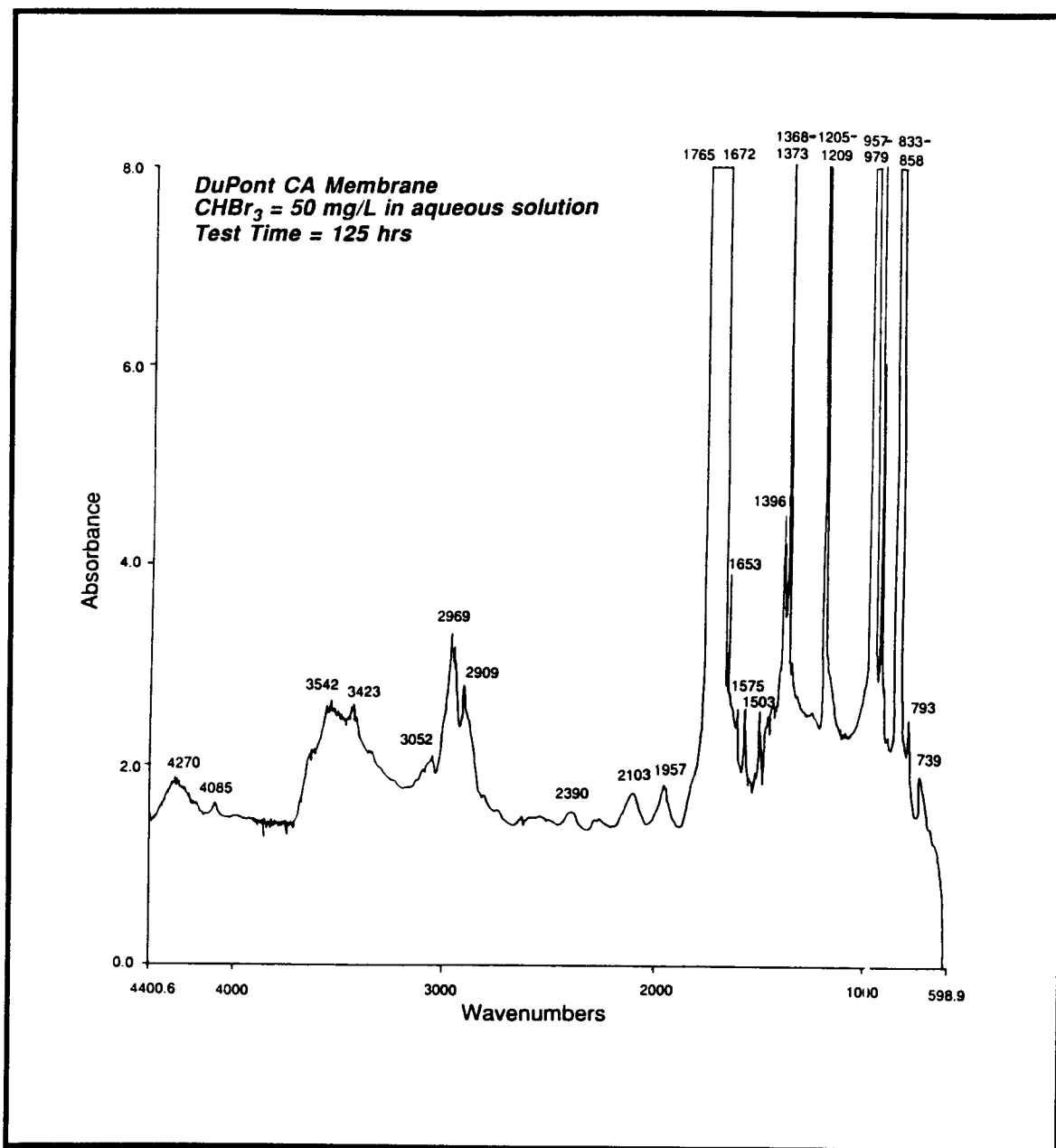


Figure 41: FTIR Spectrum for CA Membrane (CHBr₃ added)

major absorbance band was accounted for and was identified by Table VIII. Some changes in the *sizes* of the absorbance peaks were seen in Figure 40. In the sample with CHCl_3 added, increases may be seen in the O-H stretch region (3357 cm^{-1}) and in the C-O-C stretch region ($\sim 1039 \text{ cm}^{-1}$). The small peak in Figure 40 at 686 cm^{-1} may be accounted for by the C-Cl stretch in CHCl_3 . However, a strong decrease may be seen in the C=O stretch in the R-COOH group.

In comparing the spectra for the CHBr_3 added case and the baseline case, one may see some increases in C=O stretch (1765 cm^{-1}), C-H bend (1368 cm^{-1}), C-H out of plane bending (957 cm^{-1}), and benzene ring vibration (833 cm^{-1}). Two new peaks showed up, the C=O stretch (3542 cm^{-1}) and C=O stretch in COOH group (2969 cm^{-1}). Some changes in these spectra were observed; however, the weights of the samples used for the FTIR analysis was not known. Without these data, how much of the changes from the spectra are attributable to chemical bonding and how much of the changes are due to different sample weights may not be quantified.

NMR Results

NMR spectrometric analyses were performed on both dissolved CA and PA membranes. From the graphs obtained (not presented in this work), no new functional groups were seen with halocarbon addition. Each absorbance peak in the NMR scans for all the membranes exposed to halocarbons may be attributed to a normal functional group in the unexposed membrane. No new absorbance peaks were found in the scans, signifying no new bonds were formed. However, the dissolved form of these membranes may not exhibit the same chemical characteristics as the undissolved form. Hence, one has to be

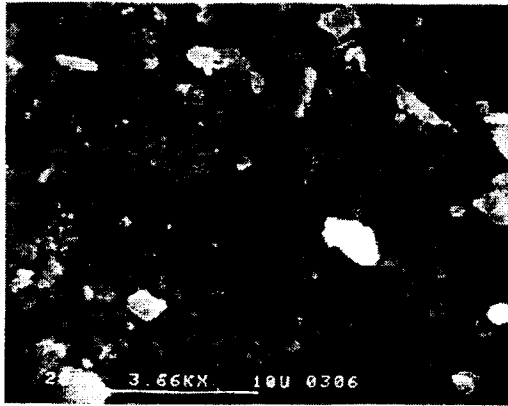
careful in drawing conclusions from this analysis.

Zachariah(1982) performed similar analysis on B-9, a PA polymer variation. In that work, benzanilide was exposed to Cl^- and Br^- . NMR scans were taken at regular intervals; it was found halogens attached to the *ortho*- and *para*-positions on the benzanilide rings. These attachments caused intramolecular hydrogen bond disruptions which led to membrane failure.

Chemical changes in the membrane are much less likely to occur with halocarbons since they are much less reactive than halogens. The NMR results show tentative results that no changes have occurred in the *dissolved* membrane samples with the addition of halocarbons. However, the question remains whether the dissolved samples exhibit the same chemical characteristics as the undissolved membrane samples.

SEM Results

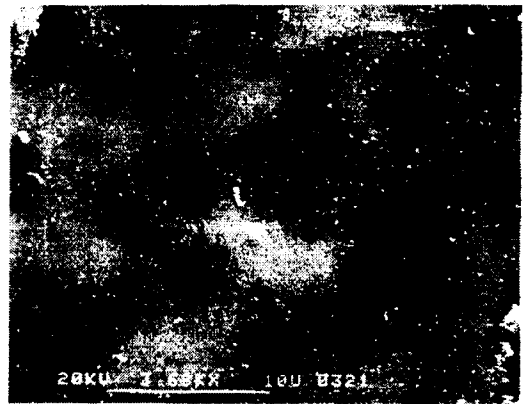
Figure 42 shows SEM photographs for an unused CA membrane, CA used in baseline testing, and CA exposed to CHBr_3 , CHCl_3 , and CCl_4 , respectively. These pictures are taken at 3670x magnification and an accelerating voltage of 20 keV. In comparing the unused and baseline test samples, the most striking difference is in pore sizes. The pores, represented as dark dots, are larger in the unused sample than in the used samples. This suggests that compaction from pressure has occurred. No change from the baseline sample is observable in the sample exposed to CHBr_3 . Some caking appeared on the surface of the sample exposed to CHCl_3 which indicates that fouling occurred. Sample cracks resulted from the fixation process that is used for SEM preparation, not from membrane defects. Some surface bacterial adhesion may be seen in the sample exposed to CCl_4 .



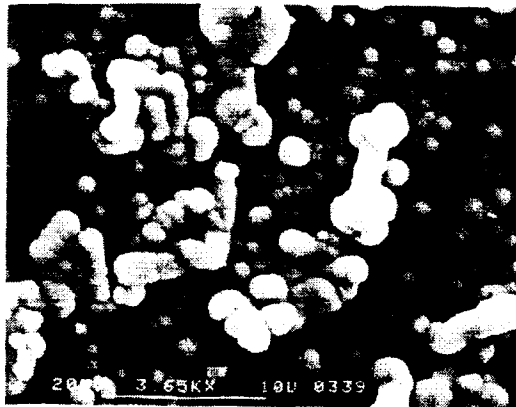
a) Unused



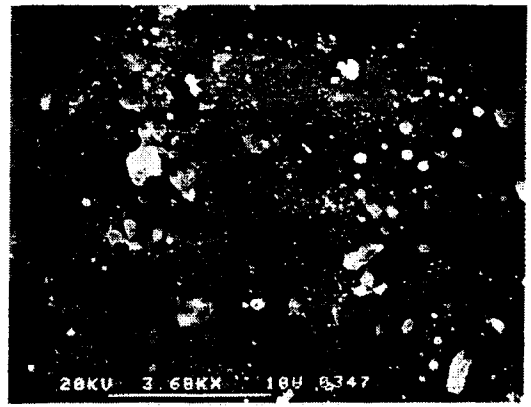
b) Baseline



c) CHCl₃ = 50 mg/L



d) CHBr₃ = 50 mg/L

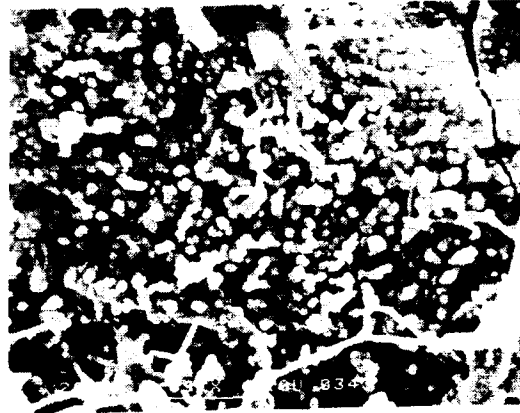


e) CCl₄ = 50 mg/L

Figure 42: SEM Photographs for CA Membrane, 3670x Magnification

Figure 43 shows SEM photographs for an unused PA membrane, PA used in baseline testing, and PA exposed to CHBr_3 , CHCl_3 , and CCl_4 , respectively. The experimental conditions are the same as for the CA membranes presented earlier. Visible differences between an unused sample and one used in baseline testing may be seen. Whereas the surface on the unused sample is smooth, the baseline test sample reveals depressions caused by pressure. The spheres are approximately 0.83 to 1.7 μm in diameter and differ in size due to depth of field; smaller spheres are further away from the microscope. The PA samples appear similar to sintered metals. Sintering is a technique which fuses spheres together to create a structure which has a high surface to volume ratio. PA membranes do not exhibit typical "pores" in the same manner as CA membranes. The sample exposed to CHBr_3 shows surface fungal growth and bacterial adhesion. This may account for decreases in solute and product water fluxes through the membrane. The sample exposed to CHCl_3 exhibited no apparent surface fouling but depressions are evident; the cracks present resulted from membrane fixation. Significant surface fouling is present in the PA sample exposed to CCl_4 , evident as white areas of the membrane. In this photograph, the top layer of spheres are no longer present; this suggests CCl_4 might have stripped away some of the bonds between top and bottom layers of the spheres.

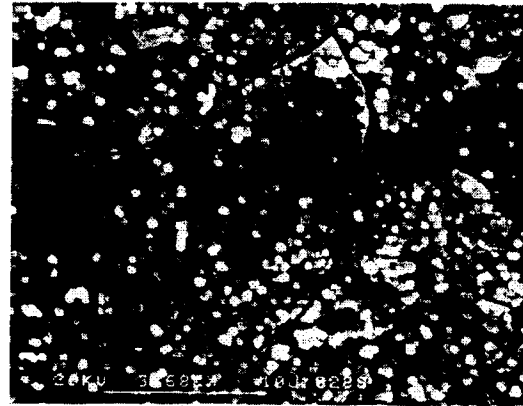
Figure 44 shows SEM photographs for an unused AC membrane, AC membrane used in baseline testing, and AC membrane exposed to CHBr_3 , CHCl_3 , and CCl_4 , respectively. Again, these pictures are all taken under the same conditions as CA and PA samples. The spheres are interconnected by polymeric strands and have uniform diameters of 2 μm . No surface fouling is evident in the samples exposed to CHBr_3 and CHCl_3 ; however, polymeric



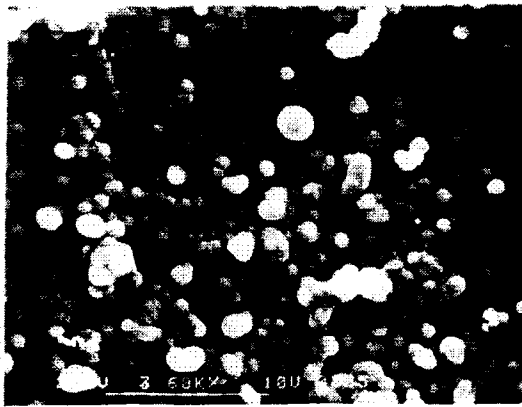
a) Unused



b) Baseline



c) CHCl₃ = 50 mg/L

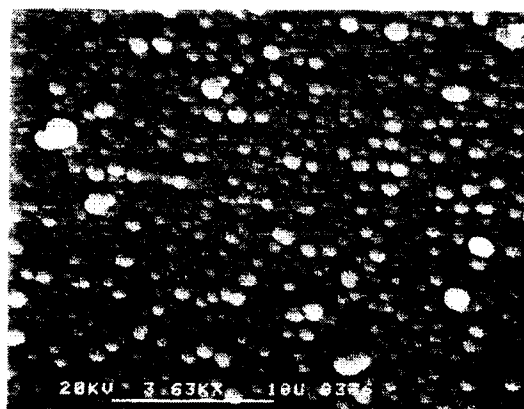


d) CHBr₃ = 50 mg/L

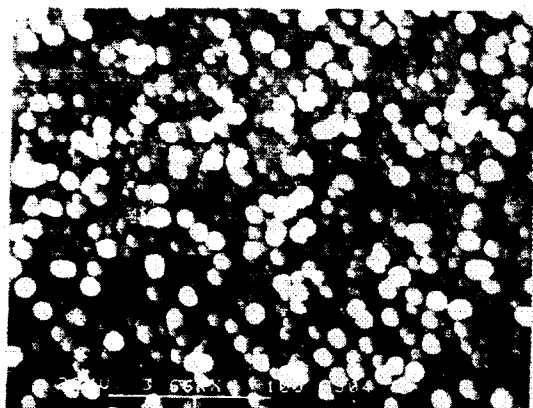


e) CCl₄ = 50 mg/L

Figure 43: SEM Photographs for PA Membrane, 3670x Magnification



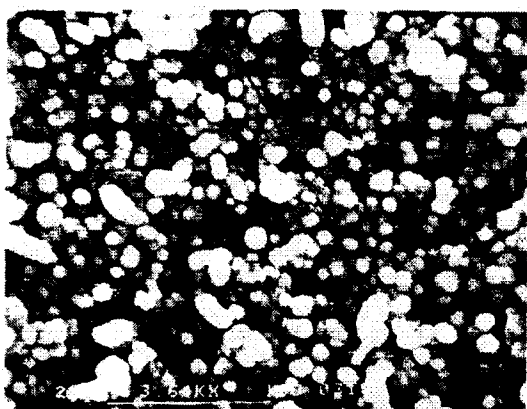
a) Unused



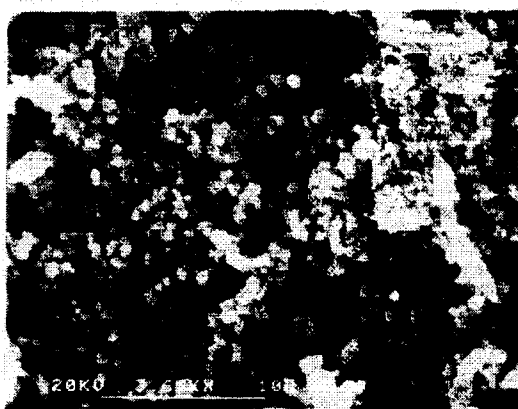
b) Baseline



c) CHCl₃ = 50 mg/L



d) CHBr₃ = 50 mg/L



e) CCl₄ = 50 mg/L

Figure 44: SEM Photographs for AC Membrane, 3670x Magnification

strands are no longer evident. This suggests some membrane dissolution may have occurred upon addition of these two chemicals.

As a further test of the ability of CCl_4 to dissolve the active layer of AC membrane, a piece of this type membrane was placed into a beaker of undiluted CCl_4 for one hour. At the end of this period, the membrane was removed and rinsed with DI water. After the rinsing, the membrane was placed into the membrane test apparatus and the water flux as well as TDS rejection were measured. The result showed the CCl_4 caused the membrane to be transparent to the solution, allowing both water and salts to pass through.

The membrane exposed to CCl_4 used for SEM examination was not the same sample used for testing as mentioned in previous sections. This sample failed after being on-line 100 hours. Membrane degradation is very evident in this ACM sample. The larger holes present in the photograph are the water transport holes beneath the active polymeric layer. The active layer appears to have been completely stripped away in some areas, thereby offering no resistance to water and solute transport. One explanation for the active layer stripping away is CCl_4 may dissolve the adhesive linking the active and porous backing layer. Once this occurs, water and solute flow may have roughed this sensitive area enough to create a hole. It is believed that this membrane sample was suddenly exposed to high CCl_4 concentration, thereby causing the failure.

11. Conclusions

The goals of this dissertation are threefold:

- 1) to examine if low weight molecular weight halocarbons cause membrane fouling/degradation,
- 2) to evaluate some hypotheses to account for the observed effects, and
- 3) to examine if fouling effects are reversible.

The four hypotheses proposed for membrane fouling/degradation effects are:

- 1) *Membrane swelling* resulting in decreased product flux and increased TDS rejection.
- 2) *Weak hydrogen bonding* resulting in increased product flow and decreased TDS rejection.
- 3) *Physical adsorption* resulting in decreased product flux and increased TDS rejection.
- 4) *Halocarbon attachment* to polymer resulting in decreased product flow and decreased TDS rejection.

The conclusions drawn from our experiments are as follows.

Flux Tests

The modified form of Merten's unsteady-state equation predicts product water volume as a function of time accurately for all cases with CA, PA, and AC membranes. The correlation coefficients between the predicted and actual data are in excess of 0.999.

High flux membranes such as AC foul faster than low flux membranes such

as CA with the same degree of pretreatment. Results from log-log flux decline parameter m evaluation show AC fouls most rapidly while CA fouls least rapidly; the exception to this trend is with addition of CHBr_3 where the order is reversed.

Organic Rejection

A correlation exists between an organic's dielectric constant ϵ and its rejection by RO membranes. Molecules with lower dielectric constant are rejected more strongly than molecules with higher dielectric constant in the case of CA membranes. Although we could not demonstrate this effect as conclusively for PA and AC membranes, this relationship holds since the rejection for all three membranes are in the same order: $\text{CCl}_4 > \text{CHBr}_3 > \text{CHCl}_3$. The order of the dielectric constants are as follows: $\text{CHCl}_3 > \text{CHBr}_3 > \text{CCl}_4$.

Halocarbon rejection also seem to depend on membrane structure and pore size. CA has the "loosest" and AC has the "tightest" structure due to varying degrees of cross-linking. CA has the largest pores while AC contains the smallest pores of the the three membranes. Our data indicate organics are rejected most strongly by AC and least strongly by CA.

Halocarbon Partitioning

Halocarbons partition the greatest into the AC membrane and equally for CA and PA membranes. CHBr_3 has the highest partition coefficient for both PA and CA membranes while CHCl_3 has the highest partition coefficient for AC membrane. Since a higher partition coefficient signifies higher adsorption, one would expect CHBr_3 to cause the most fouling on CA and PA and CHCl_3 to foul AC membrane the most. Comparing the values obtained for the log-log flux

index, we see this hypothesis is substantiated. In both CA and PA cases, CHBr_3 addition resulted in the lowest m values and CHCl_3 addition resulted in the lowest m value for AC membrane.

Membrane Fouling

Physical swelling

This hypothesis is substantiated by a combination of the void fraction tests and flux/TDS tests. The test results show decreasing void fraction with increasing concentrations of halocarbons. Also, AC void fraction decreased the most due to halocarbon addition; this is supported by the partition coefficient data which show halocarbons absorb into AC membranes.

Physical adsorption

This hypothesis is supported by partition coefficient tests as well as flux/TDS tests. We find greater partition coefficients signify greater fouling tendencies on the membrane (i.e. greater m values).

Weak hydrogen bonding

This hypothesis is not substantiated by the FTIR test. Although some changes may be seen in the sizes of the absorbances in the spectra, we may not conclude that the changes in the absorbance sizes are due to chemical changes since the membrane weight data were not known.

The NMR data shows no changes in the functional groups for the *dissolved* membrane samples in the cases of halocarbon exposure compared to the baseline cases. However, we would still need to know if there were changes in the chemical functional groups from the dissolved to the undissolved

membranes to verify that the halocarbons do cause changes in the chemical bonding.

Halocarbon attachment to polymer

This hypothesis is not substantiated by either FTIR nor NMR analysis. See explanation under *Weak hydrogen bonding*.

Fouling Reversibility

Fouling reversibility was not demonstrated in this work with AC membranes. The performance of the AC membranes did not recover as anticipated Milstead's work with CA membranes (*Milstead, 1982*). The concentrations used in our experiment were much higher than in Milstead's work. Furthermore, AC membrane seems to have a greater affinity for halocarbons than CA, as evidenced by the partition coefficient experiments.

11. Recommendations for Future Work

Membrane Fouling

Physical swelling

Replicates of the void fraction tests should be performed to demonstrate the data obtained in this study are reliable.

Weak hydrogen bonding and halocarbon attachment to polymer

Further work could be done using FTIR and NMR analyses to quantify the chemical bonding changes on these membrane samples. In the FTIR analyses, careful notes of the membrane weights should be taken to alleviate the problems shown in this work.

Fouling Reversibility

In future tests, one could try a polar solvent such as ethyl alcohol may be used to flush the membranes after exposure to halocarbons. After the flushing process for a specified time, one could resume operations without halocarbons in the feed to examine reversibility.

Effects of Concentration on Fouling

One could vary the concentration of halocarbons in the feed to examine the effects on fouling.

References

- Allegrezza, A. E. Jr., 1988, " Commercial Reverse Osmosis Membranes and Modules", Chapter 2, *Reverse Osmosis Technology: Application for High-Purity Water Production*, Bipin S. Parekh, ed., Marcel Dekker, Inc., New York & Basel, pp. 53 - 120.
- Allen, P. K. and G. L. Elser, 1979; "They Said It Couldn't Be Done-The Orange County, California Experience", *Desalination*, 30, pp. 23 - 38.
- Andersen, J.E., M.E. Heyde, and H.K. Plummer, Jr., 1981; "Irreversible Fouling Caused by Plasticization of Asymmetric Reverse Osmosis Membranes", *Desalination*, 37, pp. 307 - 11.
- Applegate, L. E., 1984; "Membrane separation processes", *Chemical Engineering*, 91(12), pp. 64 - 89.
- Applegate, R., 1986; "World's largest RO desalting facility to salvage 72.4 mgd", *Waterworld News*, pp. 17 - 19.
- Argo, D. G. and J. G. Moutes, 1979; "Wastewater reclamation by reverse osmosis", *Journal of the Water Pollution Control Conference Federation*, 51(3), pp. 590 - 600.
- Arora, M.L. and K.M. Trompeter, 1983; "Fouling of Reverse Osmosis Membranes in Wastewater Applications", *Desalination*, 48, p. 299.
- Atkins, P.W., 1982, *Physical Chemistry*, 2nd Edition, W.H. Freeman, San Francisco, pp. 318 - 20.
- Beckman, J.E., 1973; "Control of Fouling of RO Membranes When Operating on Polluted Surface Waters", Gulf Environmental Systems, San Diego, CA, Technical Report PB 223181.,
- Belfort, G., 1987, "Membrane Separation Technology: An Overview", Chapter 10, *Advanced Biochemical Engineering*, H.R. Bungus and Georges Belfort, eds., John Wiley & Sons, pp. 239 - 97.
- Besik, F., 1972; "Some Aspects of Reverse Osmosis in Treatment of Domestic Sewage", *Water and Sewage Works*, 119(10), pp. 76 - 85.
- Chian, E.S.K., W.N. Bruce, and H.H.P. Fang, 1975; "Removal of pesticides by reverse osmosis", *Environmental Science and Technology*, 9(1), pp. 52 - 59.
- Cotruvo, J. A., 1981; "THM's in drinking water", *Environmental Science and*

Technology, 15(3), pp. 268 - 74.

Cruver, J.E., 1973; Office of Saline Water Research Development. Progress Report No. 883, July, 1973, NTIS:PB223193.

Dickson, J. M., 1988, "Fundamental Aspects of Reverse Osmosis", Chapter 1, *Reverse Osmosis Technology: Application for High-Purity Water Production*, Bipin S. Parekh, ed., Marcel Dekker, Inc., New York & Basel, pp. 1 - 51.

DuPont, 1982; "Pretreatment for Colloids", *Permasep Engineering Manual*, E.I. duPont de Nemours, Inc., Wilmington, DE, pp. 1 - 4.

Eisenberg, T. N. and E. J. Middlebrooks, 1986; "Module Configurations", Chapter 7, *Reverse Osmosis Treatment of Drinking Water*, Butterworths, Boston, pp. 155 - 162.

Eykamp, W., 1976, "Fouling of Membranes in Food Processing", *Food, Pharmaceutical, and Bioengineering*, George T. Tsao, ed., AIChE Symposium Series. No. 172, 74, p. 234.

Glater, J., J. W. McCutchan, S.B. McCray, and M. Zachariah, 1981, "The Effect of Halogens on the Performance and Durability of Reverse Osmosis Membranes", ACS Symposium Series. No. 153, *Synthetic Membranes: Volume 1 Desalination*, Albin F. Turbak, ed., pp. 171 - 190.

Glater, J., L. C. Wilson, and J. B. Neethling, 1989, "Dissolved Organic Compounds at the Los Banos Desalting Facility", Chapter 43, *Aquatic Humic Substances: Influence on Fate and Treatment of Pollutants*, Advances in Chemistry Series. No. 219, I.H. Suffet and P. MacCarthy, ed., pp. 783 - 96.

Kaakinen, J.W. and C.D. Moody, 1985, "Characteristics of Reverse-Osmosis Fouling at the Yuma Desalting Test Facility", Chapter 27, *Reverse Osmosis and Ultrafiltration*, ACS Symposium Series. No. 281, pp. 359 - 82.

Kesting, R. E., 1977; "Asymmetric Cellulose Acetate Membranes", Chapter 5, *Reverse Osmosis and Synthetic Membranes, Theory-Technology-Engineering*, S. Sourirajan, ed., National Research Council of Canada, pp. 89 - 109.

Kojima, Y. and M. Tatsumi, 1977; "Operation of Reverse Osmosis Process for Industrial Waste Water Reclamation", *Desalination*, 23, pp. 87 - 96.

Kutz, S. M., D. L. Bentley, and N. A. Sinclair, 1985; "Improved Fixation of Cellulose-Acetate Reverse-Osmosis Membrane for Scanning Electron Microscopy", *Applied and Environmental Microbiology*, pp. 446 - 50.

LePore, J. V. and R. C. Ahlert, 1988, "Fouling in Membrane Processes", Chapter 4, *Reverse Osmosis Technology: Application for High-Purity Water Production*, Bipin S. Parekh, ed., Marcel Dekker, Inc., New York & Basel, pp. 141 - 183.

Loeb, S., 1980; "The Loeb-Sourirajan Membrane: How It Came About", ACS Symposium Series on Synthetic Membranes, 153(1), pp. 1 - 9.

Lonsdale, J.K., 1982; "The Growth of Membrane Technology", , 10, pp. 81 - 181.

Luck, W.A.P., 1984, *Synthetic Membrane Processes: Fundamentals and Water Applications*, Georges Belfort, ed., Academic Press, Orlando, FL, p. 21.

Malm, C. and G. Hiatt, 1971, Chapter IX, *Cellulose and Cellulose Derivatives*, N. Bikales and L. Segal, Ed., Wiley-Interscience, New York.

Mattson, M. E., 1979; "Significant Developments in Membrane Desalination-1979", *Desalination*, 28, pp. 207 - 23.

Merten, U., J.K. Lonsdale, R.L. Riley, and K.O. Voss, 1967; Reverse Osmosis Membrane Research. U.S. Office of Saline Water. Research Development Report, p. 265.

Milstead, C.E. and R.L. Riley, 1982; "Effect of Trihalomethanes on the Transport Properties of Thin-Film Composite and Cellulose Acetate Membranes", pp. 1 - 13.

Petersen, R. J., 1986; "The Expanding Roster of Commercial Reverse Osmosis Membranes", FilmTec Corporation, Minneapolis, MN, pp. 1 - 18.

Pintauro, P., 1980, "Mass Transfer of Electrolytes in Membranes", Ph.D. Dissertation, University of California, Los Angeles, Department of Engineering.

Pohland, H.W., 1989; "New Polyamide Composite Membranes for Ultrapure Fluids", Proceedings Presented at NAMS' 89, Austin, TX.

Potts, D.E., R.C. Ahlert, and S.S. Wang, 1981; "A Critical Review of Fouling of Reverse Osmosis Membranes", *Desalination*, 36, pp. 235 - 64.

Pusch, W., H.G. Burghoff, and E. Staude, 1976; "Characterization of Cellulose Acetate Membranes for Organic Solutes", *5th International Symposium on Fresh Water from the Sea*, Volume 4, Athens, Greece, pp. 143 - 56.

Reid, C.E. and E.J. Breton, 1959; "Water and Ion Flow Across Cellulosic Membranes", *Journal of Applied Polymer Science*, Volume 1(2), pp. 133 - 43.

Rickert, D.A. and J.V. Hunter, 1967; "Rapid Fractionation and Materials Balance of Solids Fractions in Wastewater and Wastewater Effluent", *Journal of the Water Pollution Control Federation*, 39, pp. 1475 - 86.

Ridgway, H., M. G. Rigby, and D. G. Argo, 1985; "Bacterial Adhesion and

Fouling of Reverse Osmosis Membranes", *Journal of the American Water Works Association*, 77(7), pp. 97 - 106.

Rudolfs, W. and J. L. Balmat, 1952; "Colloids in Sewage I: Separation of Sewage Colloids with the Aid of Electron Microscopy", *Sewage and Industrial Wastes*, 24(3), p. 247.

Selleck, R. E., Z. G. Ungun, and B. J. Marinas, 1984; "Principles of the Reverse Osmosis Process", Chapter 1 of the Final Report, Intramural Order No. 1999905, pp. 1 - 4.

Socrates, G., 1980, *Infrared Characteristic Group Frequencies*, John Wiley & Sons, Chichester, pp. 4 - 11.

Sugahara, M., T. Kitao, Y. Terashima, and S. Iwai, 1979; "Transport Properties of Thermally Conditioned Sludge Liquors in Reverse Osmosis", *International Chemical Engineering*, 19(2), pp. 322 - 28.

Sundet, S.A., 1983; "Reverse Osmosis Membrane Preparation", United States Patent 4,385,148.

Sundet, S.A., S.D. Arthur, D. Campos, T.J. Eckman, and R.G. Brown, 1987; "Aromatic/Cycloaliphatic Polyamide Membrane", *Desalination*, 64, pp. 259 - 69.

Weast, R. C., 1989, *CRC Handbook of Chemistry and Physics*, 70th Edition, CRC Press, Boca Raton, FL.

Wechsler, R., 1977; "Reverse Osmosis on Secondary Sewage Effluent: the Effect on Recovery", *Water Research*, 11(4), pp. 379 - 85.

Wilson, L., 1988, "Organic Interactions with Reverse Osmosis Membranes", Master's Thesis, University of California, Los Angeles, Department of Civil Engineering.

Winfield, B.A., 1979; "A Study of the Factors Affecting the Rate of Fouling of Reverse Osmosis Membranes Treating Secondary Sewage Effluents", *Water Research*, 13(7), pp. 565 - 69.

Wojcik, C.K., J.G. Lopez, and J.W. McCutchan, 1980; "Application of Reverse Osmosis to Reclamation of Municipal Wastewaters", *Desalination*, 32, pp. 353 - 64.

Zachariah, Michael R., 1982, "Analysis of Reverse Osmosis Membrane Degradation by Instrumental Techniques", Master's Thesis, University of California, Los Angeles, Department of Engineering.

Appendix

Representative Raw Data and Sample Calculations

Date 8/4 Du Pont 89006 ACM CCl ₄ added													
Conductivity					GC Area X 10 ⁷				Vol (L)		pH		
Hrs.	Feed	A	B	Reject	Feed	A	B	Reject	A	B	Feed	Reject	Temp
1	566	74.5	39.7	560					0.058	0.053	7.37	7.38	25.5
2	521	48.2	25.4	528	0.098	0.018	0.025	0.203	0.052	0.051	7.52	7.5	25.3
3	525	41.5	24.9	557					0.051	0.048	7.34	7.37	25.1
4	526	41.2	20.7	507	0.386	0.049	0.012	0.503	0.051	0.048	7.46	7.36	24.8
5	544	38.1	20.6	555					0.046	0.046	7.35	7.34	24.4
6	538	40	19.7	550	6.675	1.573	1.638	15.72	0.045	0.043	7.37	7.36	24.1
7	539	32.6	22.1	552					0.045	0.046	7.34	7.36	23.9
8	536	34.9	18	542	4.092	0.964	0.853	9.524	0.045	0.045	7.35	7.34	23.7
9	528	36.3	18	539					0.048	0.047	7.37	7.36	23.4
10	524	34.5	16.7	540					0.047	0.047	7.36	7.35	22.9
20	523	31.6	16.4	548	3.430	0.463	0.463	7.967	0.45	0.46	7.21	7.34	24.1
21	560	43.2	16.9	549	3.300	0.798	0.798	3.704	0.047	0.046	7.32	6.95	24.6
22	524	32.5	16.8	505					0.046	0.046	7.25	7.2	24.8
23	535	24.1	16.4	534	3.192	0.528	0.450	3.395	0.046	0.045	7.17	7.25	24.8
24	548	33.3	16.7	543					0.046	0.046	7.22	7.12	23.6

Sample Calculations

% TDS Rejection

Conductance Probe Calibration Equation:

$$C = 0.5969 \times K - 4.105$$

where: C = Concentration (mg/L)

K = Conductivity (μmho)

Taking data from time at 8 hours, $K_f = 536$, $K_A = 34.9$, $K_B = 18$

$$C_f = 0.5969 \times 536 - 4.105 = 315.8 \frac{\text{mg}}{\text{L}}$$

$$C_A = 0.5969 \times 34.9 - 4.105 = 16.7 \frac{\text{mg}}{\text{L}}$$

$$C_B = 0.5969 \times 18 - 4.105 = 6.6 \frac{\text{mg}}{\text{L}}$$

Using Equation 8, % R = $(1 - \frac{C_p}{C_f}) \times 100 \%$

$$\% R_A = (1 - \frac{16.7}{315.8}) \times 100 \% = 94.7\%$$

$$\% R_B = (1 - \frac{6.6}{315.8}) \times 100 \% = 97.9\%$$

$$\% R_{AVG} = \frac{94.7\% + 97.9\%}{2} = 96.3\%$$

% CCl₄ Rejection

Gas Chromatograph Calibration Equation:

$$C_{\text{CCl}_4} = \text{GCA} \times 12.5 \times 10^{-7} - 0.01751$$

where: C_{CCl_4} = concentration of CCl₄ (mg/L) in DI water

GCA = CCl₄ area from gas chromatograph

Taking data from time at 8 hours, $\text{GCA}_f = 4.092 \times 10^7$, $\text{GCA}_A = 0.964 \times 10^7$,
 $\text{GCA}_B = 0.853 \times 10^7$

$$C_{\text{CCl}_4,f} = (4.092 \times 10^7) \times 12.5 \times 10^{-7} - 0.01751 = 51.13 \frac{\text{mg}}{\text{L}}$$

$$C_{\text{CCl}_4,A} = (0.964 \times 10^7) \times 12.5 \times 10^{-7} - 0.01751 = 12.03 \frac{\text{mg}}{\text{L}}$$

$$C_{\text{CCl}_4,B} = (0.853 \times 10^7) \times 12.5 \times 10^{-7} - 0.01751 = 10.64 \frac{\text{mg}}{\text{L}}$$

$$\% R_{\text{CCl}_4,A} = \left(1 - \frac{12.03}{51.13}\right) \times 100\% = 76.5\%$$

$$\% R_{\text{CCl}_4,B} = \left(1 - \frac{10.64}{51.13}\right) \times 100\% = 79.2\%$$

$$\% R_{\text{AVG}} = \frac{76.5\% + 79.2\%}{2} = 77.8\%$$

Osmotic Pressure Calculation

Assumption : Molecular weight of solids = molecular weight of NaCl

Using Equation 4, $\Delta\pi = \frac{(\Delta C)RT}{\text{MW}}$, and data from time at 8 hours

$$\text{MW} = 22.98 \frac{\text{g}}{\text{mol}} (\text{Na}) + 35.45 \frac{\text{g}}{\text{mol}} (\text{Cl}) = 58.43 \frac{\text{g}}{\text{mol}} = 58430 \frac{\text{mg}}{\text{mol}}$$

$$R = 0.0821 \frac{\text{L-atm}}{\text{mol-}^\circ\text{K}}$$

$$T = 23.7^\circ\text{C} = 296.9^\circ\text{K}$$

$$\pi_f = \frac{315.8 \frac{\text{mg}}{\text{L}} \times 0.0821 \frac{\text{L-atm}}{\text{mol-}^\circ\text{K}} \times 296.9^\circ\text{K}}{58430 \frac{\text{mg}}{\text{mol}}} = 0.13 \text{ atm} \times 14.7 \frac{\text{psi}}{\text{atm}} = 1.94 \text{ psi}$$

$$\pi_A = \frac{16.7 \frac{\text{mg}}{\text{L}} \times 0.0821 \frac{\text{L-atm}}{\text{mol-}^\circ\text{K}} \times 296.9^\circ\text{K}}{58430 \frac{\text{mg}}{\text{mol}}} = 0.007 \text{ atm} \times 14.7 \frac{\text{psi}}{\text{atm}} = 0.10 \text{ psi}$$

$$\pi_B = \frac{6.6 \frac{\text{mg}}{\text{L}} \times 0.0821 \frac{\text{L-atm}}{\text{mol-}^\circ\text{K}} \times 296.9^\circ\text{K}}{58430 \frac{\text{mg}}{\text{mol}}} = 0.003 \text{ atm} \times 14.7 \frac{\text{psi}}{\text{atm}} = 0.04 \text{ psi}$$

Water Transport Coefficient (A) Calculations

Using Equation 1, $J_w = A(\Delta P - \Delta\pi)$, and data from $t = 8$ hours

$$J_{WA} = 0.045 \frac{\text{L}}{\text{hr}} \times 24 \frac{\text{hr}}{\text{day}} \times \frac{1 \text{ gal}}{3.78 \text{ L}} \times \frac{1}{2 \text{ in}^2} \times 144 \frac{\text{in}^2}{\text{ft}^2} = 22.22 \frac{\text{gal}}{\text{ft}^2\text{-day}} \text{ (GFD)}$$

ΔP = applied pressure = 400 psi

$$\Delta \pi = \pi_f - \pi_A = 1.94 \text{ psi} - 0.10 \text{ psi} = 1.84 \text{ psi}$$

Rearranging Equation 1, we get

$$A_A = \frac{J_w}{\Delta P - \Delta \pi} = \frac{22.22 \text{ GFD}}{400 \text{ psi} - 1.84 \text{ psi}} = 0.056 \frac{\text{GFD}}{\text{psi}}$$

Solute Transport Coefficient (B) Calculations

Using Equation 2, $J_S = B(\Delta C)$, and data from $t = 8$ hours

$$J_{SA} = C_A \times J_{WA} = 16.7 \frac{\text{mg}}{\text{L}} \times 22.22 \frac{\text{gal}}{\text{ft}^2\text{-day}} \times 3.78 \frac{\text{L}}{\text{gal}} = 1402.7 \frac{\text{mg}}{\text{ft}^2\text{-day}}$$

$$\Delta C = C_f - C_A = 315.8 \frac{\text{mg}}{\text{L}} - 16.7 \frac{\text{mg}}{\text{L}} = 299.1 \frac{\text{mg}}{\text{L}}$$

Rearranging Equation 2, we get

$$B_A = \frac{J_{SA}}{\Delta C} = \frac{1402.7 \frac{\text{mg}}{\text{ft}^2\text{-day}}}{299.1 \frac{\text{mg}}{\text{L}} \times 28.32 \frac{\text{L}}{\text{ft}^3}} = 0.166 \frac{\text{ft}}{\text{day}}$$

Partition Coefficient (K_s) Calculations

Procedure: Soak round pieces of membrane with 2 in. diameters in solutions of known concentration for 10 days. Extract halocarbons using 8 mLs of TMP.

Dilute 0.5 mLs of TMP extract in 8.5 mLs of DI water and inject into GC column.

Data: Wet membrane weight + pan = 1.3240 g

Dry membrane weight + pan = 1.2352 g

Pan weight = 1.0210 g

Wet membrane thickness = 0.0070 in
 Dry membrane thickness = 0.0072 in
 Membrane diameter = 2 in
 Membrane type = DuPont 89006 ACM
 CHCl₃, CHBr₃, CCl₄ Concentration = 2,000 $\frac{\text{mg}}{\text{L}}$

$$GCA_{\text{CHCl}_3} = 2.09 \times 10^7$$

$$GCA_{\text{CHBr}_3} = 6.11 \times 10^6$$

$$GCA_{\text{CCl}_4} = 2.63 \times 10^6$$

$$\eta_{\text{CHCl}_3} = \text{GC column efficiency for CHCl}_3 \text{ detection} = 99.78 \%$$

$$\eta_{\text{CHBr}_3} = \text{GC column efficiency for CHBr}_3 \text{ detection} = 90.19 \%$$

$$\eta_{\text{CCl}_4} = \text{GC column efficiency for CCl}_4 \text{ detection} = 99.75 \%$$

GC calibration equation for CHCl₃:

$$C_{\text{CHCl}_3} = \frac{GCA_{\text{CHCl}_3} \times 5.59 \times 10^{-7} - 0.01798}{\eta_{\text{CHCl}_3}}$$

GC calibration equation for CHBr₃:

$$C_{\text{CHBr}_3} = \frac{GCA_{\text{CHBr}_3} \times 12.8 \times 10^{-7} + 0.00532}{\eta_{\text{CHBr}_3}}$$

GC calibration equation for CCl₄:

$$C_{\text{CCl}_4} = \frac{GCA_{\text{CCl}_4} \times 12.5 \times 10^{-7} - 0.01751}{\eta_{\text{CCl}_4}}$$

Taking CHBr₃ adsorption as an example:

$$C_{\text{CHBr}_3} = \frac{(6.11 \times 10^6) \times 12.8 \times 10^{-7} + 0.00532}{0.9019} = 8.67 \frac{\text{mg}}{\text{L (diluted soln)}}$$

This is the diluted concentration.

To find the concentration in TMP:

$$C_{\text{CHBr}_3} = \frac{8.67 \frac{\text{mg}}{\text{L (diluted soln)}} \times 9 \text{ mL of diluted soln}}{0.5 \text{ mL TMP}} = 156.1 \frac{\text{mg}}{\text{L TMP}}$$

To find the mols of CHBr_3 per g of wet membrane:

$$\frac{156.1 \frac{\text{mg}}{\text{L TMP}} \times 0.008 \text{ L TMP}}{(0.303 \text{ g wet membrane}) \times 252770 \frac{\text{mg}}{\text{mol}}} = 1.63 \times 10^{-5} \frac{\text{mol CHBr}_3}{\text{g wet membrane}}$$

To find the mols of CHBr_3 per g of soaking solution:

$$\frac{2000 \frac{\text{mg}}{\text{L}}}{252770 \frac{\text{mg}}{\text{mol}} \times 1000 \frac{\text{g soln}}{\text{L soln}}} = 7.91 \times 10^{-6} \frac{\text{mol CHBr}_3}{\text{g soln}}$$

Using Equation 11, $K_s = \left(\frac{\text{mol organic}}{\text{kg wet membrane}} \right) : \left(\frac{\text{mol organic}}{\text{kg solution}} \right)$, we get

$$K_s = \frac{1.63 \times 10^{-5} \frac{\text{mol CHBr}_3}{\text{g wet membrane}}}{7.91 \times 10^{-6} \frac{\text{mol CHBr}_3}{\text{g soln}}} = 2.06$$

K_s for the other halocarbons, concentrations, and membranes were performed similarly.

Membrane Void Fraction (ϵ) Calculations

Using the above data, calculate dry and wet membrane densities

$$v_w = \pi \times (1 \text{ in})^2 \times 0.0070 \text{ in} = 0.022 \text{ in}^3 \times \left(2.54 \frac{\text{cm}}{\text{in}} \right)^3 = 0.36 \text{ mL}$$

$$v_d = \pi \times (1 \text{ in})^2 \times 0.0072 \text{ in} = 0.023 \text{ in}^3 \times \left(2.54 \frac{\text{cm}}{\text{in}} \right)^3 = 0.38 \text{ mL}$$

$$w_w = 1.3240 \text{ g} - 1.0210 \text{ g} = 0.303 \text{ g}$$

$$w_d = 1.2352 \text{ g} - 1.0210 \text{ g} = 0.2142 \text{ g}$$

$$\rho_w = \frac{0.303 \text{ g}}{0.36 \text{ mL}} = 0.84 \frac{\text{g}}{\text{mL}}$$

$$\rho_d = \frac{0.2142 \text{ g}}{0.38 \text{ mL}} = 0.56 \frac{\text{g}}{\text{mL}}$$

Using Equation 13, $\Delta V = \frac{\rho_d(w_w - w_d)}{\rho_d w_d}$, we get

$$\Delta V = \frac{0.56 \frac{\text{g}}{\text{mL}} \times (0.303 \text{ g} - 0.2142 \text{ g})}{0.56 \frac{\text{g}}{\text{mL}} \times 0.2142 \text{ g}} = 0.414$$

Using Equation 12, $\varepsilon = \frac{\Delta V}{1 + \Delta V}$, we get

$$\varepsilon = \frac{0.414}{1 + 0.414} = 0.293$$